Sensors and Their Applications for Connected Health and Environment

by

Nai-Yuan Liu

A Dissertation Presented in Partial Fulfillment
of the Requirements for the Degree
Doctor of Philosophy

Approved September 2018 by the
Graduate Supervisory Committee:

Erica Forzani, Chair
Gregory Raupp
Julianne Holloway
MaryLaura Thomas
Paul Westerhoff

ARIZONA STATE UNIVERSITY

December 2018

ABSTRACT

Connected health is an emerging field of science and medicine that enables the collection and integration of personal biometrics and environment, contributing to more precise and accurate assessment of the person's state. It has been proven to help to establish wellbeing as well as prevent, diagnose, and determine the prognosis of chronic diseases. The development of sensing devices for connected health is challenging because devices used in the field of medicine need to meet not only selectivity and sensitivity of detection, but also robustness and performance under hash usage conditions, typically by non-experts in analysis. In this work, the properties and fabrication process of sensors built for sensing devices capable of detection of a biomarker as well as pollutant levels in the environment are discussed. These sensing devices have been developed and perfected with the aim of overcoming the aforementioned challenges and contributing to the evolving connected health field. In the first part of this work, a wireless, solid-state, portable, and continuous ammonia (NH_3) gas sensing device is introduced. This device determines the concentration of NH_3 contained in a biological sample within five seconds and can wirelessly transmit data to other Bluetooth enabled devices. In this second part of the work, the use of a thermal-based flow meter to assess exhalation rate is evaluated. For this purpose, a mobile device named here mobile indirect calorimeter (MIC) was designed and used to measure resting metabolic rate (RMR) from subjects, which relies on the measure of O_2 consumption rate (VO_2) and CO_2 generation rate (VCO_2), and compared to a practical reference method in hospital. In the third part of the work, the sensing selectivity, stability and sensitivity of an aged molecularly imprinted polymer

(MIP) selective to the adsorption of hydrocarbons were studied. The optimized material was integrated in tuning fork sensors to detect environmental hydrocarbons, and demonstrated the needed stability for field testing. Finally, the hydrocarbon sensing device was used in conjunction with a MIC to explore potential connections between hydrocarbon exposure level and resting metabolic rate of individuals. Both the hydrocarbon sensing device and the metabolic rate device were under field testing. The correlation between the hydrocarbons and the resting metabolic rate were investigated.

ACKNOWLEDGMENTS

First of all, I would like to express my greatest appreciation to my advisor Dr. Erica S. Forzani for the guidance and support of my Ph.D. study and research with consideration and patience not just academically but mentally.

Second, I would like to thank Dr. Gregory Raupp, Dr. Julianne Holloway, Dr. Mary Laura Thomas, and Dr. Paul Westerhoff for taking time to serve on my committee. I am grateful to have them as my committee members. They have provided a lot of valuable advises on my research.

Third, I would like to thank Dr. Yue Deng, Dr. Francis Tsow and Dr. Devon Bridgeman for their help in polymer optimization, hardware design, and fabrication. I would like to thank Dr. Leslie Thomas for providing the idea of how important monitoring on urine-ammonia level is and providing urine samples for me to do experiments; Dr. Kulick for providing me subjects and equipment to validate my mobile indirect calorimeter.

At last, I would like to say that it is my pleasure to work with so many amazing scholars and researchers down the road. Without them, I would not have such a fantastic experience in the journey toward my PhD degree.

TABLE OF CONTENTS

Page

CHAPTER Page

Page

LIST OF TABLES

LIST OF FIGURES

Figure Page

Figure Page

CHAPTER 1

BACKGORUND AND INTRODUCTION

1.1. Connected Environment and Health

The idea of connected health has been reported as a social-technical model for healthcare management and delivery [1]. Connected health & Environment is the extended idea of connected health that all the health data of a person and the environmental data that would affect the health of a person could be gathered together for early-stage diagnosis for doctors, research about the influence of pollutants to human health or even just for personal health condition tracking. By addressing the effect of environmental pollutants to human health altogether with the health condition of a personnel, it allows the possibility of all kinds of research and applications in medical community. To accomplish this, two goals need to be fulfilled: (1) a robust chemical detecting system for health condition and environment, (2) a data collection unit that all the data are gathered.

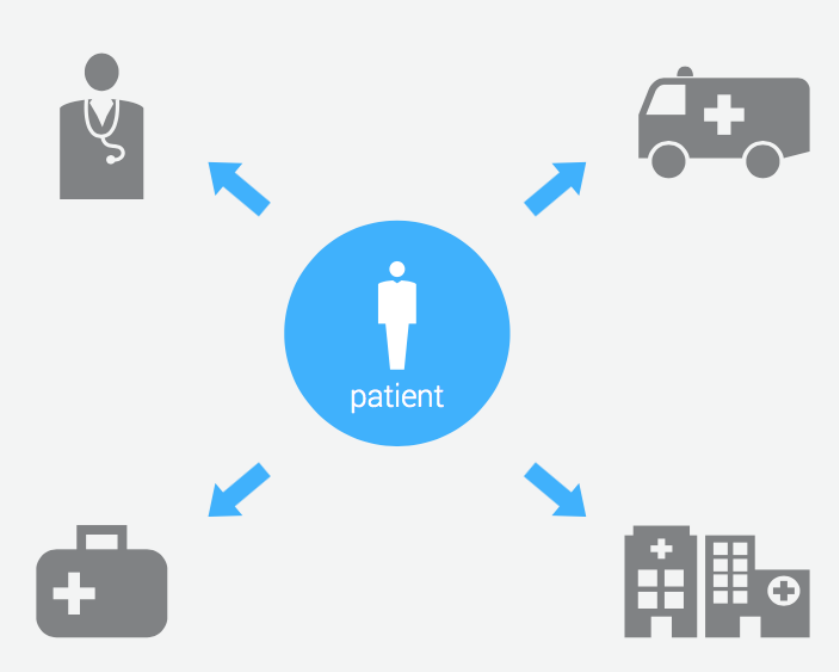

Figure 1-1. The idea of connected health, reported as been reported as a social-technical model for healthcare management and delivery [2].

The chemical detecting system needs to be portable and fast-responding, and easy to use, which measurements could be done in the field without any further data processing. The sensor needs to be very selective to the components depending on the purpose. The reusability of the sensor is also very important since real-time or continuous monitoring is preferable. Reusable sensors also increase simplicity of the detecting system, making the device more accessible to people in different disciplines. Ideally, the device needs to be automatic without additional labor work. For information acquisition on human beings, non-invasive measurement is essential to achieve continuous monitoring and the acceptance of the technology for the public.

An ideal data storage unit should be portable and wireless. All the data detected through different sensing devices needs to be gathered altogether and transmitted wirelessly for

convenience and simplicity. A smart device is the most ideal electronics that could fulfill these goals. A platform that allows professionals, researchers and patient, etc. to easily access needs to be established. One of the most famous examples is the platform Apple Inc. has created. The health app in every Apple's smart device gathered all the health data that could be accessible to different people depending on the protocols. [3]

In this work, I will focus on the chemical detecting system and discuss about the properties and fabrications of sensors and some of their applications for detecting the hydrocarbons level in the environment; how it correlates with the resting metabolic rate and the biomarker in human body to evaluate one's health condition.

1.1.1. Environment: Volatile Organic Compounds (VOCs)

Volatile organic compounds (VOCs) are organic chemicals emitted from anthropogenic and biogenic sources with high vapor pressure at room temperature [4], such as acetone, ethanol and benzene…etc., some of which are harmful to human health [5]. According to the United States Environmental Protection Agency (EPA), VOCs are among the major pollutants for indoor and outdoor air quality, which are emitted from furniture, appliances, and construction materials and combustion of vehicle fuels [6, 7]. Harmful VOCs typically are not acutely toxic, but have long-term health effects [8]. In this work, I will be focusing on discussing about hydrocarbons detection (a large portion of (VOCs) and its correlation with the resting metabolic rate.

1.1.2. Heath: Ammonia and Oxygen/Carbon Dioxide

Ammonia

A research survey conducted by the Mayo Clinic has shown that there is a significant need for real-time monitoring of biomarkers related to kidney and liver function in the

human body due to increasing diagnoses of disorders of the aforementioned organs, such as acute kidney injury/chronic kidney disease [9, 10], liver disease [11-13], urea cycle disorders [14-16], disturbances of acid-base regulation [17-20] and protein metabolism end energy balance [21, 22]. Ammonia is a promising biomarker for this purpose, since a person's ammonia levels are abnormally high when their regular kidney or liver function is poor [14, 16-25]. In this work, I will be focusing on discussing about the creation of a urine-ammonia sensing device.

Oxygen/Carbon dioxide

Oxygen and carbon dioxide level are measured to evaluate the environment quality or the health condition of people. For instance, the carbon dioxide is the main compound in the atmosphere causing global warming. In this work, I will be focusing on the measurement of biological oxygen and carbon dioxide to evaluate the resting metabolic rate on personnel. Oxygen consumption (VO_2) rate and carbon dioxide rate (VCO_2) production rate in breath was measured based on colorimetric technology, which are used to determine the resting metabolic rate according to the Weir equation [26].

1.1.3. The Design of The Sensing Device

To design a mobile sensing device, typically, there are several steps needed to be followed. First of all, the sensing mechanism needs to be chosen, which is dependent on the detecting range, the detection limit and the resolution. For example, when an adult consumed a high amount of protein, in consequence, the total ammonia (NH_3) concentration in his or her body fluid will change rapidly in a small period of time. In this case, we need to know the normal range of total ammonia in her body fluid. The sensing mechanism needs to be able to tell the concentration difference in this range. As the total

NH_3 concentration will change throughout the time, the sensing mechanism needs to be able to tell the change in a specific amount of time depending on the purpose. The absorbance change in specific time period is also defined as resolution.

Once the mechanism is determined, the stability, reproducibility and repeatability are what needed to be considered. Take the same example mentioned in previous paragraph. First of all, the sensor needs to always give the same response when exposed to the same amount of analyte (reproducibility). Then it needs to function well even in a long period of time (stability). Reusability is always favorable in the aspect of sensing technology. Therefore, in this case, we need to know how repeatable the sensor could be used before being disposed.

After all these are determined, the printed circuit board and other components (such as a pump, a drying fan, or a pre-conditioning column, etc.) will then be designed and coordinated with sensing components. In the sense of connected health and environment, the PCB will be wirelessly connected to a smart device through Bluetooth. Finally, the cost of the sensor and sensing device need to be considered depending on the purpose.

1.2. State of Art Gas Detection Techniques

1.2.1. Gas Chromatography- Mass Spectrometry (GC-MS)

GC-MS is by far the most accurate instrument for quantification analysis of gas. In general, all the gas could be quantified by GC-MS. The detecting mechanism is divided into two parts: First, the gas chromatograph separates different compounds based on their different retention time, which is the time used for the compounds to pass through the column. In the end of the column is where the mass spectrometer is. The mass spectrometer

will then quantify the amount of compounds by ionizing them to generate charged molecules or molecule fragments to measure their mass-to-charge ratios [27, 28]. Although GC-MS [27, 29-31] is accurate for gas measurement, it's often expensive and difficult to maintain. GC-MS separates and identifies targets from complex mixtures, but requires expensive instrumentation (~$300,000) and pre- concentration steps that preclude high reproducibility and real-time implementation.

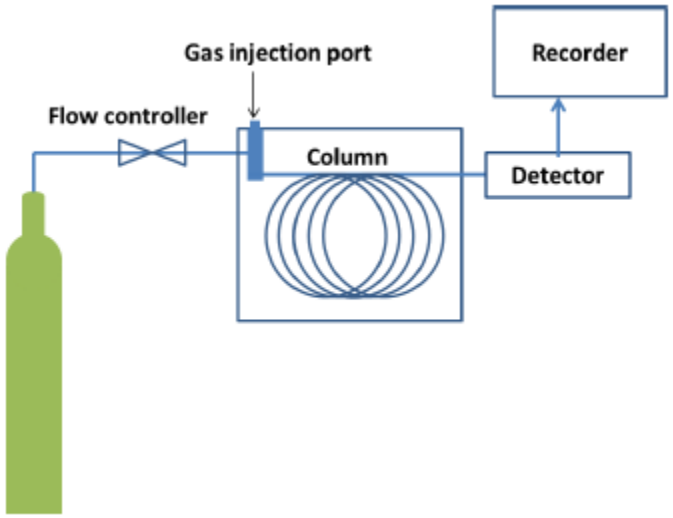

Figure 1-2. Schematic diagram of gas chromatograph [28].

1.2.2. Metal Oxide Semiconductor (MOS)

The adsorption and desorption of gases on the surface of MOS materials will change the conductivity of the material, which could be used to quantify the concentration of the target gas [32]. The conductivity change is based on carrier concentration change of the MOS material due the reduction or oxidation of the target gas once it adsorbs on the surface of MOS [33, 34]. Research has shown that MOS sensors are responsive a variety of gases, including VOCs and non-VOCs, e.g. ethanol, acetone and ammonia, etc. [35]

This selectivity is the main challenge for this kind of sensor [32] [36-40]. Also, MOS sensors usually requires high temperature working environment, which address high energy consumption problem.

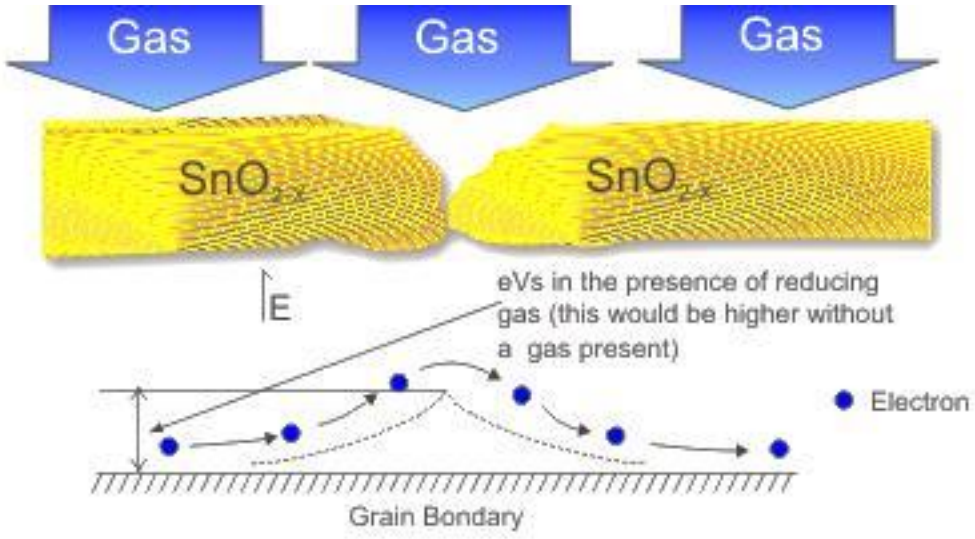

Figure 1-3. The schematic of the mechanism of how metal oxide semiconductor works [41].

1.2.3. Photo Ionization Detection (PID)

In a PID, high-energy UV photons bombarded compounds, which turn into positively charged ions. The ions produce an electric current, which is the signal output of the detector. The signal is later converted to concentration [42]. There have been many patents regarding gas detection with PID [16, 17]. The primary use of PID is for monitoring VOCs. However, some non-VOC gases (e.g. ammonia) are also detected by PID [18, 19]. PID has been particularly useful due to its portability.

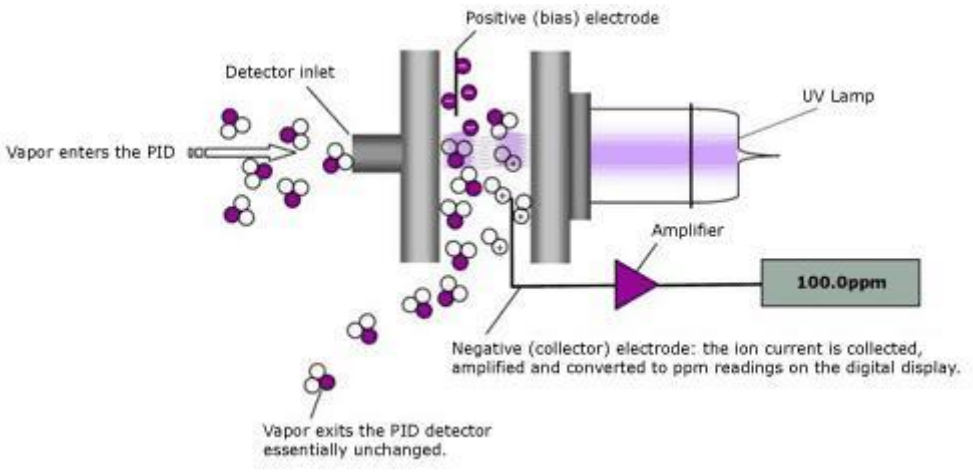

Figure 1-4. The schematic of a photo ionization detector [43].

1.2.4. Electrochemical Gas Sensors

Electrochemical gas sensors measure the concentration of a target gas by oxidizing or reducing the target gas at an electrode and measuring the resulting current. An ion-selective electrode for liquid solution converts the activity of a specific ion dissolved in a solution into an electrical potential. The ISE for ammonia used in this work has an additional membrane, which allows only gaseous ammonia to pass through. I used this electrode as a reference method for measuring gaseous urine-ammonia.

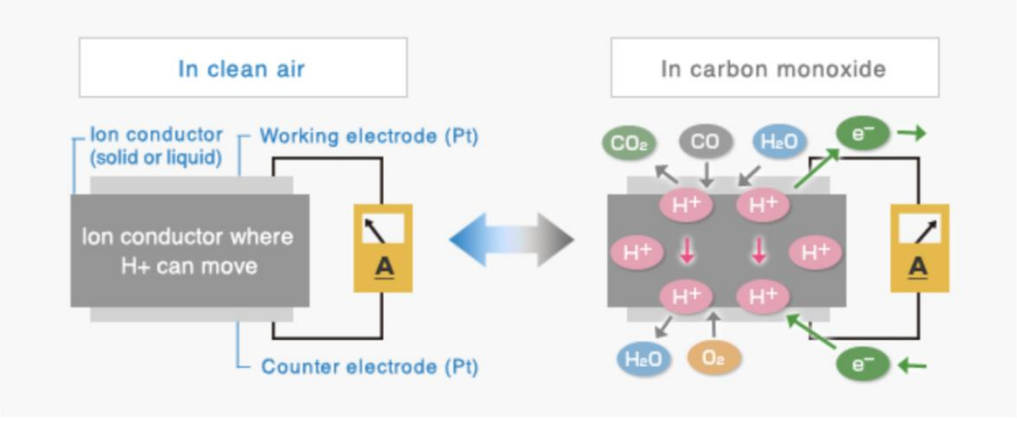

Figure 1-5. The schematic of a electrochemical gas sensor [44].

1.2.5. Enzyme Methods/Spectrophotometry

In general, enzymatic assays involve multiple incubation steps, require processing times greater than one hour, and require significant operator labor. The analyte is usually detected by UV or Visible light spectrophotometry. For NH_4^+ detection in blood and urine, enzymatic assays are the only technique that meets the FDA's standards [45-47] for clinical research, given the complexity of biological samples.

1.3. Quartz Tuning Fork (QTF) Resonator for VOCs

Quartz is a piezoelectric material. This material accumulates charge in response to applied mechanical stress and vice-versa, which is the basic principle used in the operation of the quartz tuning fork. Quartz tuning forks have been used in many applications, where require precise timing, including wristwatch and microcontroller integrated circuit. Mechanical resonations are generated when a voltage is applied the prongs. The tuning forks require very low power consumption and are very stable and precise [26-28]. In chemical sensing, QTF surface is usually coated with a selective sensing material. Target analyte adsorbs on the prongs, resulting in the mass change or the prongs. This change will then decrease the resonant frequency of the material. Based on the mass change, the concentration of the material could be calculated.

1.4. Colorimetric Sensor Assays for NH_3 and CO_2/O_2

This sensor consists of a thin membrane embedded with an ammonia-sensitive pH dye attached to the end of a fiber optic cable [36-40, 48]. These devices possess high sensitivity, but, further instrumental improvements are required for use with biological

samples. In this work, the ammonia and carbon dioxide/oxygen sensors utilize this technique.

1.5. Dissertation Overview and Summary

This document consists six chapters. Chapter 1 (this chapter) provides the idea of connected health and environment and focus on the role of chemical detecting system to accomplish this idea. Chapter 2 gives an example of how to create a mobile chemical sensor and its application. In this example, I will introduce a device that is able to detect urine-ammonia as a biomarker of kidney or liver disorder in real time. Chapter 3 gives an example of the improvement on mobile sensing device for healthcare. In this example, I will describe the flow resistance problem of the mobile indirect calorimeter and improvement I made. Chapter 4 gives an example of the improvement on mobile sensing device for environment. I will discuss the aging problem of the VOC sensor and its improvement and fabrication. Chapter 5 gives an example of the connection of health condition and environment with the chemical detecting system. I will discuss the study on the correlation of different worker's resting metabolic rate and the surrounding VOC level measured by the devices discussed in chapter 3 and 4. Lastly, in chapter 6, I will conclude the work and discuss possible future work.

CHAPTER 2

THE CREATION OF A NEW MOBILE CHEMICAL SENSOR AND ITS APPLICATION: THE DETECTION OF URINE AMMONIA BIOMARKER IN REAL TIME

2.1. Background and Introduction

The determination of concentration of total ammonia (ammonia (NH_3) and ammonium (NH_4^+)) in biological samples has traditionally presented technical challenges. Urine total ammonia concentration is not generally determined, and medical doctors have been trained to estimate urine NH_4^+ concentration via the utilization of a flawed indirect indicator (i.e., urine anion gap) [49, 50]. However, nitrogen balance is significantly impacted by a number of physiological conditions, and knowledge of the precise total ammonia level of blood, urine, and other biological samples (e.g., breath, sweat), is known to be of great benefit for the diagnosis and/or treatment of several disease states. For instance, blood NH_4^+ is an important marker used to inform treatment decisions for patients with *urea cycle disorders* [14, 25, 51, 52]. Dynamic changes in kidney total ammonia generation (i.e., renal ammoniagenesis) are stimulated by systemic conditions of acid-base balance, potassium balance, and others; thus, an enhanced moment by moment understanding of urine total ammonia levels in patients prone to acid-base or potassium disturbances (e.g., critically ill, hospitalized patients) would augment immediate clinical knowledge and could be leveraged to serve as an early warning signal of rapidly changing (and otherwise under-recognized) deleterious systemic conditions [22]. Given the complex interactions of kidney and liver adaptations for total ammonia

homeostasis, disorders of the kidney and/or liver may produce rapid changes in total ammonia levels. For instance, acute hepatic dysfunction or decompensation is associated a rise in blood total ammonia levels [13] while acute kidney dysfunction is associated with a rapid decrease in urine total ammonia levels [53]. In the outpatient setting, serial monitoring of total ammonia levels of biologic samples (including breath, sweat, blood, and urine) could provide a baseline level of total ammonia, departures from which would be a strong predictive signal of pending metabolic decompensation in patients with advanced liver disease or a predictive signal of pending kidney dysfunction. In the inpatient setting, patients with indwelling urinary catheters at high risk of acute kidney injury could be monitored for rapid decreases in urine total ammonia concentration as the first sign of generalized kidney tissue distress. Utilizing that technique could lead to rapid identification of acute kidney injury within moments (compared to several hours or days using the lagging, traditional markers, including serum creatinine). In each of these scenarios, specific treatments to ameliorate either the underlying organ distress or predictable byproducts of organ dysfunction could be employed in a much more rapid, more individualized, and more effective manner than occurs today in modern medical practice. Additionally, increasing the percentage of dietary protein in terms of total "Calories In" has become a method for healthy weight management in bariatrics (as well as in exercise science). Reported short-term benefits include: i) optimal maintenance of muscle tissue, ii) improved satiation, and iii) insurance against malnutrition (sufficient essential amino acid intake is more assured) [21]. However, a detailed analysis of these relatively short-term studies is lacking, and the long-term metabolic effects and other health consequences of significantly increased dietary protein intake have been largely

unexplored. An understanding of the rate of storage of consumed amino acids versus the rate of immediate metabolic oxidation (for work-energy and heat production) can be greatly enhanced by measurement of nitrogen balance, which may be performed by an analysis of urine for major nitrogen-containing molecules (e.g., urea, creatinine, and total ammonia). Currently, accurate quantification of these analytes is cumbersome because lab-bench analysis methods are required. Since urine total ammonia has been proposed as a marker of nitrogen balance [21, 22], real-time urine total ammonia monitoring could allow the end user to better estimate amino acid utilization [22].

Most measurement techniques for NH_3 detection in human samples rely on breath or blood (plasma) [54]. Metal-oxide based sensor technologies [36-40] are frequently used for NH_3 analysis. However, this type of sensor exhibits limited specificity for NH_3 and can be confounded by ethanol, acetone, methane, hydrogen, nitric oxide, and nitrogen dioxide [55]. For blood (plasma), ion selective electrodes (ISE) have been optimized to detect NH_3 and ammonium (NH_4^+) in clinical applications [55]. In fact, our research has demonstrated ISE's are highly accurate when compared to gold standard enzymatic methods (see below). However, in our experience ISE's can be implemented for bed-side reading in near-real time detection, but they require labor since the Ammonia Electrode [56] needs to be calibrated each day before use to minimize measurement drift because of the limited stability of sensing membranes. Given the complexity of biological samples, few sensor technologies have been approved by the United States Food and Drug Administration (FDA) for clinical research. For NH_4^+ detection in blood and urine, enzymatic assays are the only technique that meets the FDA's standards [45-47]. In general, enzymatic assays have limited enzyme storage lifetime, involve multiple

incubation steps, require processing times greater than one hour, and involve significant operator labor. Alternatively, NH_3 can be detected via absorption spectroscopy by instruments such as Nephrolux™ (Pranalytica, Santa Monica, CA) [57], which uses a tunable laser and an acoustic detector to perform sub-parts per billion (ppb) zero background measurements of NH_3 in the presence of interferents like CO_2 and water vapor such as in breath. While spectroscopic techniques are extremely sensitive, they usually have bulky components making them inconvenient for personalized use. Moreover, optical components in absorption spectroscopy are prone to misalignments and unsuitable for personalized use [58].

Gas chromatography – mass spectrometry (GC-MS) [29-31] and selective ion flow tube – mass spectrometry (SIFT-MS) [59-63] are accurate for NH_3 measurement but are expensive, and instruments are difficult to maintain. GC-MS separates and identifies NH_4^+ and NH_3 from complex mixtures, but requires expensive instrumentation (~$300,000) and pre-concentration steps that preclude high reproducibility and real-time implementation [30, 31, 64, 65]. SIFT-MS was developed for real-time detection of low molecular weight volatiles, including NH_3, in different biological samples (skin and urine headspace, breath, etc.) but is also expensive (~$200,000) [59-63] and rather difficult to maintain.

Many new emerging sensing methods have been proposed and are being developed for the detection of NH_3 including: (1) colorimetric sensors, (2) spectroscopic based sensors, (3) nanomaterial based sensors, and (4) contactless conductivity based sensors. (1) Colorimetric sensors are used for measurement of NH_3 in wastewater and blood [66-68]. This type of sensor consists of a thin membrane embedded with an NH_3-sensitive pH dye

attached to the end of a fiber optic cable. These devices possess high sensitivity, but further instrumental improvements are required for use with biological samples. (2) Spectroscopic methods of NH_3 measurement include pulsed quantum cascade laser spectroscopy [69-71] and optical micro-ring resonators [72]. While large (table-top) measurement systems exist, these lack the small size, low weight, and low cost desirable for portable individual monitoring (such as at a hospital bedside). (3) Nanomaterial based chemiresistors [73-78] and electrochemical sensors [79, 80] exhibit detection limits matching the clinically relevant NH_3 levels (breath- NH_3 in ppb and blood- NH_3 in µmol/L) under well-defined, near ideal laboratory conditions. However, detection of NH_3 in complex samples using these sensors requires further improvement to obtain the selectivity and lifetime necessary for continuous monitoring conditions. (4) Finally, Toda et al. reported a contactless conductivity based NH_3 sensor [81]. However, the acid solution used must be replaced after each measurement, making continuous measurement impractical [81].

Human urine NH_3 levels are high and provide an opportunity for development of new continuous sensors [55]. NH_4^+ ions in liquid are volatile and rapidly turn into NH_3, therefore in the medical field, there is currently no standard technique for instantaneous urine NH_4^+ measurement. A urine reagent stick is in wide clinical use to determine 10 different urine parameters (including specific gravity, pH, protein, leucocytes, nitrites, blood, ketones, glucose, bilirubin, and urobilinogen) [82]. Commercial electronic readers of these urine dipsticks do not include measurements of excreted NH_3 [83]. However, NH_3-detection reagent sticks are commercialized for use in water samples [84]. The operation of dipsticks is based on irreversible chemical reactions, and therefore they are

single-use devices. Although dipsticks are quick and easy to use, they only provide a semi-quantitative assessment of parameters, and do not demonstrate the accuracy and continuous real-time monitoring capability desired in critical applications.

This work introduces for first time a Colorimetric Optoelectronic Dynamics Analyzer (CODA) for real-time and continuous urine total ammonia detection using very small amounts of urine. The device uses a sensor embedded with an NH_3-sensitive sensing probe based on a pH dye. Unlike existing detection methods for human body fluids, which directly measure dissolved NH_4^+, the new sensing platform detects total ammonia as NH_3 in urine headspace by converting liquid NH_4^+ to gaseous NH_3 by alkaline exposure of the fluid before measurement, which provides the device with extraordinary selectivity. Although similar sensing methods based on this concept have been studied [68, 85], they have only been applied to waste water and pure solution testing. The handheld, solid-state device introduced here utilizes a red LED light source and photodiodes. The photodiodes transduce the color change of the sensor to an electronic signal, which can be wirelessly transmitted to smart devices for readouts. The wireless connection feature allows flexibility to accommodate a variety of situations, and the operational method has been demonstrated to be accurate, providing concentration levels comparable to the ISE method.

2.2. Material and Methods

2.2.1. Sensing Mechanism and Sensor Preparation

This ammonia (NH_3) sensor is based on Bromophenol Blue (BpB) from Sigma-Aldrich. It is used as a pH indicator that changes color form yellow at pH 3.0 to blue at pH 4.6 [86]. NH_3 contributes to an alkaline environment to make the color change on BpB as it forces the dissociation of H^+, which the overall reversible chemical reaction could be described as follows:

$$2NH_3 + BpBH_2 \leftrightarrow (NH_4)_2BpB \qquad \text{Equation 2-1}$$

(blue)

The kinetics include two steps: (1) First, the NH_3 molecules adsorb on the sensing substrate. (2) Then the reaction (Equation 2-1) happens on the substrate. The overall reaction is a basically a simplified form of acid-base reaction, which happens extremely fast. Therefore, the rate limiting step is the mass transfer (adsorption) [87]. The sensor substrates were cut into a rectangular shape (2.7 cm * 1.2 cm) and laminated so that they fit the sensing chamber of the Colorimetric Optoelectronic Dynamics Analyzer (CODA).

2.2.2. Optoelectronic Analyzer, Instrument, and Signal

The CODA introduced in this work has a horizontal gas flow channel passing through the sensing chamber, which contains a 610 nm LED at the top of the sensor and four photodiodes (a sensing/reference pair and a sensing/reference backup pair) beneath the sensor (Figure 2-1a, b). The target gas is injected into a sensing chamber, where it is

exposed to the sensor which then exhibits a color change proportional to the concentration of NH_3 in the target gas. The photodiodes were mounted on the printed circuit board (PCB), which was integrated with a Bluetooth unit, allowing signal transmission to an Android phone. An app was created to provide a user interface to show the signal read by the photodiodes (Figure 2-1c). The sensor contains a reference area and a sensing area (Figure 2-1d). Typically, the background response from the reference and sensing areas when the sensor is in the chamber is around 1.2 V. A pair of photodiodes simultaneously and continuously read the response of the reference and the sensing areas every 0.2 seconds. The absorbance is calculated by taking the negative logarithm of the signal response from the sensing area (Ssens.) divided by the signal response from the reference area (Sref.) as follows in Equation 2-2:

$$Absorbance = -log(\frac{S_{sens.}}{S_{ref.}}) \qquad \text{Equation 2-2}$$

Calibration curves for the NH_3 sensor were performed for a concentration range of 2 - 1000 ppm for NH_3 by plotting measured absorbance change versus known concentration of the sample.

(a)

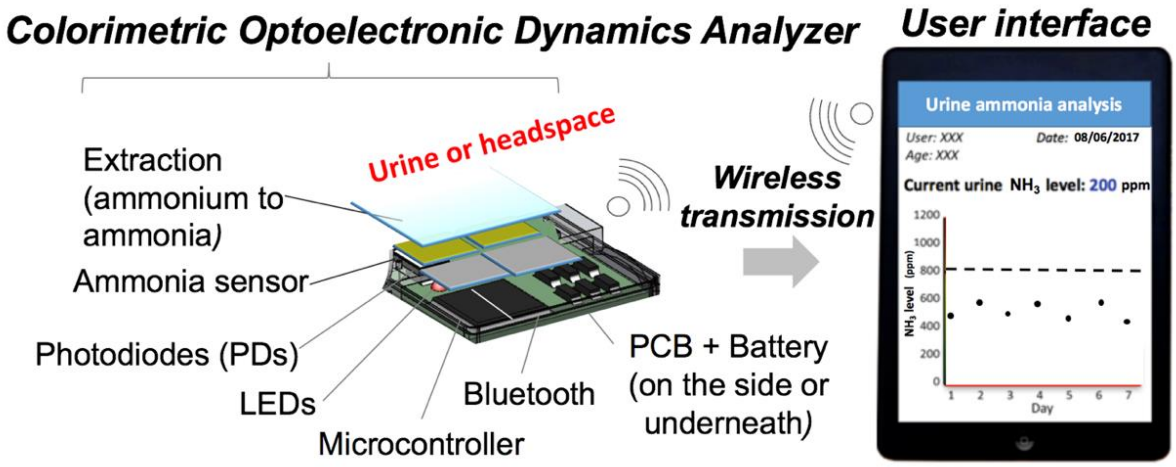
Colorimetric Optoelectronic Dynamics Analyzer
User interface
Urine or headspace
Extraction (ammonium to ammonia)
Ammonia sensor
Photodiodes (PDs)
LEDs
Microcontroller
Bluetooth
PCB + Battery (on the side or underneath)
Wireless transmission
Urine ammonia analysis
User: XXX
Age: XXX
Date: 08/06/2017
Current urine NH3 level: 200 ppm
NH3 level (ppm)
Day

(b)

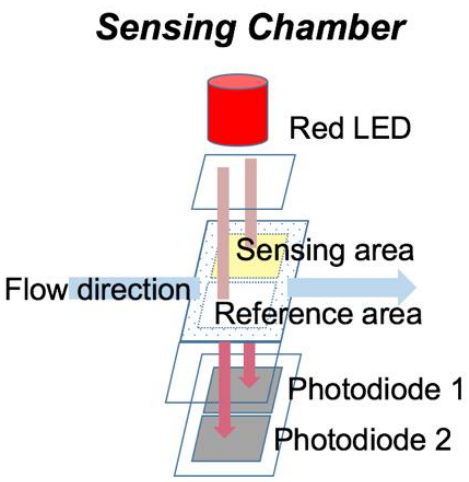
Sensing Chamber
Red LED
Sensing area
Flow direction
Reference area
Photodiode 1
Photodiode 2

(c)

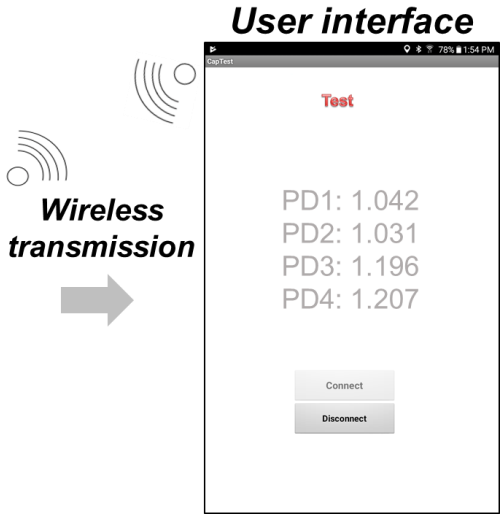
User interface
Wireless transmission
Test
PD1: 1.042
PD2: 1.031
PD3: 1.196
PD4: 1.207
Connect
Disconnect

(d)

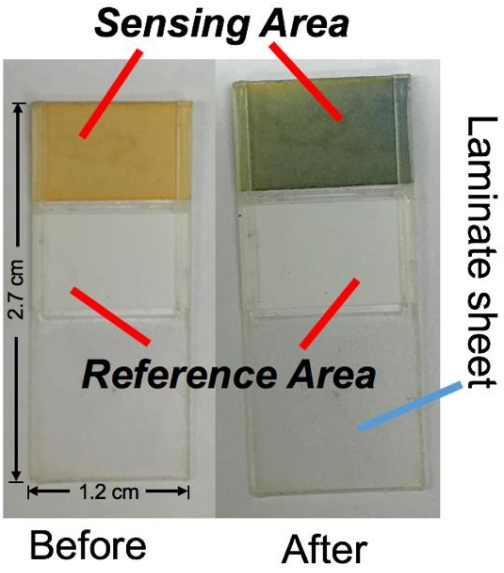

(e)

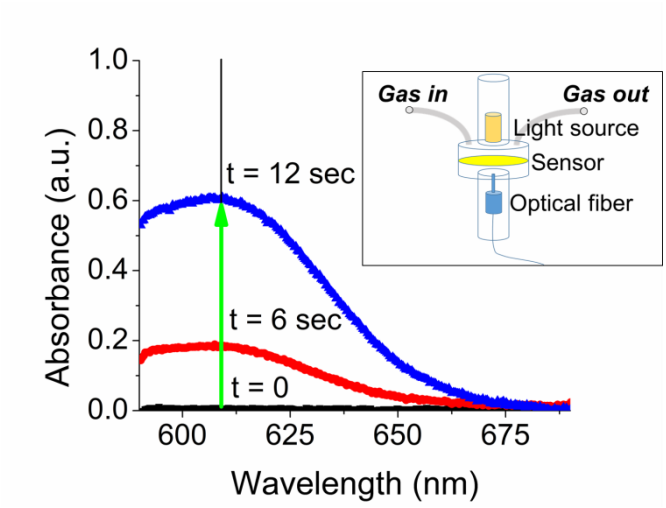

Figure 2-1. The schematic of the Colorimetric Optoelectronic Dynamics Analyzer (CODA). (a) The main components of the CODA (real dimensions added). (b) Schematic of the sensing chamber, and (c) screenshot of the actual user interface, including photodiodes for measuring the signal of the sensing area and the reference area. By comparing the changes on the -log of signal ratio between the sensing and reference areas, the concentration of ammonia (NH_3) gas can be determined via absorbance. CODA is able to measure total ammonia level in biological samples up to 59 mmol/L every 2 minutes. (d) The color change of the sensor from orange to blue after exposure to NH_3. (e) Spectrum of the absorbance change of the sensor obtained with a JAZ

Spectrophotometer (JS) instrument's sensor chamber (illustrated in the insert). Spectrum before (t=0) and after (t>0) exposure to NH_3, indicating the maximum absorbance change wavelength (609 nm) are shown. Insert: Schematic of JS's sensing chamber. The optical fiber is on the top of the chamber, while the tungsten light source is at the bottom of the chamber. The gas travels from the left tube and discharges into ambient from the right tube.

In order to ensure there was no interference between photodiode readings from sensing and reference areas of the sensor, a cross-talking test was performed. In this test, we individually masked either the reference area or the sensing area with black thick ink to block light and we conducted the measurement for 30 seconds to check if response was zero for the blocked area, and unaffected for the unblocked sensor areas. The cross-talking test results are shown in Supplemental Information, Table A.1 and Table A.2 in Appendix A. For both masked substrates, the cross-talking test shows a minor signal change that was not significant important under sensing conditions, and could be further improved by creating a thicker barrier between photodiodes or decrease the distance from the sensor to the detector.

Optoelectronic instrument

A JAZ Spectrophotometer (JS) from Ocean Optics was used to conduct the sensitivity tests for the different sensor materials and spectrum measurement before and after exposure to NH_3. Fig. 1e insert presents a schematic of the JS measurement device. Whatman no.1 filter paper was cut into a round shape to fit the JS sensing chamber. An NH_3 sensor integrated in the shape of a sandwich with an NH_3 extraction membrane was used for spectrum measurement. The sensor/membrane assembly consisted of five parts: 1) the distribution layer (filter paper), which makes sure the liquid disperses

homogeneously 2) the alkaline layer (impregnated with NaOH solution), extracting NH_3 from the sample 3) a polytetrafluoroethylene (PTFE) membrane, precluding liquid from reaching the indicator layer 4) the indicator layer (substrate impregnated with Bromothymol Blue), and 5) the mask made of tape, which protects the sensing probe. A synthetic urine feed (NH_4^+ solution with other ions simulating urine: NaCl, KH_2PO_4, $CaCl_2$, $MgSO_4$) was injected from the top of the integrated NH_3 sensor membrane. The JS quantifies the NH_3 level in sample. The NH_3 sensing mechanism is further discussed in Section 2.2.3.

Optoelectronic sensor signal

As mentioned previously, Bromophenol Blue (BpB) was used as a colorimetric sensing probe for NH_3 detection. A BpB solution has a yellow/orange color when it is exposed to a pH level below 3 and a blue color when exposed to a pH above 4.6. The acid/base equilibrium between NH_4^+ (acid) and NH_3 (conjugate base) is determined by the pH of the solution in the overall reaction $OH^- + NH_4^+ \leftrightarrow H_2O + NH_3$. NH_3 has a vapor pressure of 1062 kPa and a pK_a of 9.25 at room temperature [88]. Biologically relevant pH conditions are below the pKa of the NH_4^+/ NH_3 equilibrium. For example, at a relatively high urine pH of 8, only 6.6% of the total NH_4^+/ NH_3 is present as NH_3 (gas) [88, 89]. Because of the dynamic nature of biological pH and the variable ratio of urine NH_4^+ to urine NH_3, an alkaline solution is needed to increase the sample pH greater than ~12 to ensure 100% conversion of NH_4^+ (liquid) to NH_3. NH_3 causes the sensing surface to become more alkaline, shifting the pH value higher and causing a yellow to blue color transition (Figure 2-1d). By quantifying the color change using the CODA, we can

determine the corresponding NH_3 concentration derived from the sample.

2.2.3. Gas Sample Preparation

Ammonia bags

The NH_3 gas samples used in this work were diluted with 100 ppm and 1000 ppm calibration NH_3 gas purchased from Calibration Technologies, Inc. Dilutions of gas samples in laboratory compressed air were prepared from 100 and 1000 ppm of NH_3 calibration gas. These calibration gases were directed into a 40 L bag using a micro diaphragm gas pump for a predetermined amount of time. Additional clean air was also directed into the bag for a controlled amount of time until the concentration of NH_3 in the bag reached the desired level. The target NH_3 gas concentration was prepared by manipulating the ratio of time of NH_3 gas injection to air injection. An alternative NH_3 bag was prepared by injecting 5 µl of ammonium hydroxide in a 1 L Tedlar^{TM} bag and left in ambient room temperature for 30 minutes to validate the calibration curve for the sensors (respective results shown in

Table 2-2).

Urine headspace bags

A test sample of urine was preconditioned by adding NaOH to a sample of urine, to ensure that the pH of the sample was greater than 12. The preconditioned urine sample was subsequently added to a 4 L Tedlar^{TM} bag and purged with dry air until the bag was full. The Tedlar^{TM} bag was left at ambient room temperature to ensure gas equilibration. This means that all of the NH_4^+ in the urine reacted with the base and turned into its conjugated phase NH_3 in urine headspace. Subjects of this part of the study were approved by the Institutional Review Board of Arizona State University (IRB protocol # 1012005855). Five test subjects participated voluntarily, providing written consent to participate in the study. Three of the subjects are males and the rest are females. All subjects are healthy adults aging between 21 to 27. All tests for this study were conducted from February 2016 - January 2018. The subjects had a small meal (Lean Cuisine), and drank a Whey Protein (GNC Holding Inc., PA or US Nutrition Inc., NY) shake with concentrations of protein ranging from 0 to 1.2 g of protein per Kg of body mass to produce a variable and wide range of urine total ammonia. The subjects urinated periodically at 0, 0.5, 2.5, and 3.5 hours from the intake. Urine samples were collected and analyzed as soon as possible, using ISE method and the CODA.

2.2.4. Sensor Detection Procedure

The sensitivity, reversibility, and reusability of the sensors were tested using an NH_3 flow system, which contains a micro diaphragm gas pump, a three-way valve, one 40 L

air bag, one 40 L sample bag, and the sensing chamber. Tests were conducted by placing one sensor in the sensing chamber each time. The three-way valve was first switched to connect with the air bag for a few seconds so that the sensor could be purged in air before it was exposed to the sample for a few seconds. In order to study the sensitivity of the sensor for different sample exposure times, sampling times varied from 1, 5, 20 and 180 seconds. After exposure to NH_3, the valve was switched to allow dry air to pass through the system for a few seconds to test the sensor substrates' reversibility.

2.2.5. Preconditioning Column for Automatic Sampling

An automatic sensing system is designed to facilitate the inpatient setup. In order to do so, a pre-conditioning column is designed to automatically extract the ammonium (NH_4^+) to ammonia (NH_3). The extraction column (Figure 2-2) has a cylinder-like structure with beads coated with Hydroxide (OrOH) inside. At the top of the column there are two tubes. One is for inlet and the other is for outlet. The setup allows the liquid sample to go through these beads and elevate the pH level to above 11. Thymolphthalein was used as an indicator to visually determine when the pH level is over 10.5 (The indicator develops a blue color at this pH from colorlessness). The sample can be injected to the column through the middle of cylinder-like structure. Simulation were done the estimate the lifespan for the extraction column.

Figure 2-2. The actual look of the extraction column.

The extraction column was packed with beads coated with OrOH of different diameters (d) into a porous structure with porosity, ε_p. The permeability (κ) of the system for a given porosity and particle size was estimated by Carman-Kozeny relation [90].

$$\kappa = \alpha \frac{d^2 {\varepsilon_p}^3}{(1-\varepsilon_p)^2} \qquad \text{Equation 2-3}$$

The α was calculated as 1/36K, where K is a constant for fixed beds, which is 5 [91]. Brinkman equation given by:

$$\frac{\rho}{\varepsilon_p}\frac{\partial u}{\partial t} + \nabla \cdot \left[-\frac{\eta}{\varepsilon_p}(\nabla u + (\nabla u)^T) + pI\right] + F = -\frac{\eta}{\kappa}u \quad \text{Equation 2-4}$$

$$\nabla \cdot u = 0 \quad \text{Equation 2-5}$$

were used to model the flow of urine through this medium, where ρ denotes the density of urine (1000 kg m^{-3}), u represents the velocity, p refers to pressure, F related to other forces (e.g. gravity). Equation 2-5 above implies that the fluid flow is incompressible in the domain. Boundary conditions for the flow were set as follows: Boundary 1: u .n = u_0 (inlet), where u_0 is the linear flow velocity at the inlet; Boundary 2 and Boundary 3 : u = 0 (wall); Boundary 4: p = 0 (outlet). With these domain and boundary settings, the velocity field was determined and the solution obtained was further used to solve the mass transport process using COMSOL 5.0 [92].

Mass transport of water with the tube was described by the diffusion-convection equations

$$\frac{\partial C}{\partial t} + \nabla \cdot (D_i \nabla C_i + C_i \mathrm{u}) = R \quad \text{Equation 2-6}$$

where C_i denotes the concentration of the species, D is the diffusion coefficient, u represents the velocity, and R refers to the rate of consumption of species i. These equations were applied to the two components of the extraction process, where species 1 is the stationary hydroxide fixed beds, beads coated with OrOH, and species 2 is the ammonium (NH_4^+) entering the column and species 2. The OrOH reacts with NH_4^+ and produce gas-phase ammonia. The diffusion coefficient is set to $2*10^{-9}$ (m^2 s^{-1}) as a

standard diffusion coefficient for water solution. As the column is short and the inlet velocity is fast, the convection effect was assumed to dominate over diffusion. The rate of consumption, R, was assumed to be the chemical reaction described as the following:

$$NH_4^+{}_{(aq)} + Cl^-{}_{(aq)} + OrOH \rightarrow NH_{3(g)} + H_2O_{(l)} + OrCl \qquad \text{Equation 2-7}$$

, which could be simplified as the following:

$$NH_4^+{}_{(aq)} + OH^-{}_{(aq)} \rightarrow NH_{3\,(g)} + H_2O_{(aq)} \qquad \text{Equation 2-8}$$

The reaction rate is given by:

$$R = -kC_1C_2 = -k_0C_2 \qquad \text{Equation 2-9}$$

, where k is the rate constant, C_1 is the concentration of OH^- and C_2 is the concentration of NH_4^+. The initial concentration of OH^- is 1706 mol m^{-3}. The concentration of the binding OH^- is estimated experimentally by coating known amount of OrOH to the beads. The OH^- has an excess amount compared to NH_4^+ in the liquid solution, so C_1 was assumed to be constant, which makes $kC_1 = k_0$. As the reaction of $NH4^+$ and OH^- is an acid-base reaction, the reaction finished in pico-second [93]. Therefore, the k_0 was assumed to be an extremely large number, which was set to 170.6 (s^{-1}), to be numerically calculable. Moreover, this reaction is a reversible reaction, but has a tendency toward the

NH_3 side. With the excess amount of OH^-, the reaction was assumed to be a complete conversion, which also ensured the pH value is over 10.5.

In this work, the control variables are the initial concentration of inlet NH_4^+ solution, the porosity and inlet velocity. We also work beyond these parameters to see how the geometry of the column affects the depletion of stationary hydroxide (OH^-). Experiments were done by using different concentrations NH_4Cl as the samples to verify the modeling results. Table 2-1 shows the denotations and the parameters used in the modeling.

Table 2-1. Denotation

Symbol	Meaning	Parameters
p	Pressure	(atm)
u	Velocity	(m s^{-1})
ρ	Density	1000 (kg m^{-3})
p_0	Outlet pressure	(atm)
u_0	Inlet velocity	0.0035, 0.05, and 0.5 (m s^{-1})
F	Gravity force	1 (N)
α	Kozeny constant	0.0056
d	Diameter of the beads	2 (mm)
k	Rate constant	0.1 (m^3 s^{-1} mol^{-1})
k_0	Rate constant	170.6 (s^{-1})
C_1	Concn. of OH^- on binding sites	(mol m^{-3})
C_2	Concn. of NH_4^+	(mol m^{-3})
D	Diffusion coefficient	2*10^{-9} (m^2 s^{-1})
ε_p	Porosity	0.34, 0.66 and 0.90

2.3. Results and Discussion

2.3.1. Choice of the CODA Wavelength

The color of the light source for the CODA was selected based on the spectral changes NH_3 exposure induced on the sensing probe (BpB). Round sensors made of Whatman no. 1 filter paper impregnated with BpB were placed in the sensing chamber of the JS

instrument, and the spectrum of each sensor was recorded before and after exposure to NH_3. Figure 2-1e shows visible spectrophotometric changes of a BpB-based sensor, and significant increases of absorbance in the range of 575 - 625 nm are clearly observed. Based on these results, the LED color was chosen to be red, wavelength: 610 nm. Once the detection wavelength and the first screening of sensor substrate were chosen, the CODA was constructed and used to proceed with the rest of the study.

2.3.2. Reproducibility of Sensor Response

Figure 2-3 compares the absorbance response of sensors in the CODA. Four replicate sensors were made and placed in the CODA. Next, the sensors were exposed to NH_3 for 180 seconds followed by dry air for additional 60 seconds to determine recovery. The sensors show similar response characteristics with rising absorbance upon the injection of NH_3, and decreasing absorbance upon purging with dry air. The sensor responses included 0.58 a.u. with a standard deviation of 0.03 a.u. for measurements performed in multiple sensors from a same batch and a response dispersion across sensor substrates of 5% or less.

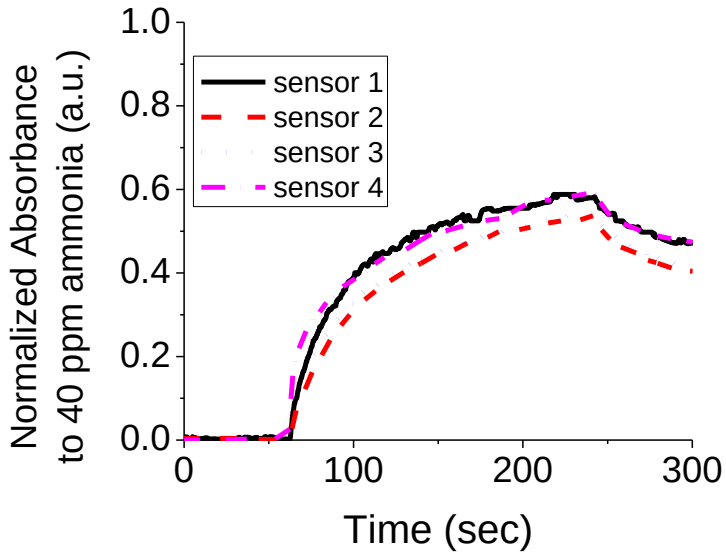

Figure 2-3. The reproducibility of the sensors was determined using four different sensors to detect 40 ppm of ammonia (NH_3) through the CODA. The sensors show similar absorbance response.

2.3.3. Sensor Calibration to Ammonia

Two calibration curves were developed for the NH_3 sensors with the CODA, using 5 second sampling times with NH_3 gas levels ranging from 2 ppm to 1000 ppm. In one case, a Langmuir model [94] was applied (Figure 2-4a), and exhibited a R^2 value greater than 0.99. For the 5 second sampling times, the calibration equation is as follows, where A^L represents the absorbance derived from Langmuir model and C represents the corresponding concentration:

$$A^L = 1.85\ C / (1122.28 + C) \quad \text{Equation 2-10}$$

We name “Langmuir-like” to the equation describing the sensor response vs. concentration because: (1) The ammonia/ammonium molecules have no-null interactions that may take the adsorption behavior apart from the purely described “Langmuir” behavior [95], and (2) there is a chemical reaction coupled to the adsorption process of ammonia onto the substrate with the sensing probe.

In the other case, the calibration curve was divided into two ranges for fitting linear regressions: 2 – 150 ppm and 150 - 1000 ppm. Both measurement ranges showed R^2 values greater than 0.98 (Figure 2-4b). The calibration equations are as follows, where A^1 represents the absorbance derived from linear model from 0 – 150 ppm, A^2 represents the absorbance derived from linear model from 150 – 1000 ppm, and C represents the corresponding concentration:

$$A^1 = 0.00131\,C + 0.01027 \quad for \quad 0\,ppm < C \leq 150\,ppm \qquad \text{Equation 2-11}$$

$$A^2 = 0.0007\,C + 0.19445 \quad for \quad 150\,ppm \leq C \leq 1000\,ppm \qquad \text{Equation 2-12}$$

(a)

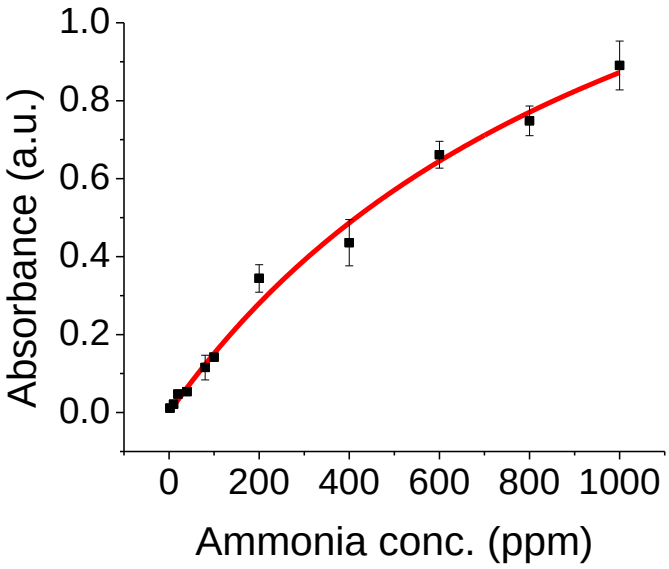

(b)

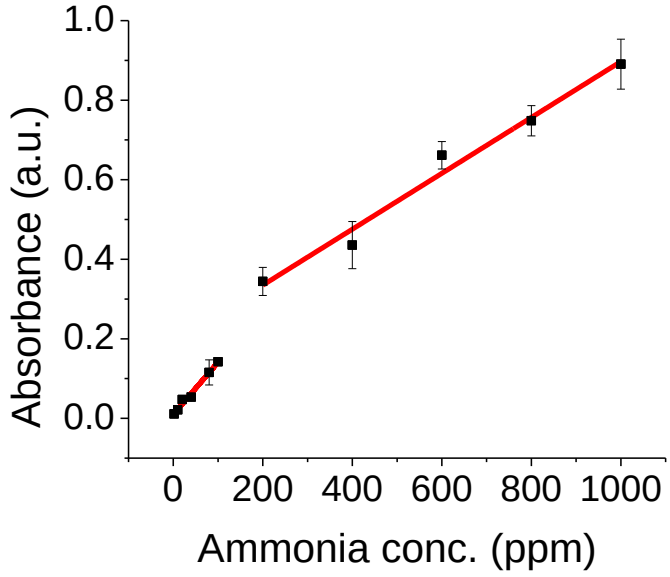

Figure 2-4. Calibration curves were developed by measuring 2 ppm to 1000 ppm of ammonia (NH_3) with CODA in 5 seconds. (a) Langmuir model was also used to fit the entire NH_3 concentration range measurement with an R^2 equal to 0.99. (b) A linear fitting was used to fit the lower-range concentration measurements (2-100 ppm) with an R^2 equal to 0.98 and another linear fitting was used to fit higher range concentration measurements (200-1000 ppm) with an R^2 equal to 0.99.

In a different set of fittings, linear regressions for absorbance changes assessed at 1 second exposure of NH_3 were also obtained, and compared to those obtained at 5 second exposure of NH_3. These regressions were used to test an unknown sample concentration, resulting from a mixture of ammonium hydroxide and air inside a bag.

Table 2-2 shows the results assessed for the unknown concentration sample by the sensor, using a 1- and 5- second sample exposure, and the corresponding calibration curves. Both calibration curves (from the 1-second and 5-second exposure data), yielded the same concentration of the prepared NH_3 bag of unknown concentration, indicating self-consistency of the calibrations. Additionally, these results indicate consistency between each pair of photodiodes (PD1 (sensing) / PD3 (reference) shown as PD1 and PD2 (sensing) / PD4 (reference) shown as PD2) in the system, as both pair of photodiodes yielded the same response.

Table 2-2. Ammonia concentration (ppm) output from calibrations performed with 1-sec and 5-sec sampling times in the NH_3 sensors

	1 sec PD1[1]	1 sec PD2[2]	5 sec PD1[3]	5 sec PD2[4]
Run 1	868	875	956	932
Run 2	980	1035	919	914
Run 3	1018	998	1021	968
Mean	955	970	966	938
Std. Dev.	64	68	42	23

[1-2] Recovered with 1-second calibration curve from Photodiode 1, and Photodiode 2, respectively
[3-4] Recovered with 5-second calibration curve from Photodiode 1, and Photodiode 2, respectively

2.3.4. Sensor Selectivity to Ammonia

To confirm the sensor is only selective to NH_3, the sensor was exposed to several interferents (e.g., acetone, 2-butanone, and methylene chloride) reported to exist in urine headspace [29]. Figure 2-5 shows the selectivity of the sensor to NH_3. Even with relatively high concentration of interferents (e.g. 100 ppm acetone), the sensor only showed a significant response to NH_3. This test confirmed the selectivity of the sensor in the harsh environment of the urine headspace sample.

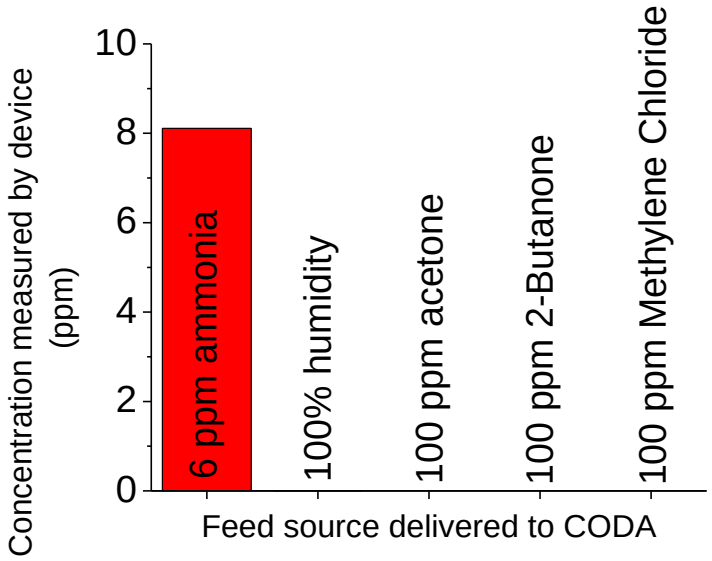

Figure 2-5. The concentration of several compounds existing in urine headspace was measured with the CODA in this work. The NH_3 sensor only shows response to ammonia.

2.3.5. Sensor Reversibility and Reusability

A healthy adult may urinate every 2-3 hours (8-9 times per day) [96]. Current methods to quantify NH_4^+ in urine for clinical medicine require the patient to collect all excreted urine for 24 hours. There is no clinically used method for instantaneous urine NH_3 measurement. Figure 2-6a shows the absorbance response of the PTFE-based sensor to alternating exposure to 100 ppm of NH_3 and dry air repeatedly over 1.2 hours. The sensor was continuously exposed to a repeating cycle of NH_3 for 5 seconds followed by dry air for 120 seconds. The sensor was re-used for over 60 detection cycles without degradation in performance. For practical, clinical application one 5-second ammonia measurement could be taken every 24 minutes to cover 24 hours of monitoring, although much more frequent testing is also possible. Figure 2-6b shows the measured concentrations from the

continuous test after signal analysis, and use of calibration equations. It is important to note that the sensor required a conditioning period of 5-7 exposures. After this conditioning period, the concentration output remained fairly constant throughout the multiple exposures to NH_3 and detection events of the same concentration. The detection concentration error was lower than 20%, and could be further improved with a better enclosure of the CODA, which will preclude from ambient light interference.

(a)

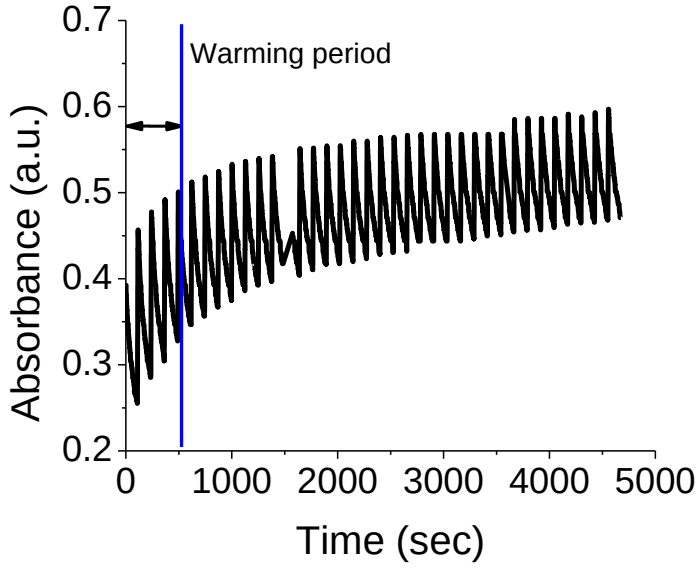

(b)

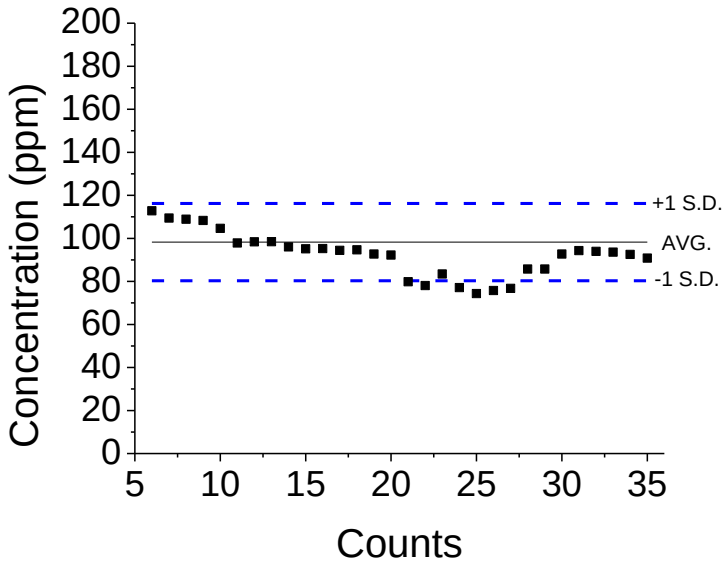

Figure 2-6. (a) The reusability of a sensor was determined by exposing 100 ppm of ammonia to a sensor for 5 seconds and then to dry air for 2 minutes for each measurement. (b) 35 measurements were conducted in 1.2 hours before the sensor saturated. About 80% of the measurements were within ±1 standard deviation.

2.3.6. Evaluation of Ion Selective Electrodes as Reference Method

In this work, an ion selective electrode (ISE) (Ammonia High Performance Ion Selective Electrode) from Thermo Fisher Scientific was used as a reference method for total ammonia (NH_3 + NH_4^+) detection. The ISE was chosen due to the relatively inexpensive cost per sample compared with Gold Standard Methods, which are based on enzymatic methods. In addition, ISE enabled the processing of near real-time real urine samples, and the evaluation of results under conditions that were more compatible with the ISE, the intended use of the CODA. In order to evaluate the accuracy of ISE, the Gold Standard Method from Biovision [97] was used. The method is based on enzymatic reactions, and enables accurate detection of total ammonia expressed as NH_4^+ levels. In

the assay, NH_3 or NH_4^+ is converted to a product that reacts with an enzyme and redox probe to generate color (at Optical Density, OD of 570 nm, which can be easily quantified by a plate reader. The kit can detect 1 nmol (~20 μM) of NH_3 or NH_4^+ [97]. A linear regression of the averaged data for 3 samples at each concentration is shown in Figure 2-7a, and was in agreement with the manufacturer specifications. The curve was used to assess total ammonia levels from urine, which were also determined by ISE. Figure 2-7b shows the averaged results of urine samples analyzed with the Gold Standard Method (enzymatic) and ISE. The ISE method had an error smaller than 1% when compared with Gold Standard Method, therefore, the ISE method was established as reference method.

(a)

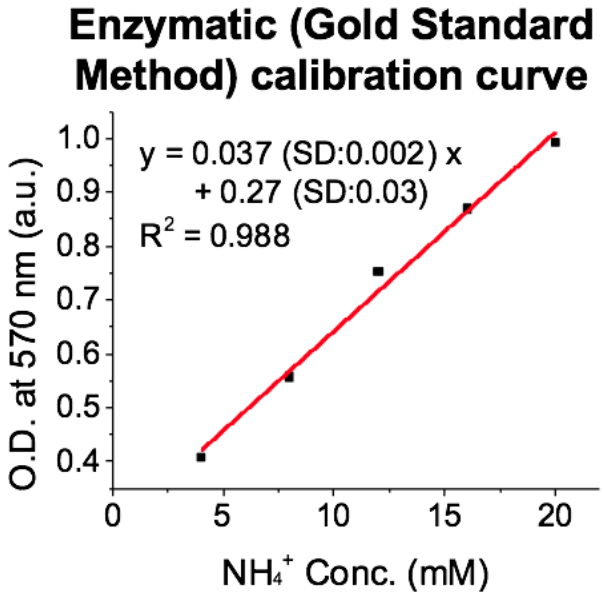

(b)

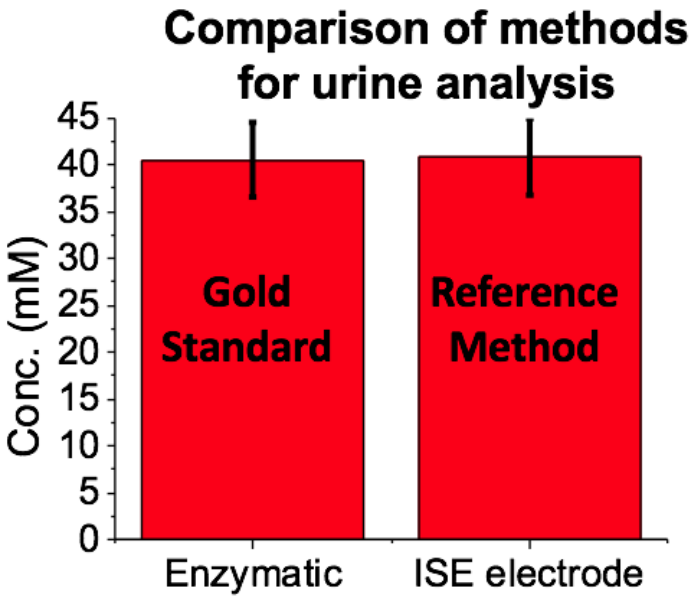

Figure 2-7. Evaluation of accuracy of the reference method, ISE. (a) The evaluation was performed with the gold standard method based on enzymatic reactions from Biovision. The calibration curve of the Biovision method is shown and was used to extract the

ammonia levels that were compared to the total ammonia level assessed from the ISE. (b) Averaged urine levels of 40.5 mM from Biovision test compared to averaged urine total ammonia levels of 40.9 mM from ISE, showing ISE method with an error smaller than 1%.

2.3.7. Sensor Use with Urine Samples

To confirm the feasibility of the CODA and its use of the sensor in real conditions, a urine sample analysis was performed and measurements were recorded from a calibrated batch of sensors, and results were compared with those assessed from the ISE method. Subjects were first asked to urinate and then to eat a small meal and drink a protein shake as described in the experimental section. Next, the samples were measured by the ISE electrode and afterwards measured with the CODA. Figure 2-8a presents an example of the measurements from one subject, which had protein shake with 1 g of protein per kg of body mass. A similar result can also be found in literature using SIFT-MS [98]. Figure 2-8b shows a correlation plot of results assessed from 5 subjects that had a wide range of protein concentration intake (details shown in experimental section), and urine samples were collected and analyzed with ISE (first) and CODA (second). A total of 20 samples (4 samples per subject) were processed. A good agreement between the measurement with CODA and ISE electrode was found with a regression coefficient > 0.9. However, the slope of the correlation showed smaller values assessed from CODA with respect to ISE method. This was due to an inadequate urine storage performed for some of the collected samples, as well as sample pH. It was observed the higher the pH of the urine sample, the more critical was the timing between collection and analysis due to the loss of NH_3 as a gas. This fact remarked the importance of the implementation of a true

continuous sample collection and analysis system. In this regards, the team is making progress that hope to report in a follow up publication.

Despite the detected problem, analysis of Receiver Operating Curve (ROC) for the assessed results was performed. Figure 2-8c shows the analysis of the analytical performance of CODA, with a ROC, using ISE method to determine True diagnostic ability as its discrimination threshold varied from 5, 10, 15, 20, 30, 40 mM NH_4^+ (read total ammonia levels). The concentration range covers the normal ammonia total level in urine. Rapid change of total ammonia level in urine could therefore be captured as an early warning for *acid-base and/or potassium disturbances.* As it can be observed, the overall accuracy of the method was 92%, which is a satisfactory result.

Table *2-3* shows comparative features of the traditional methods used for total ammonia detection in connection to the newly proposed method based on CODA. The setup discussed in this work requires two manual steps: (1) the preparation of preconditioned urine to produce ammonia and (2) the switching the valve to control the sensing time. The team is developing an automatic system that has a preconditioning membrane and electronic valves allowing the omission of these steps. Challenges are that the membrane needs to work for at least 24 hours to meet the need of medical applications. . The ultimate goal is to apply CODA as a diagnostic device. With the planned changes accuracy could be improved over 92%.

Table 2-3. Comparative table of methods for total ammonia detection.

Method	Enzymatic (Gold Standard)	ISE (Reference Method)	CODA
Accuracy error		>99% compared with Gold Standard	92% compared to Reference Method
Time per sample	60+ min	< 5 min	< 2 min*
Cost per sample	$ 5+	< $0.35	< $0.03

* as envisioned with automated sampling

(a)

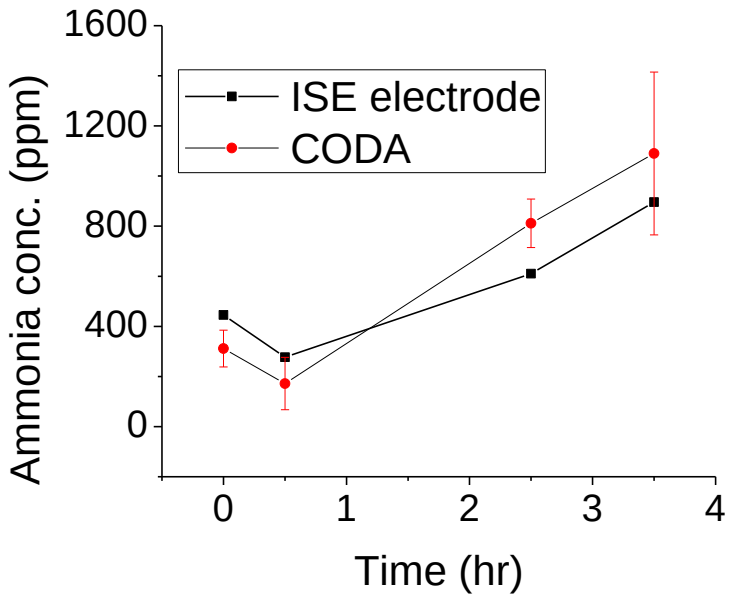

(b)

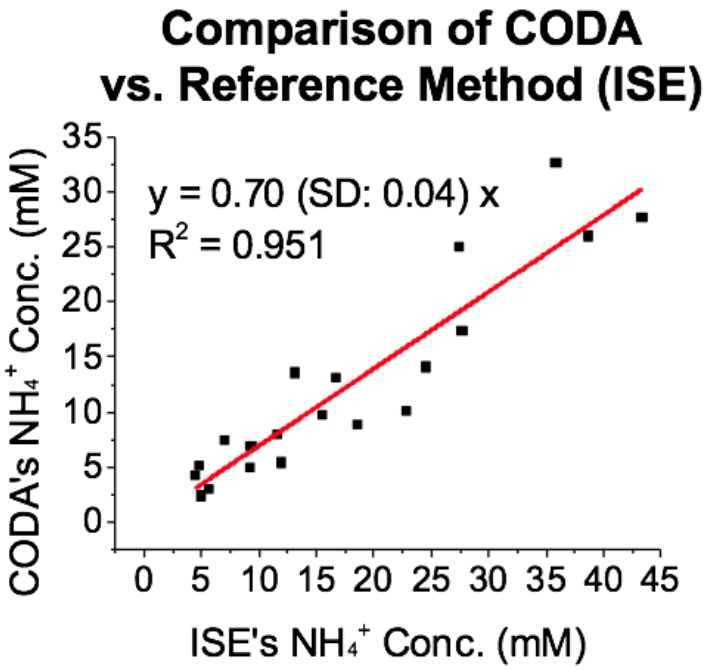

(c)

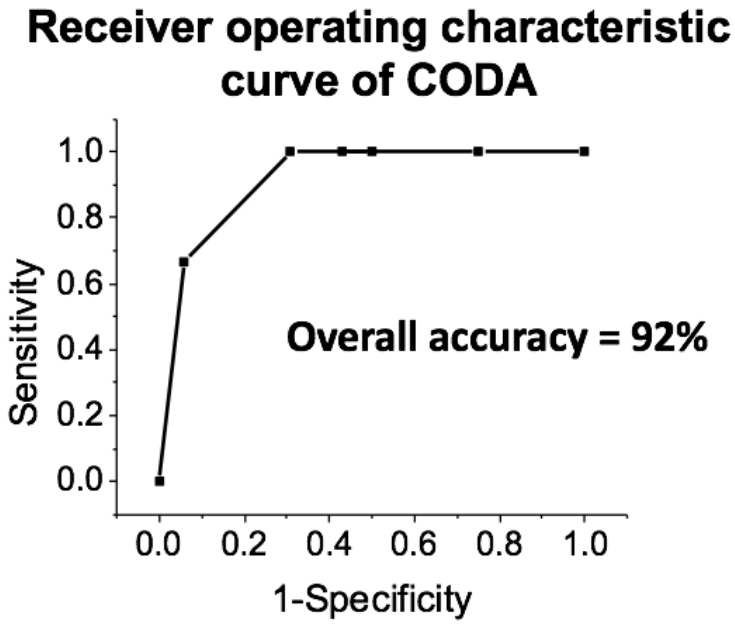

Figure 2-8. (a) Measurements of ammonia in urine headspace collected with the CODA and an ISE electrode for 3.5 hrs after the subject drank a protein shake. Both devices

show ammonia concentration levels dropped 0.5 hr after drinking the protein shake but continued to rise until the experiment ended. (b) The accuracy of the CODA was determined by systematically comparing its measurement to an ammonia ISE electrode (reference method). The measurement of the CODA was converted to NH_4^+ level in liquid solution for clinical practical use by Medical Professionals. (c) Analytical performance of CODA: Receiver operating characteristic (ROC), using ISE method to determine True diagnostic ability as its discrimination threshold varied from 5, 10, 15, 20, 30, 40 mM NH_4^+ (read total ammonia levels).

2.3.8. Pre-conditioning Column for Continuous Measuring

Reusability

The concentration of the incoming NH_4^+ does not affect the concentration profile of the stationary hydroxide (OH^-) site in the concentration range of NH_4^+ that is typically encountered in urine samples (3.6 –100.0 mM). The concentration of OH^- is primarily affected by the inlet velocity (Discussed in Section: *Variables: boundary conditions – inlet velocity u_0* later). In this model, the concentration of OH^- was set to a certain level to determine how many times this column could be used before the OH^- is depleted. It has been determined experimentally that each injection takes 0.8 seconds to reach the target amount of the sample (200 ul). The concentration of NH_4^+, the inlet velocity, and the porosity were set to values of 37.8 mM, 0.05 m s^{-1} and 0.34, respectively. Figure 2-9 shows the concentration profile at the (a) 1^{st}, (b) 10^{th}, and (c) 20^{th} injection, with the bluish portion representing the full consumption of the OH^- within the column, which we denote that the pH of the sample is over 10.5 for the sample as we assume the consumption of the OH^- results in alkalization of the sample. The result shows that at the end of the 20^{th} measurement almost all of the OH^- in the column's midsection has been depleted, which leads to the conclusion that after the 20^{th} cycle, there is no more OH^- able to alkalinize the sample. Therefore, we couldn't ensure the sample's pH is still over 10.5.

(a) (b) (c)

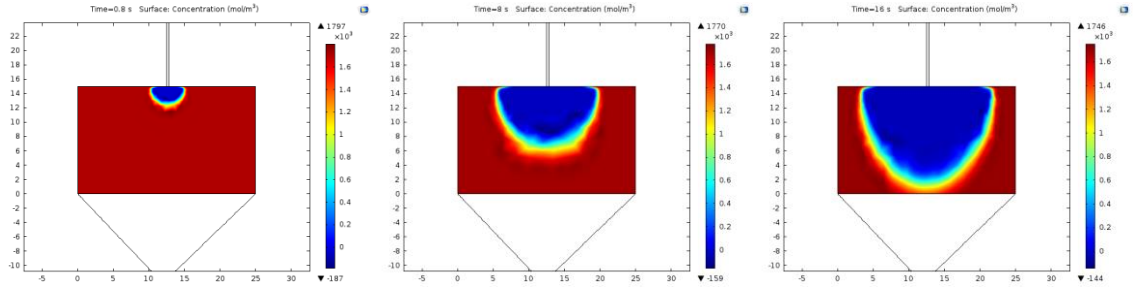

Figure 2-9. The concentration of NH_4^+, the inlet velocity and the porosity were set to values of 37.8 mM, 0.05 m s^{-1} and 0.34, respectively. The result shown here is concentration profile for the (a) 1th, (b) 10th, and 20th measurement.

Variables: Porosity

The porosity of the extraction column was estimated based on ratio of the beads' volume to the cylinder. The target column is a cylinder with the diameter of 2.5 cm and height of 1.5 cm. The volume ratio occupied by the Styrofoam beads was derived by estimating the number of beads in a single layer, the number of layers in the cylinder, and the average diameter (0.2 cm) of the beads. The concentration of NH_4^+ and the inlet velocity were set to values of 37.8 mM and 0.05 m s^{-1}, respectively. Figure 2-10 shows the concentration profile at the 20th cycle as the porosity is set to values of (a) 0.34, (b) 0.66 and (c) 0.90 to better understand its effect on the stationary hydroxide (OH^-) concentration profile. When the porosity is high the OH^- depletes slightly faster.

(a) (b) (c)

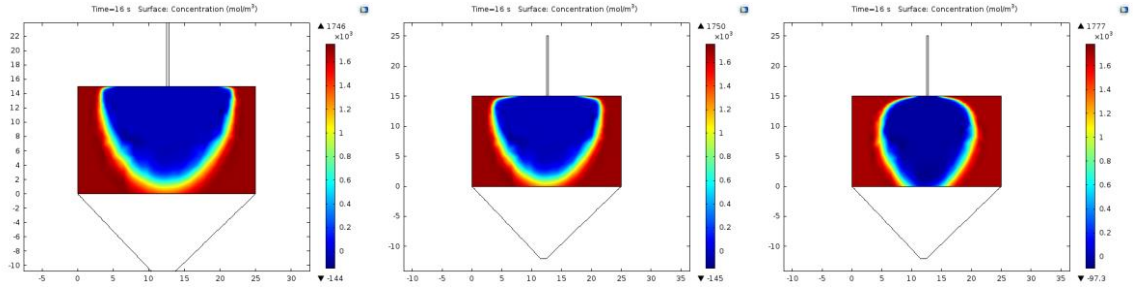

Figure 2-10. The concentration of NH_4^+ and the inlet velocity were set to values of 37.8 mM and 0.05 m s^{-1}, respectively. The result shown here is the 20th measurement with porosity of: (a) 0.34, (b) 0.66, and (c) 0.90.

Variables: Boundary conditions – inlet velocity u_0

The boundary condition was estimated based on the real experiment, depending on the setup. In our extraction column, the inlet velocity was determined based on the average velocity that the water droplet reached the column, which was 0.05 m s^{-1}. Low (0.0035 m s^{-1}) and high velocities (0.5 m s^{-1}) were used to better understand the effect of the inlet velocity on the concentration profile within the column. Figure 2-2 shows the concentration profile at the 20th cycle under different inlet velocity: (a) 0.0035, (b) 0.05 and (c) 0.5 m s^{-1}. The concentration of $NH4^+$ and the porosity are set to the valued of 37.8 mM and 0.34, respectively. The model clearly shows that the inlet velocity dominates the effect to the stationary hydroxide (OH^-) concentration over porosity.

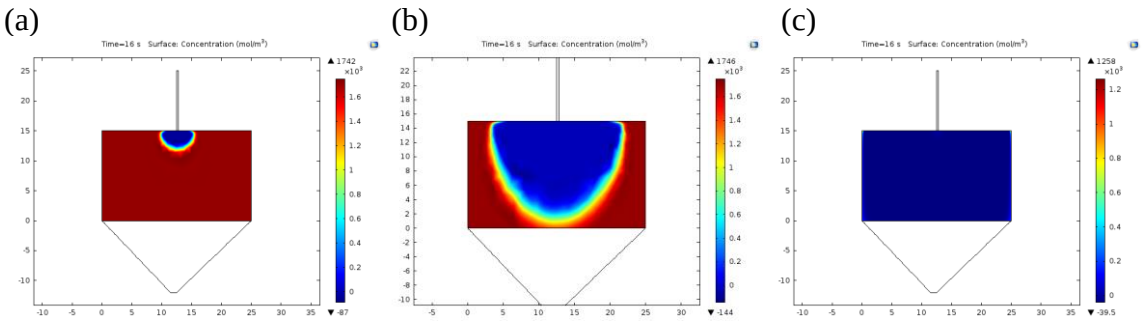

Figure 2-11. The concentration of $NH4^+$ and the porosity are set to the values of 37.8 mM and 0.34. The result shown here is the 20th measurement with inlet velocity of: (a) 0.0035 m s^{-1}, (b) 0.05 m s^{-1}, and (c) 0.5 m s^{-1}.

Variables: The initial NH_4^+ concentration of the samples

Most urine samples have initial concentrations ranging from 3.6 to 100.0 mM. Within this range there is not much difference between the OH^- concentration profiles after the 20th measurement because the reaction is an acid-base reaction, which occurs immediately after the NH_4^+ from the sample makes contact with the OH^- within the column. Since the OH^- is in excess with respect to the incoming $NH4^+$, the $NH4^+$ is totally converted to NH_3, which is released as a gas. The depletion is mainly caused by the fluid going through extraction column, which is described in previous section (Section: *Variables: boundary conditions – inlet velocity u_0*). Figure 2-12 shows the result of the concentration profile after the 20th cycle with a range of initial NH_4^+ concentrations (37.8, 100.0 and 3780.0 mM). The inlet velocity of the sample and the porosity was set to the values of 0.05 m s^{-1} and 0.34, respectively. The results show that only under extremely high concentrations (3780.0 mM) of NH_4^+ the concentration profile of OH^- changes. The OH^- depletes more quickly for samples with a high initial concentration NH_4^+.

(a) (b) (c)

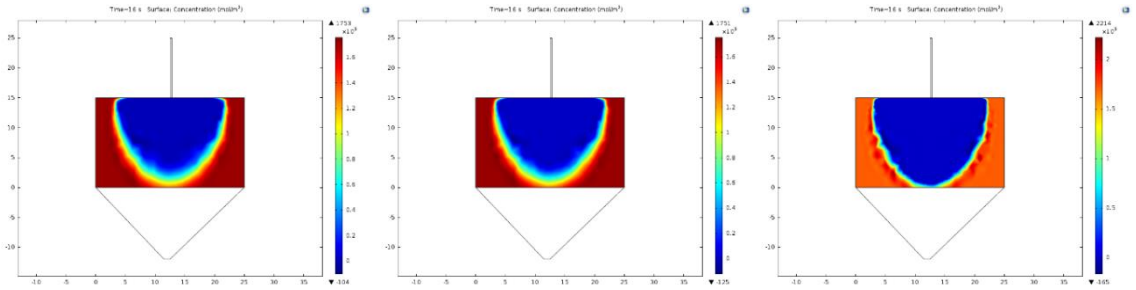

Figure 2-12. The inlet velocity of the sample and the porosity was set to the values of 0.05 m s^{-1} and 0.34, respectively. The result shown here is the 20th measurement with NH_4^+ concentrations of: (a) 37.8 mM, (b) 100.0 mM, and (c) 3780.0 mM.

Variables: Geometry

A model was created determine the effect of the column's geometry on its depletion rate. Changing the geometry will as well change the amount of packed bed (beads), but the binding OH^- remains the same. Two different column lengths (1.5 cm and 3 cm) were tested with all other parameters were kept constant. The concentration of NH_4^+ and the porosity were set to the values of 37.8 mM and 0.34, respectively. Figure 2-13a and Figure 2-13b show the concentration profiles corresponding to the two configurations. Doubling the length of column increases the columns lifespan from 20 to 55 cycles. Doubling the length also allows more efficient use of the column. The OH^- closer to the wall is mostly depleted in comparison with other cases. Figure 2-13c shows the concentration profile with a thinner width configuration (2.0 cm in diameter) that shortened the lifespan of the column from 20 cycles to 17 cycles.

(a) (b) (c)

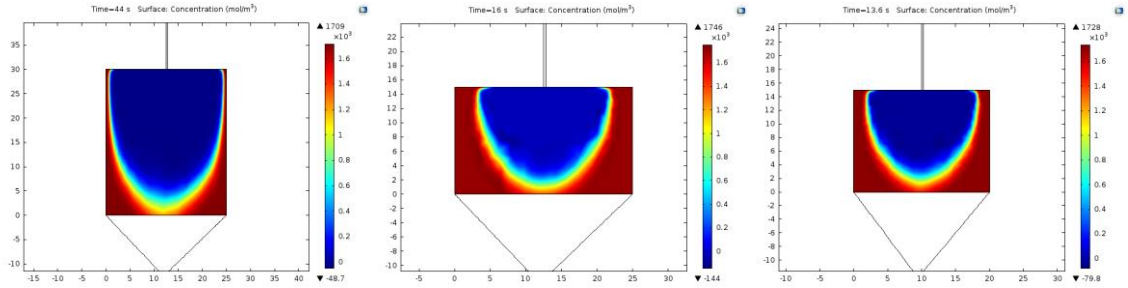

Figure 2-13. The concentration of NH_4^+ and the porosity were set to the values of 37.8 mM and 0.34, respectively. The result shows the concentration profile how the hydroxide (OH^-) is depleted with the configuration of: (a) 3 cm in length and 2.5 cm in diameter, (b) 1.5 cm in length and 2.5 cm in diameter, and (c) 1.5 cm in length and 2.0 cm in diameter.

Model verification

An experiment was performed where NH_4Cl was introduced to the column several times in the following sequence: 8 cycles of 37.8 mM, 5 cycles of 18.6 mM, and 5 cycles of 3.6 mM; 20 measurement cycles in total. Figure 2-14a and Figure *2-14*b show the cross-sectional concentration profiles of the top layer of the extraction column based on modeling. Thymolphthalein was used as an indicator to visually determine when the pH level is over 10.5 (The indicator develops a blue color at this pH). The Figure 2-14c shows the top layer of the extraction column before any sample is introduced and Figure 2-14d shows the same column after the 20th injection cycle. Figure 2-14d clearly shows almost no bluish color within the column, which indicates the sample's pH level is below 10.5.

(a) (b)

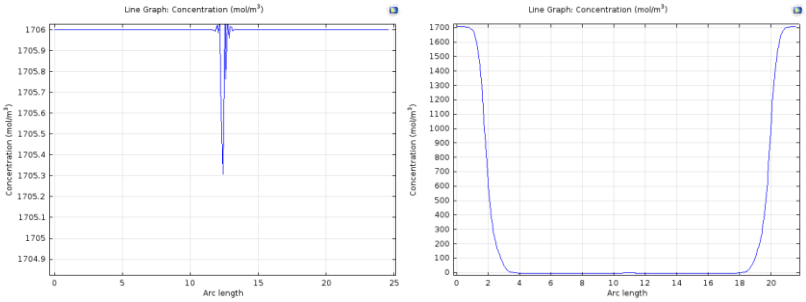

(c) (d)

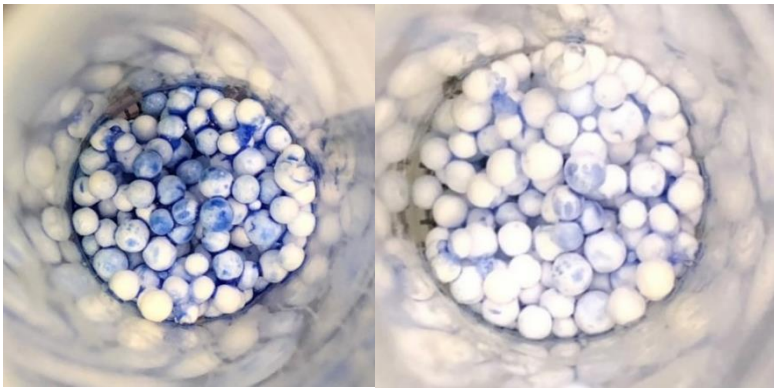

Figure 2-14. The modeling results of 20 cycles were shown for the before the cycle (a) and after the 20th cycle (b). As a comparison, the experimental result was compared by showing the pH of the column with color change on Thymolphthalein before the cycle (c) and at the 20th cycle (d).

2.4. Conclusion

The Colorimetric Optoelectronic Dynamics Analyzer (CODA) discussed provides specificity, fast-response and accurate measurements for NH_3 gas concentrations ranging from 2 ppm to 1000 ppm (corresponding to 0.1 mmol/L to 50 mmol/L of NH_4^+ in liquid). Comparing the current standards, CODA measures 30-time faster and allows much less labor work to do the measurement. The sensor is very selective to NH_3, especially considering the high amount of interferents in urine headspace. The sensor shows good

reusability in long sampling periods, enabling daily use for medical applications. CODA can accurately monitor the total ammonia level in urine, as evidenced by comparison to measurements from a commercial reference method (ISE electrode). The device connects wirelessly to smart devices, which provides flexibility for measurements for inpatient, outpatient, or personal health monitoring. As such, this sensor could potentially be a great asset to the medical community, providing a convenient alternative to the slow and bulky measurement techniques that are currently in widespread use.

Acknowledgments

Many thanks to: 1- Drs. Lenore Dai and Kyle Squires from the School of Engineering for Matter, Transport and Energy, and Ira A. Fulton Schools of Engineering, respectively for their support and the Entrepreneurial Professor Award to Dr. Forzani, 2- Drs. Francis Tsow and Devon Bridgeman for the assistance on device electronics, and Dr. NJ Tao, Director of the Center of Bioelectronics and Biosensors, Biodesign Institute, for his constant encouragement to this work.

Publications

1. Nai-Yuan Liu, Pinar Cay-Durgun, Tianmiao Lai, Mark Sprowls, Leslie Thomas, Mary Laura Lind and Erica Forzani, *A handheld, colorimetric optoelectronic dynamics analyzer (CODA) for measuring total ammonia of biological samples*, IEEE: Journal of Translational Engineering in Health and Medicine, 2018, 6 (1), pp 1-10

2. Pinar Cay-Durgun, Nai-Yuan Liu, Stephenie Brown, Leslie Thomas, Mary Laura Lind and Erica Forzani, Development of *An Extraction Membrane in A Handheld Analyzer for Non-invasive, Real-time Monitoring of Kidney and Liver Disorders*, 11th International Congress Membranes and Membrane Processes, San Francisco, CA, USA (2017)

3. Nai-Yuan Liu, Tianmiao Lai, Afsaneh Khosravi, Pinar Cay-Durgun, Mary Laura Lind, Erica Forzani and Leslie Thomas, *An Ammonia Sensor for a Handheld Analyzer for Non-Invasive, Real-Time Monitoring of Kidney and Liver Disorders*, AIChE annual meeting, San Francisco, CA, USA (2016)

CHAPTER 3

THE IMPROVEMENT OF AN EXITING MOBILE SENSING DEVICE FOR HEALTHCARE: A FLOW METER MODIFICATION IN A MOBILE INDIRECT CALORIMETER (MIC)

3.1. Background and Introduction

Resting metabolic rate (RMR), also known as resting energy expenditure is defined as the amount of energy expended by a person at rest.[99] and represents over 65% of total daily energy expenditure (TEE). Furthermore, RMR can represent 80-90 of TEE in sedentary people [100]. Therefore, evaluating an individual's RMR is important to help the assessment of daily caloric intake needs for weight management. The most common methods used to assess RMR is indirect calorimetry, which determines RMR based on the oxygen consumption rate (VO_2) and carbon dioxide production rate (VCO_2), via the Weir Equation [101]. Traditional indirect calorimetry instrument are metabolic carts, which are expensive, bulky and requires trained personnel for correct use. To get around with this, equations were created to estimate RMR that accounts for age, gender, weight and height [102]. However, it has been proved that the used of equations can render estimations that are 600-900 kcal/day from the true values assessed with indirect calorimetry measurement [103]

To overcome the above problem, a mobile indirect calorimeter was developed to facilitate personal use for RMR tracking [48, 104]. The device uses a differential-pressure based flow meter and a colorimetric-based chemical sensor to determine VO_2 and VCO_2. Breath is delivered into the sensing chamber, where the O_2 and CO_2 react with a sensor

chip, inducing color changes for determining exhalation O_2 and CO_2 concentrations. VO_2 and VCO_2 were calculated based on the breath O_2 and CO_2 concentrations, and breath flow rate. The performance of the device and colorimetric sensor have been validated by over 300 measurements against the Gold Standard, the Douglas bag method [104]. In addition, this mobile indirect calorimeter has been further used in human subjects to confirm functionality [105, 106].

In order to investigate an alternative to existing technology, we modified the commercial device to explore the utility of a new flow sensor for breath analysis.

Some commonly used flow meters are described as follows: (1) Fleisch-type meters use small capillary tubes to create laminar flow, which provide good linear relation, but they suffer from clogging and are hard to clean [107]. (2) Orifice-differential pressure sensor-based flow meters are simple, robust, and inexpensive, but they might offer high flow resistance [108]. (3) Variable-orifice flow meters provide less flow resistance by having an orifice size proportional to flow [109]. However, they are prone to wear out mechanically over time. (4) Pitot tube flow meters are inexpensive and have very low flow resistance, as their flow rate is proportional to the stagnation pressure. However, the sensitivity of this kind of tube is usually very low and is limited to low and steady flows [110]. While the field of flow meters has been well studied, flow measurement for breathing conditions with a wide range of flow rates has not been reported systematically, and it is important to investigate direct breath flow measurement due to special conditions such as temperatures above room temperature and possible condensation from humidity.

In this work, we used an orifice plate (diameter of 6.8 m) combined with a thermal flow

meter with the inlet and outlet located before and after the orifice plate for breath flow rate measurement. The thermal flow meter converted differential thermal energy change into flow rate [111]. Unlike other flow meters, a thermal flow meter enables to work at low flow resistances. Comparative study between this modified device and a metabolic cart was conducted to validate the performance of the new system.

3.2. Materials and Methods

3.2.1. The MIC from This Work

The MIC measured VO_2 and VCO_2 from breath and determined RMR according to the Weir Equation [26]. When breath O_2 and CO_2 flow through the sensor chip, they induced a color change on the sensor because of specific chemical reactions. The device had a light source and photodiodes to determine the absorbance change during the chemical reaction. The photodiodes transduced the absorbance of the sensor to a digital signal, which was wirelessly transmitted to a smart device for data processing. The absorbance was calculated by taking the negative logarithm of the signal response from the sensing area ($S_{sens.}$) divided by the signal response from the reference area ($S_{ref.}$) as follows:

$$Absorbance = -log(\frac{S_{sens.}}{S_{ref.}}) \qquad \text{Equation 3-1}$$

A built-in calibration curve converted the absorbance to corresponding fraction of exhaled O_2 concentration (FEO_2) and fraction of exhaled CO_2 concentration ($FECO_2$). As mentioned above, our new flow meter implemented into the device allowed the

measurement of the exhalation breath rate (V_E), which was used to calculate the oxygen consumption rate (VO_2), carbon dioxide production rate (VCO_2), and RMR through the following equations:

$$VO_2 = (0.2093 - 0.01 \cdot FEO_2) \cdot VE \qquad \text{Equation 3-2}$$

$$VCO_2 = (0.01 \cdot FECO_2 - 0.0003) \cdot VE \qquad \text{Equation 3-3}$$

$$\text{RMR}\left(\frac{kcal}{day}\right) = \left[3.941\left(VO_2\left(\frac{L}{min}\right)\right) + 1.11\left(VCO_2\left(\frac{L}{min}\right)\right)\right] * 1.440 \qquad \text{Equation 3-4}$$

(Weir Equation)

where FEO_2 is the breath O_2 concentration typically measured between 0.13 to 0.19 and $FECO_2$ is the breath CO_2 concentration typically measured between 0.03 and 0.06. The fraction concentration of O_2 in atmosphere is assumed to be 0.2093 and the CO_2 to be 0.0003 based on typical atmospheric condition [112]. Since the inhalation volume and exhalation volume are very close, we also assumed they were the same in the calculation. Lastly, a built-in fan dried the flow tube to avoid water condensation buildup between measurements.

3.2.2. The Flow Meter on This Work's MIC

The flow meter of the MIC, TFM, was an off-shelf electronic component obtained from

Omron® (part number: D6F-P0010A2 [113]). It was located with the inlet and outlet connected to the exhaled breath channel in the upstream and downstream portion at each side of the 6.8-mm orifice plate. The temperature output from a thermopile or thermistor in the TFM is based on its electrical voltage change, which was subsequently measured by the microcontroller analog-to-digital converter. The TFM utilized the transduction of energy change to voltage change to measure flow rate. Usually in a TFM, there are two thermistors in the flow tube: the reference thermistor measures the temperature of the incoming gas, which is called the reference temperature (T0), and the hot thermistor, which is driven by a current to raise its temperature (TR) to some fixed level above the temperature of the gas [111]. In still gas, the hot thermistor loses heat due to energy dissipation (both radiation and convection) to balance the electrical energy that heats the thermistor, stabilizing the hot thermistor's temperature. When the gas is flowing, the heat dissipation constant (K) of hot thermistor increases and TR decreases, resulting in an increase of the flow of current. The driving circuit senses the change in the current and raises the voltage (V) across the hot thermistor to maintain a fixed temperature difference between the reference thermistor and the hot thermistor, which is described by the following equation [114, 115].

$$V = \sqrt{KR[T_R - T_0]} \qquad \text{Equation 3-5}$$

where R is resistance.

Alternatively, two thermopiles (one upstream and the other downstream of the gas flow) and a heating element in between the thermopiles can be used. This approach can

simplify the required circuitry. When there is no gas flow, the temperature as measured by the two thermopiles is the same. As gas flows, the upstream temperature (T0) is expected to be lower than the downstream temperature (TR). The resulting temperature profile converted to voltages will allow gas flow rate to be determined. The TFM used in this project uses the thermopiles approach (Figure 3-1).

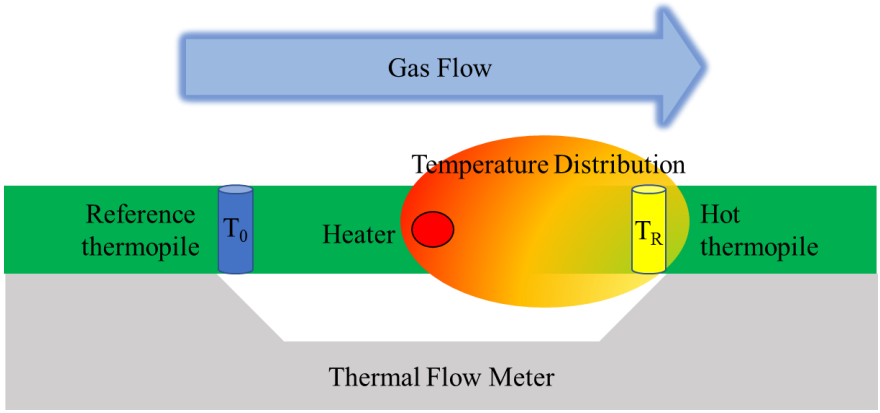

Figure 3-1. Schematic of a Thermal Flow Meter.

After placing the new TMF in the MIC, a calibration curve was built between the voltage and flow rate for a range from 20 L/min to 120 L/min, using dry air. The flow rate was integrated over time to assess the total volume which was used as criteria to determine the amount of breath to be used. The measurement of flow was set to be stopped when a total volume of 30L was collected. The reference flow used in the calibration was commercial flow sensor - Mass Flow Sensor SFM3000 from Sensirion.

3.2.3. Metabolic Cart Used as Reference Instrument

Metabolic carts are commonly used in hospitals to measure the individual's RMR. Here we used Medical Graphics (MG) Ultima™ Cardi® as a reference equipment. This

instrument provides RMR measurement based on breath-by-breath analysis, is FDA-cleared, and is typically used for assessments of patients' RMR or energy expenditure under exercise conditions at institutions such as Mayo Clinic. To validate the new MIC, 16 subjects were recruited (see details below) and measured by connecting the mouthpiece of the MG to the MIC in sequence with a T-joint, which only allowed exhalation breath to go through (Figure 3-2). Unlike the MIC, the MG only samples in average ~25% of the breath for breath O_2 and CO_2 measurement. Therefore, a factor of 1.25 was applied to the exhalation rate (V_E) measured by the MIC (accordingly to VO_2, VCO_2 and RMR) to compensate for the loss of the breath.

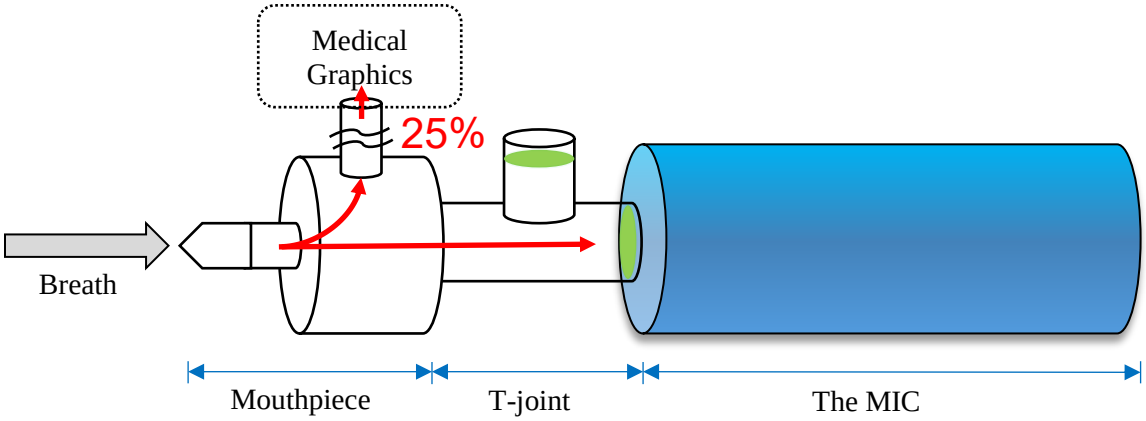

Figure 3-2. The schematic of sequence of how the MIC connected to the MG.

3.2.4. Subjects

Sixteen (16) healthy adults, including 9 males and 6 females, were included in the study. The number of subjects was chosen to discriminate average RMR of 1800 and 2000 kcal/day with standard deviation of 200 kcal/day (typical clinical variability) and to reach a power of 0.80 and alpha 0.05. The subjects' age ranged from 27-57 years and BMIs

ranged from 18-46 kg/m^2. The measurements of the resting metabolic rate were performed early in the morning following standard clinical protocol approved by the Institutional Review Board of Mayo Clinic (IRB protocol # 16-003321). The protocol required subjects to fast with no strenuous exercise for the last 12 hours, or no moderate exercise for 4 hours prior to the measurement. The subjects remained in a comfortable sitting position in a darkened room with room temperature at ~23 ^{o}C. The subjects were asked to rest for 30 minutes before the measurement and then to breathe normally through the setup (Figure 3-2) and during the measurement.

3.3. Results and Discussion

Based on experience from other studies[103, 105, 106], predicative RMR equations such as Mifflin - St. Jeor or Harris - Benedict are average population estimations based on the physical characteristics of the subjects (age, gender, height and weight), and do not necessarily represent actual measured RMR values. In the case of this study, similar conclusions have been found. Table. 1 shows the comparison between the RMR calculated by the Mifflin - St. Jeor Equation (MSJE) [116] and the RMR measured with our reference instrument, Medical Graphics (MG). As it can be observed, absolute differences ranging from 20% to 41% were observed for most of the subjects (11/16, ~68% of the subjects). These differences translated into energy expenditure assessments with differences between 300 and 880 kcal/day, which is a significant amount that could cause weight gain in someone targeting weight loss. For this reason, we believe that the only way to assess the true RMR of an individual is measuring it. Indirect calorimetry is the recommended method. Therefore, the goal of this paper is to compare the result

between a modified self-designed device with a solid well-established reference indirect calorimetry method.

Table 3-1. The comparison between the RMR calculated by the Mifflin - St. Jeor Equation (MSJE) and the RMR measured with Medical Graphics (MG).

Subject #	Weight (kg)	Height (cm)	Age (yr)	Gender	MSJE RMR (kcal/day)	MG RMR (kcal/day)	Difference: MG RMR -MSJE RMR (kcal/day)	Differential Percentage (MG RMR -MSJE RMR) / MG RMR (%)
1	68	170	46	F	1968	1758	-210	-11
2	85	190	27	M	2335	2547	211	9
3	60	163	27	F	1751	1997	246	14
4	84	189	27	M	2319	2983	664	29
5	61	164	27	F	1767	2315	548	31
6	66	161	59	F	1956	1150	-806	-41
7	111	180	47	M	2631	2133	-498	-19
8	48	161	50	F	1732	1366	-366	-21
9	83	176	58	M	2381	1694	-687	-29
10	150	183	57	M	3089	2261	-827	-27
11	66	161	54	F	1931	1218	-713	-37
12	102	182	52	M	2578	1700	-879	-34
13	102	159	45	F	2234	1706	-528	-24
14	101	175	56	M	2544	2510	-35	-1
15	78	186	57	M	2388	1808	-580	-24
16	110	186	57	M	2708	1983	-725	-27

*MSJE RMR = Resting metabolic rate calculated based on Mifflin St-Jeor Equation: For women: 10 x weight (kg) + 6.25 x height (cm) – 5 x age (y) – 161, For men: 10 x weight (kg) + 6.25 x height (cm) – 5 x age (y) + 5
*MG RMR = Resting metabolic rate measured by Medical Graphics

Figure 3-3 shows the calibration curve of the new MIC. Since the built-in calibration curve ranging from 0 – 120 L/min was not linear, it was divided into 7 linear segments (0 – 10, 10 – 20, 20 – 30, 30 – 40, 40 – 50, 50 – 90 and 90 – 120 L/min) to optimized the performance of the firmware of the device and reduce calculation time.

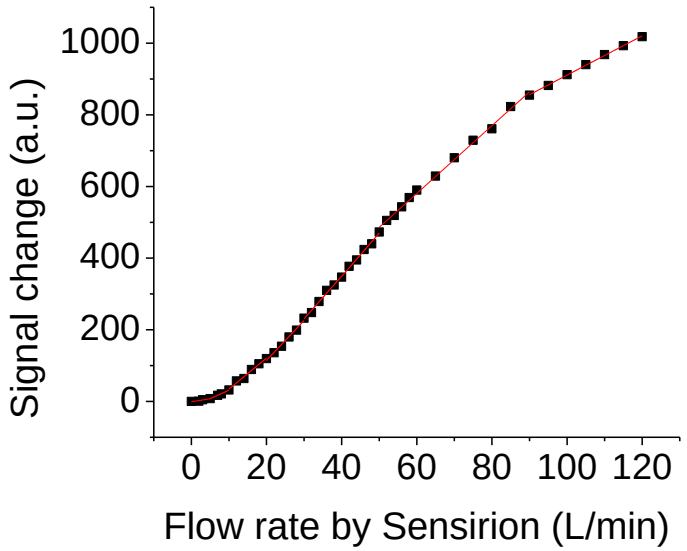

Figure 3-3. The calibration curve of flow rate ranging from 0 to 120 L/min.

Figure 3-4 shows an example of breath exhalation flow rate (VE) measured by the MIC and the reference Sensirion flow sensor. The exhalation flow rate measured by the new MIC was recovered by using the calibration curve built from the Sensirion flow sensor and corrected by standard pressure and dry conditions before the comparison. The interrogation showed the ability of the device to monitor exhalation flow rate in a breath-by-breath manner. Note this accuracy was maintained during the first 10 weeks of the use of the flowmeter. However, a degradation of performance was observed over time as

shown as follows (see below).

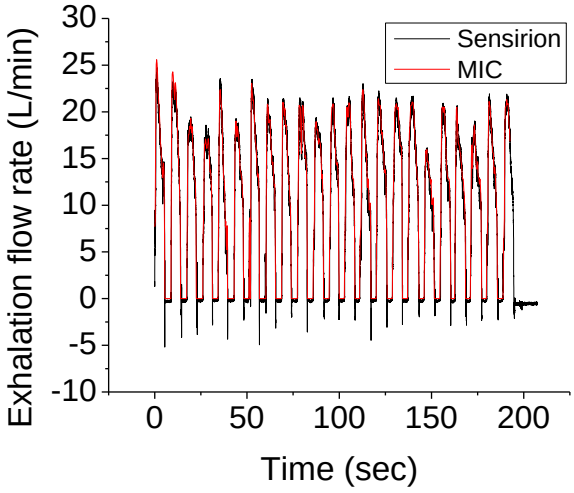

Figure 3-4. A breath-by-breath exhalation flow rate monitoring was measured by our modified device and Sensirion.

To evaluate the performance of the new MIC over time, 16 subjects' RMR were measured using the MIC and the MG simultaneously. As mentioned before, a factor of 1.25 was applied. Figure 3-5a, 5c, and 5e show that VO_2, VCO_2, and RMR measured by the new MIC and the MG correlated very well. All of them had regression coefficient (R^2) greater than 0.96. On average, the measured RMR from the MIC were about 5.9% less than the MG for VO_2, 5.3% for VCO_2, and 6.6% for RMR. Figure 3-5b ,5d, and 5f show the Bland-Altman plot of the percentage difference between the new MIC and the MG for VO_2, VCO_2, and RMR defined as (MIC – MG) / MG * 100%. All the results for VO_2, VCO_2, and RMR were within the range of mean value ±1.96 standard deviation, showing a reasonable performance. However, we identified +/- 10% should be a practical acceptance limit of performance since +/- 10% is the physiological variability of RMR

[112], and therefore, percentage differences larger than +/- 10% , which were observed for VO_2, VCO_2, and RMR, were found to be inadequate for acceptance criteria of good performance.

(a)

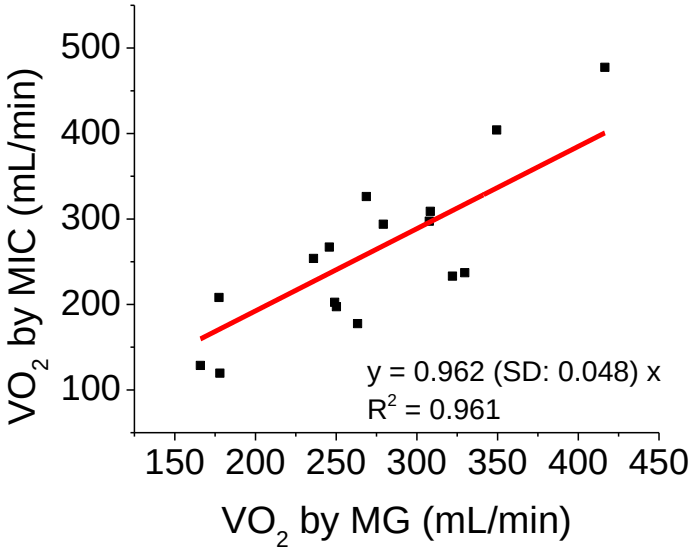

(b)

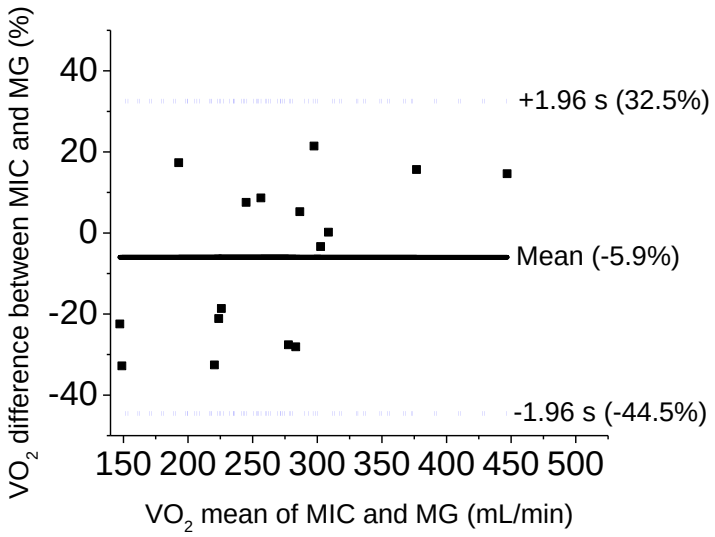

(c)

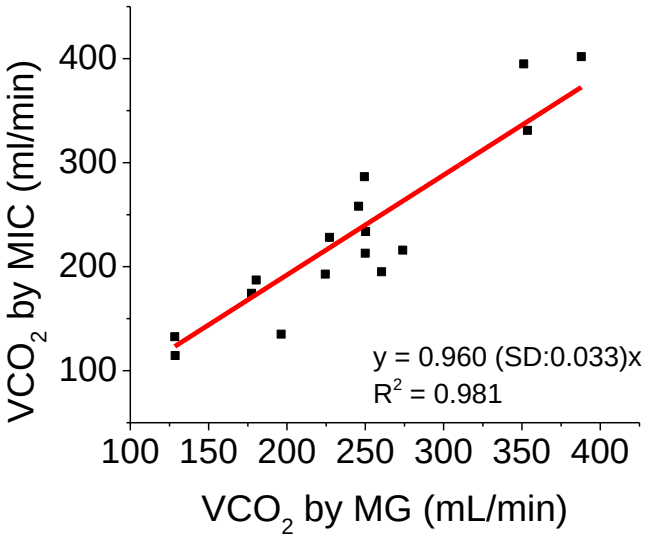
400
300
200
100
VCO2 by MIC (ml/min)
y = 0.960 (SD:0.033)x
R2 = 0.981
100 150 200 250 300 350 400
VCO2 by MG (mL/min)

(d)

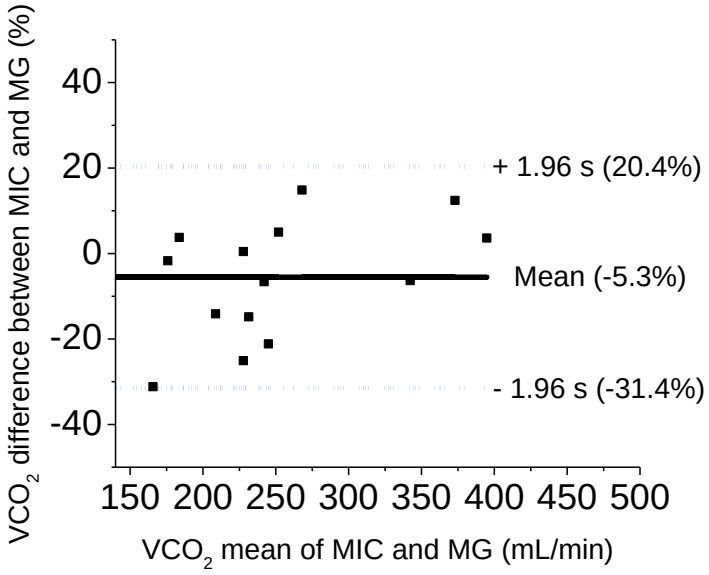
40
20
0
-20
-40
VCO2 difference between MIC and MG (%)
+ 1.96 s (20.4%)
Mean (-5.3%)
- 1.96 s (-31.4%)
150 200 250 300 350 400 450 500
VCO2 mean of MIC and MG (mL/min)

(e)

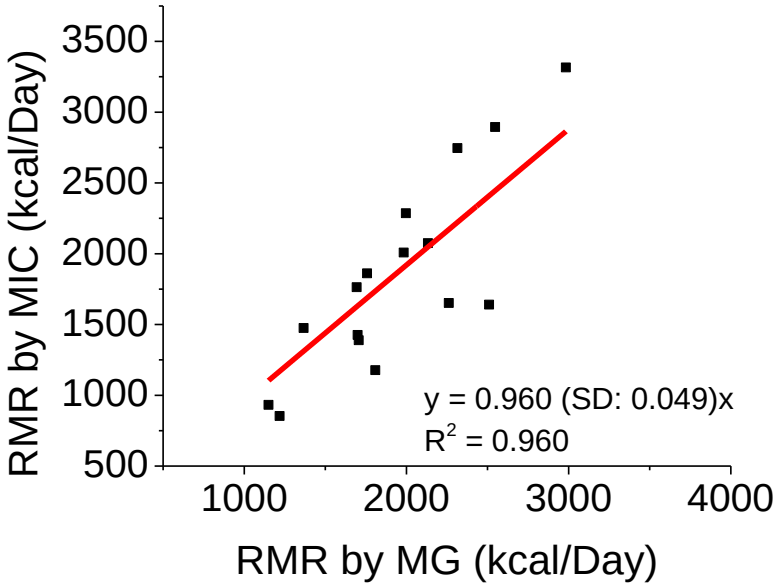

(f)

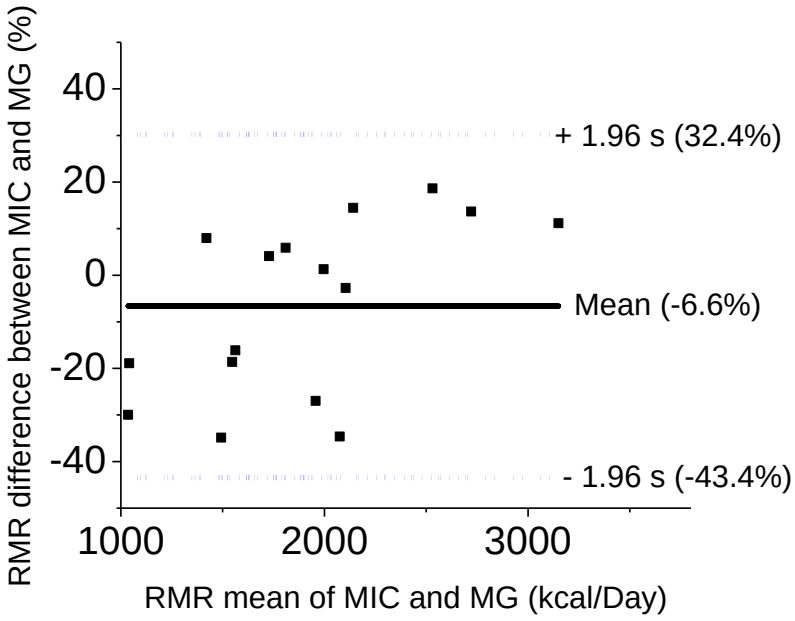

Figure 3-5. Comparison between the new MIC and the MG instrument. Linear correlations and Bland-Altman analysis for VO2 (a)(b) and VO2 (c)(d) and RMR (e)(f).

In order to quantify the lack of the new MIC device's performance, we further analyzed the results, defining three categories based on absolute percentage differences: a) <10%, b) 10-20%, and c) > 20%. Figure 3-6 shows a pie chart that categorizes the absolute percentage difference between the measured results from the new MIC and the MG. Twenty-five percent (25%) of the measurements had a difference larger than 20%, 44% had a difference between 10~20% and only 31% had a difference within +/-10%. In summary, 69% of the measurements had a difference of over 10%.

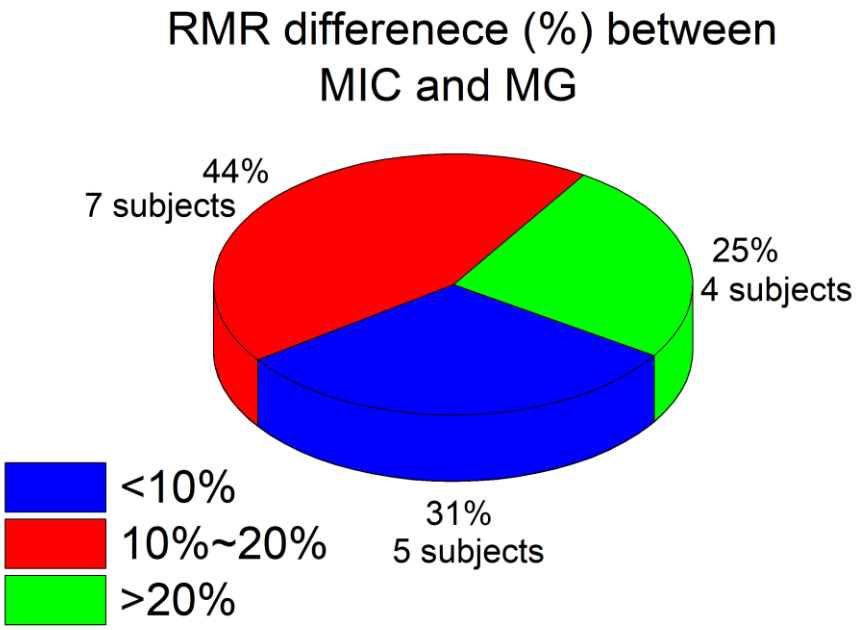

Figure 3-6. Pie chart distribution for RMR difference (%) between the modified MIC and MG.

As mentioned before, we analyzed the exhaled O_2 and CO_2 concentration outputs from

the modified MIC vs. the MG, and no significant difference was found (not shown). However, we found the difference to be caused by V_E (see more details below). In fact, we noticed a degradation of V_E performance from the TFM over time. Figure 3-7 shows the error of V_E between MG and MIC on each subject over the period of use. A clear increase of error was built up over time (as the number of subject increased), with V_E measured from the modified MIC systematically lower with respect to V_E from MG.

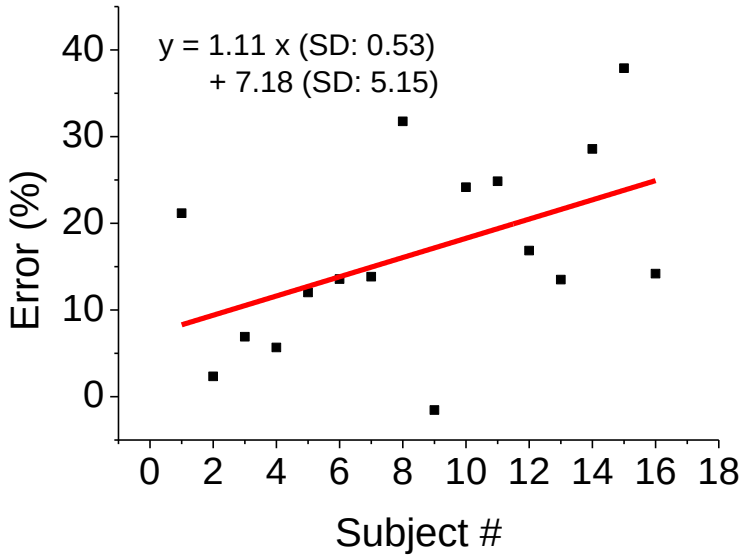

Figure 3-7. Absolute percentage difference of V_E between the MG and MIC calculated as Error (%) = $|(VE_{MIC} – VE_{MG})/VE_{MG} * 100\%|$ for each subject. The subjects 1-16 were measured between a period in time starting on 02-20-2017 and ending on 02-05-2018.

Figure 3-8 shows a breath-by-breath example of the measurement of a subject with the modified MIC after the performance degradation was detected. As opposite to the patterns observed before, the degradation where relatively constant maximum exhalation rates were observed in each cycle from the beginning to the end of the measurement (see Figure 4), this pattern shows significantly lower exhalation rates at the beginning of the

measurement. The recorded flow rate before 280 seconds was about 2 times lower than after the flow rate recorded in the remaining second portion of the measurement. Further investigation needs to be done to learn more about this phenomenon, and only a hypothesis can be discussed at this time.

A possible reason for failure is that the condensation of moisture in breath over time may cause damage in the TFM's thermopile and the mechanisms involved to reach adequate behavior. Before the start of the measurement, the humidity around the thermopiles is the same as the humidity of the environment. After the measurement starts, a sudden disturbance from the moisture of breath condensing on the surface of thermopiles takes place.

In a new TFM, the thermopile seems to be immune to humidity condensation (probably due to hydrophobic coatings). In a used TFM, the thermopiles may suffer a damage of their coatings and a breath humidity condensation, which is a phase change that releases heat, and may dramatically change the energy flow, changing the TFM working conditions, and causing an erroneous reading. As the measurement continues, the condensation reaches a steady state and no longer perturbates the system with further heat release, and therefore, the temperature in the system would reach equilibrium so that the TFM can function correctly.

Using tubing before the flow meter inlet to trap humidity could possibly reduce the condensation onto the thermopiles. In addition, a systematical correction algorithm can also be applied to accommodate the effect of condensation. These modifications are possibilities to mitigate the above-mentioned problems. However, the TFM in its current form is not suitable to be used as a flow meter for a gas sample that has high humidity or

temperatures significantly different from ambient temperatures.

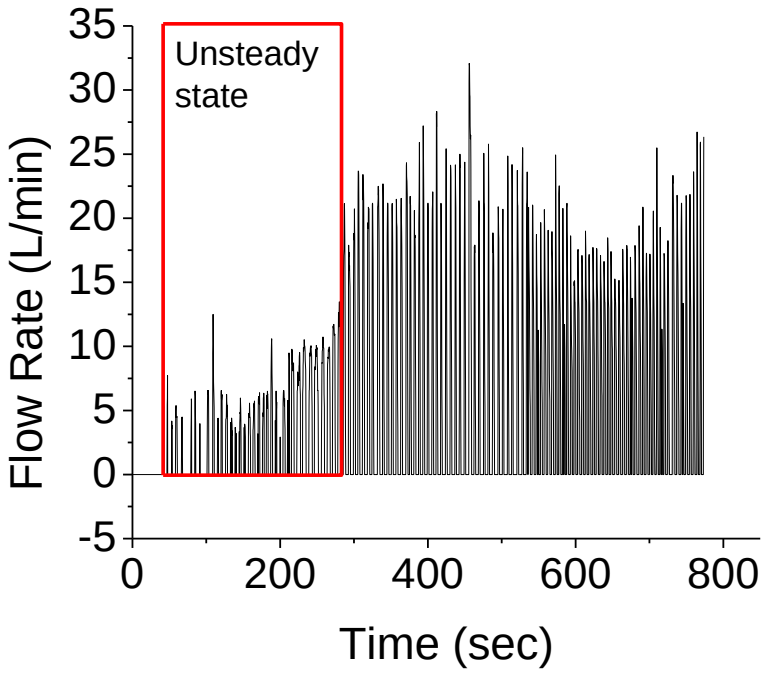

Figure 3-8. An example of a breath flow rate recording on the modified MIC after the performance degradation was detected.

3.4. Conclusion

To conclude, we observed a 6.6% underestimation of RMR output in the new MIC. Although initial calibration of the TFM sensor done at a range from 0-120 L/min rendered accurate values with respect to reference commercial flowmeters, the original calibration failed to be applied after using the TFM over a period of 3-4 months. Furthermore, VO_2 and VCO_2 were measured to render RMR measures by the modified MIC and MG in parallel, and 69% of the measurements showed a difference between the two methods that was greater than 10%, which could have been caused by moisture from

the breath collection or from the degradation of the TFM sensitivity to the flow. Further investigation needs to be done to confirm this assumption. Nevertheless, the TFM is not suitable for highly humid gas sample measurement, such as human breath.

Acknowledgments

The authors would like to thank Arizona State University and Mayo Clinic for their support.

Conflict of Interest

E.F., X.J., D.B., F.T., and N.T. work for Breezing^{TM}, indirect calorimeter tracker used as a base device of the modified indirect calorimeter device studied in this work.

Publications

Nai-Yuan Liu, Yue Deng, Francis Tsow, Xiaojun Xian, Nongjian Tao, Jane J Dean, Janet L Wilson, Doina Kulick, and Erica Forzani, *Evaluation of a thermal-based flow meter for assessment of mobile resting metabolic rate measures*, Journal of Sensors, 2018, doi: 10.1155/2018/9186475

CHAPTER 4

THE IMPROVEMENT OF AN EXITING MOBILE SENSING DEVICE FOR ENVIRONMENT: THE LIFE-TIME BOOST ON A QUARTZ TUNING FORK SENSOR

4.1. Background and Introduction

Volatile organic compounds (VOCs) are organic chemicals emitted from anthropogenic and biogenic sources with high vapor pressure at room temperature [4], such as acetone, ethanol and benzene…etc., some of which are harmful to human health [5]. According to the United States Environmental Protection Agency (EPA), VOCs are among the major pollutants for indoor and outdoor air quality, which are emitted from furniture, appliances, and construction materials and combustion of vehicle fuels [6] [7]. Harmful VOCs typically are not acutely toxic, but have compounding long-term health effects [8]. Monitoring personal exposure to VOCs is needed. A plethora of analytical methods has been developed to monitor VOC concentrations. PID is well-known for its portability and simplicity to handle, but not very selective to specific analyte [42]. GC-MS with its supplemental detection method such as thermal conductivity (TCD) [117], differential mobility (DMD) [118], and flame ionization (FID) [119] is another one, which has high selectivity, but is very expensive, bulky and requires expertise to handle. MOS sensors for VOCs are also reported [35] However, they are power-consuming and not very selective. Some other personal VOC monitors have also been recently developed [120].

A wireless wearable monitor based on quartz tuning forks (QTF) sensors for environmental VOCs has been developed by our group [121]. Quartz tuning forks are

mass sensitive resonators useful in biosensors [122, 123]. The QTF sensors are coated with polymer films that are sensitive and selective to target VOCs. For instance, the molecular imprinted polymers (MIP) are highly selective to hydrocarbons. The MIPs are formed in the presence of a specific molecule template that is extracted later, leaving binding sites complementary cavities with chemical affinity to the molecules similar to the original molecule template or its family [124]. When target VOCs molecules are adsorbed onto the polymer, a change in resonant frequency (induced from loaded mass change on the QTF sensor) is detected. The QTF sensing mechanism gives the possibility to develop fast response, high sensitivity and portable devices for personal VOC exposure detection compared to any other methods mentioned before. Studies has shown the validation of the specifications of the QTF-based VOC device [125] and the ability for the device to provide timely response to VOCs exposure level, helping to identify potential health risks [126]. The device developed in our group, compared to other works, has the characteristics as follows: (1) A replaceable pre-calibrated sensor cartridge has been created to improve to avoid laboratory calibration procedures dependent on expertise. (2) A much smaller device volume VOC device has been designed and mass-produced, including highly integrated components. (3) A user interface with embedded guidance has been created as a mobile application in a phone or tablet.

In this part of work, we will describe the fabrication of the QTF sensors for the wireless, wearable device for hydrocarbons detection and their properties. Many studies have been done on the molecularly imprinted polymer structure [124], including thermal stability [127], chemical and physical adsorption calculations and evaluations [128-130]. Previous work done by our group demonstrates evidences of MIP aging and its effect on MIP

sensing properties [131]. We have built MIP-modified QTF sensors, and systematically tested the stability of the material. MIP is a porous and adsorptive sensing material [132-134], and we have observed an aging effect on the sensing material with a concomitant decay of sensor sensitivity over time. Comparative study about the selectivity to hydrocarbons between fresh and aged sensors has been investigated.

4.2. Materials and Methods

4.2.1. Quartz Tuning Fork Sensors

The QTFs are piezoelectric crystal resonators with high mass sensitivity, thermal and mechanical stability, and self-sensing capability [135]. The QTF sensors used in the present experiments have a native resonant frequency of 32.768 KHz and a dimension of 4 mm x 0.6 mm x 0.35 mm (manufactured by Jiangcheng Electronic Limited Company), which renders a mass sensitivity of 20 ng/mm^2.

4.2.2. Molecularly Imprinted Polymer (MIP) Preparation

The MIP is synthesized using divinylbenzene (mixture of o-, m-, p-, Sigma Aldrich) as both monomer and cross-linker, o-xylene (Sigma Aldrich) as both template and solvent, and azobisisobutyronitrile (AIBN, Sigma Aldrich) as initiator, under argon environment, 85◦C, and overnight. In addition, MIPs using styrene (Sigma Aldrich) and the above mentioned components were synthesized to study the effect of the ratio of monomer (styrene)-to-cross- linker (divinylbenzene) on the sensitivity of the polymer to xylene.

4.2.3. MIP Treatment and QTF Sensor Coating

After synthesis, the polymer is cracked into smaller pieces (estimated size: 1mm-5mm) first and smashed using ball milling machine (PQ-NO 4 Planetary Ball Mill, Across International) to obtain consistent particle size. The QTF forks were pretreated with isopropanol and dodecane thiol overnight, then dipped in dried toluene and phenyl trimethoxy silane for 5 hours and dried with argon before being coated. The uniform polymer particles (estimated size: 1μm-10μm) are then dispersed in o-xylene solvent and the mixture is coated onto QTFs with a metal needle syringe or with Spin Coater Model P6700. To show the sensitivity of the optimized QTF sensors, pure polystyrene (PS), pure MIP and the mixture of MIP and PS with the ratio of 19:16 were coated to the QTF. One group of MIP+PS-modified QTF sensors was left at -4C refrigerator for 14 days before testing its sensitivity and selectivity to hydrocarbons to compare with the sensitivity of those which are freshly made to study the aging effect.

4.2.4. QTF Sensing Device Mechanism

Figure 4-1 shows the schematic and appearance of the devices. The personal VOC device based on QTF sensors consists of four functions: (1) Collection and delivery: the air sample is collected and delivered via an alternating channel valve-activated mechanism with a purging channel, delivering a VOC-free baseline for 120 s and a sampling channel, delivering the gas sample to analyze for 60 s. Environment hydrocarbons are tested through the sampling channel. Humidity of air sample is balanced by a Nafion® tube. (2) Sensing and detection: after the air sample is produced, it passes a sensor chamber with a MIP- modified QTF sensor inside, and the sensing

signal from the sampling vs. purging channels are compared and assessed. (3) Signal conversion and data transfer: the resonant frequency shift of the MIP-modified QTF sensor is the sensor signal output, which allows the detection of gas phase analyte concentration due to the mass loading effect of the adsorption of molecules onto the MIP. (4) Data transmission and signal processing: the differential sensor signal is transmitted to a smart phone via Bluetooth®, where raw signal is captured, and further processed to provide concentration output. Detailed descriptions of the circuit have been provided in a previous publication [125].

(a)

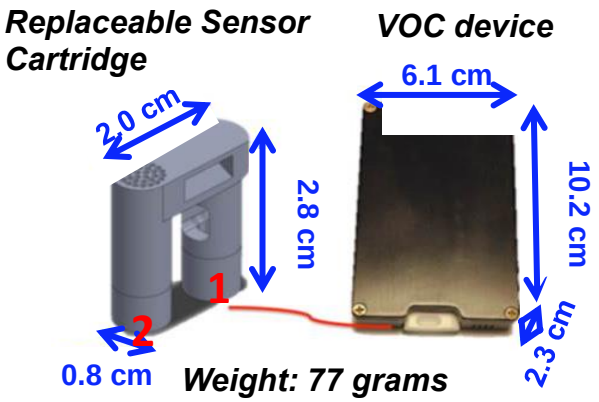

(b)

Figure 4-1. The schematic [136] (a) and the appearance of the VOC replaceable cartridge and device.

4.3. Results and Discussion

Previous work has shown that the study on optimizing the ratio between the MIP, styrene monomer and DVB [131]. *Figure 4-2* shows the sensitivity of different ratio of materials coated on the QTFs. The result shows the template (o-xylene) mixing without monomer gives the highest response.

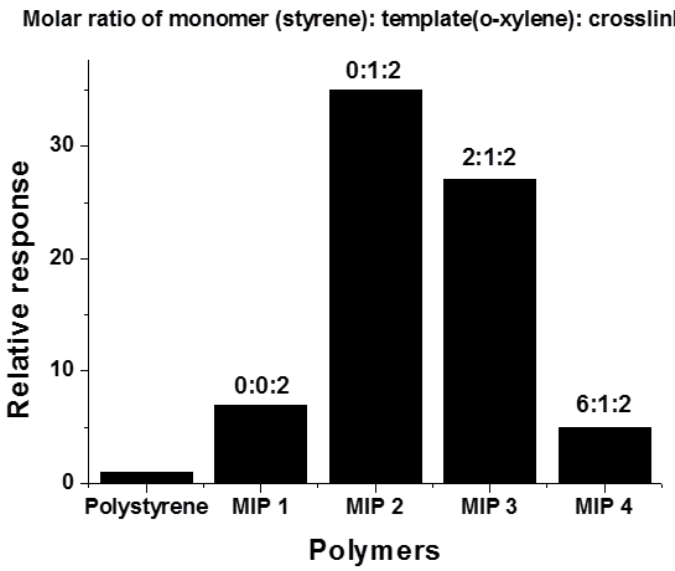

Figure 4-2. Response of TF sensors modified with different MIPs and commercial polystyrene (Aldrich). The MIP-modified TF sensor response is normalized to the PS-modified TF response. Different MIPs were synthesized with different ratios of styrene as monomer, o-xylene as template, and divinylbenzene (DVB) as cross linker. The MIP synthesized with no monomer (styrene), and pure cross-linker (DVB) had the higher sensitivity, and was selected as MIP of choice. [136]

Figure 4-3 shows the selectivity between the fresh and aged sensors that was coated with MIP and polystyrene (PS) to different hydrocarbons. Common environmental pollutant gases, such as formaldehyde, ethanol, acetone, dowanol, ammonia, NO_2, ozone, hydrogen sulfide and carbon monoxide, were also tested with the device. None of them shows response to the QTF sensor. T-test was performed between fresh MIP+PS and fresh MIP as well as fresh MIP + PS and aged MIP + PS. There is no significance difference for both comparisons, which the p-value are 0.2629 for fresh MIP + PS versus fresh MIP and 0.8709 for fresh MIP+PS versus aged MIP + PS.

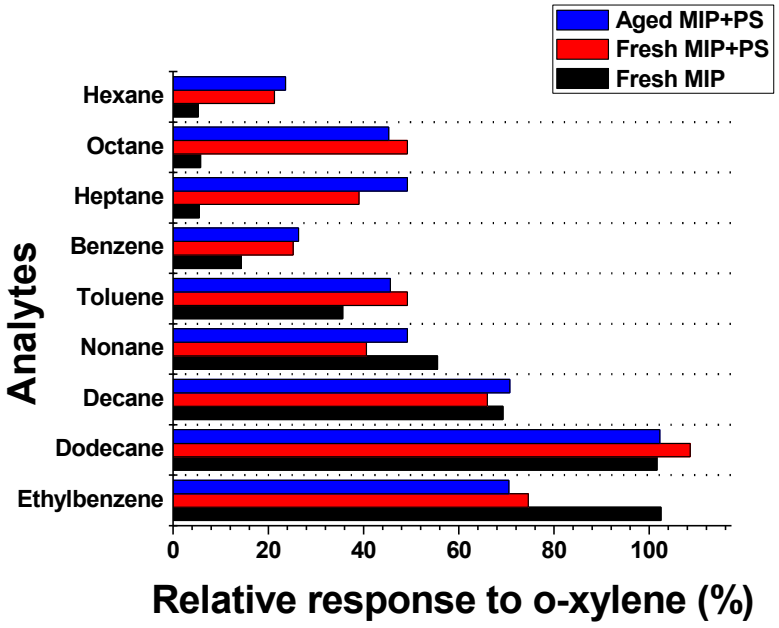

Figure 4-3. MIP selectivity. Response of MIP of choice to different analytes.

To confirm the response to analytes is caused by the coating of MIP on the sensor, the sensitivity between different coatings was compared. 40 ppm of xylene was used to evaluated the sensors. Figure 4-4 shows a comparison between the coating of pure PS, the Non-imprinted polymer (NIP) and the mixture of PS and MIP with the ratio of 19 : 16. The mixture of PS and MIP is the most responsive among the different coatings. PS shows 0 response to xylene, proving the analyte is only responsive to MIP. NIP is slightly responsive to xylene, since there are no sites for hydrocarbons to adsorb.

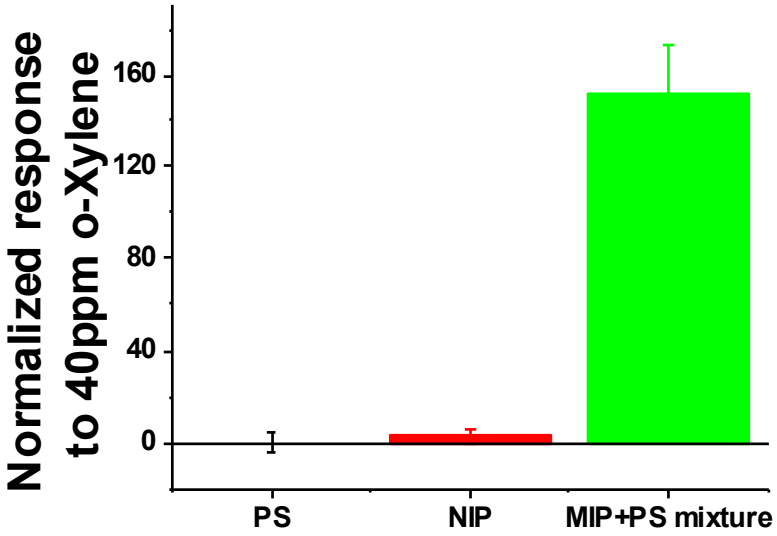

Figure 4-4. The sensitivity of the QTF with pure coating of PS, pure coating of MIP and the mixture of PS and MIP with the ratio of 19 :16. 40 ppm of xylene were used to evaluate the performance of the coatings for the QTFs.

In previous study in our group, the stability of the pure MIP-modified was found to lost its sensitivity within 2 weeks [131]. PS was used to increase the stability of the QTF sensor throughout the time. The sensitivity of the MIP + PS-modified QTF sensors are tested over a year, stored at -4˚C (Figure 4-5). It was found that storage of the MIP + PS-modified QTF sensors under low temperature allows achieving sensitivity stabilization for more than four months at ~75% level of the original sensitivity of Day 1. [131]

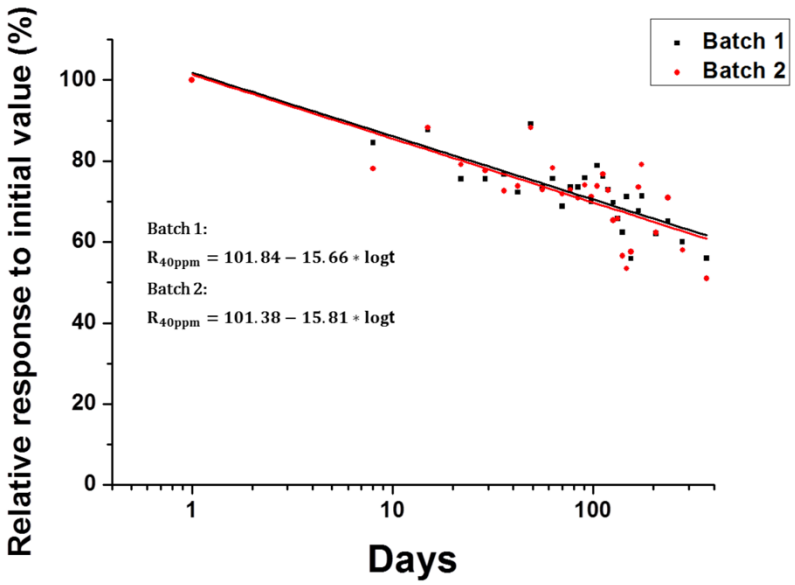

Figure 4-5. The MIP + PS modified QTF sensor response vs time in a year, stored at -4˚C. [131]

4.4. Conclusion

In summary, we explored aging effect of the MIP in connection to its gas adsorption capability, using a MIP+PS-modified QTF sensor located inside a recently developed personal wearable wireless VOC device. The QTF sensors still show good sensitivity and selectivity to environmental hydrocarbons even been aged for 2 weeks. Polystyrene was shown to provide good stability to the MIP modified QTF sensors throughout the time. The MIP+PS-modified QTF shows good sensitivity to environmental hydrocarbons pollutants and has an extraordinary life time; the signal detected by the sensors could be well-transmitted to smart devices. The properties mentioned shows this detecting system is a good candidate for connected health and environment application.

Acknowledgments

The authors would like to thank NIH/NIEHS (GEI, #5U01ES016064 and SBIR 1R44ES021678 program) for their financial support in the development of the quartz tuning chemical sensor, and Dr. Tao for his support for our work.

Publications

Yue Deng, Nai-Yuan Liu, Francis Tsow, Xiaojun Xian and Erica Forzani, *Adsorption Thermodynamic Analysis of a Quartz Tuning Fork Based Sensor for Volatile Organic Compounds Detection*, ACS Sensor, 2017, 2 (11), pp 1662–1668

CHAPTER 5

THE SENSING DEVICES APPLICATION FOR CONNECTED HEALTH AND ENVIRONMENT: RESTING METABOLIC RATE INTEGRATION WITH ENVIRONMENTAL SENSING

5.1. Background and Introduction

Resting metabolic rate (RMR) is the most useful parameter in assessing people's metabolic activity [137], which provides information for patients with a variety of health concern [115, 138] and is the only way for professionals to properly estimate caloric needs of an individual to fit a person's wellness and weight goals [21].

Although epidemiological equations were developed for calculating RMR [139], it is necessary for an individual to assess their RMR value by measurement directly [105] for better accuracy since one's RMR value varies from the predictive equations and relies on many physiological parameters [137]. Methods to measure people's RMR have been developed in the past decades, including direct calorimetry [140] and indirect calorimetry (IC) [141]. Laboratory bench based instruments to measure RMR have been developed, such as the metabolic cart [137]. However, these bulky instruments are developed for professional use and are not accessible to regular users. As reported by our group and others, although there is no statistically significant difference between measured RMR and predicted RMR as population averages, difference exists for an individual's RMR, and the variance may be big [142, 143]. In recent years, hand-held and mobile devices have been developed for personal use [104, 144], which make it practical for individuals

to monitor their RMR daily and design an evident based personal wellness and fitness plan, rather than using epidemiological equations to estimate their metabolism.

Persistent organic pollutants (POPs) are toxic chemicals that are resistant to degradation and can adversely affect human health and the environment [145]. It has been reported that increase in body burden of some POPs (i.e. organochlorines) may decrease oxidative enzymes and RMR [146-151], which is correlated with weight loss [147]. Volatile organic compounds (VOCs) is among the top air pollutants for both indoor and outdoor environment [4] that presents harm to human health and the environment [152]. Furthermore, VOCs in blood can diffuse across the pulmonary alveolar membrane. Given the similarity and overlap of POPs and VOCs, we hypothesize that VOCs in the alveolar breath correlates with metabolism [153]. Nevertheless, we are unaware of any report that directly associate VOCs exposure with RMR. Therefore, it is important to study the effect of environmental VOCs exposure at personal level and its correlation with human metabolism.

Mobile trackers enable the tracking of individuals' VOCs exposure in real-time. In this paper, we present the first study that directly tracks personal VOCs exposure and correlates it with individual's RMR differences between the measured value from portable IC device and predicted value using predicative equation. We tracked 17 sedentary office lifestyle participants' VOCs exposure with a portable monitor. During the same period, their RMRs were measured using a portable IC. In addition, to study the effect of high concentration VOCs exposure, we tracked another participant who is an auto mechanic. Results showed that there is no obvious RMR-VOCs correlation for

sedentary office lifestyle workers. However, correlation is found for the auto mechanic. Further investigation on active working professionals with high VOCs exposure level is needed to confirm this finding.

5.2. Materials and Methods

5.2.1. Participants

A total of 36 participants were recruited from the greater Phoenix area in 2016. The recruitment criteria includes overall good health, free from any medications that might affect metabolic rate and no tobacco use. Female subjects who were pregnant and/or lactating were excluded. We have obtained the Arizona State University Institutional Review Board approval prior to the study (IRB protocol # 1012005855 for the RMR measurement and IRB protocol # 1304009100 for the VOCs measurement). All participants provided written informed consent before participating in the study.

5.2.2. Measurements

Physical parameters, including height, weight, gender, age, and body fat percentage (BF %) were recorded. Body compositions was determined by Tanita bio-impedance scale (model: BC-554 IRONMAN® Body Composition Monitor). Height was measured with a wall-mounted stadiometer. These parameters were used to calculate RMR from the epidemiological equation. Summary of all sedentary office lifestyle participants has been included in Table 1. As mentioned in the introduction, 1 participant is an auto mechanic, who represented subject exposed to higher than typical VOCs concentration. This

specific participant is a 23 year old male. His weight is 93.6 kg and height is 1.75 m. His BMI is 30.6 kg/m2.

Table 5-1. Sedentary office lifestyle participants' physical parameters.

	N	Age	Weight (kg)	Height (m)	BMI (kg/m^2)	Fat (%)
All participants	35	27.8±4.5 (23-47)	63.2±13.4 (45-86)	1.69±0.1 (1.42-1.91)	21.9±2.4 (17.2-26.7)	16.9±5.7 (6.0-29.2)
Males	19	29.5±5.3 (23-47)	72.3±9.99 (52.8-86)	1.78±0.05 (1.70-1.91)	22.7±2.6 (18.1-26.7)	13.8±4.1 (6-19.6)
Females	16	25.2±2.2 (23-30)	52.4±7.33 (45-70)	1.58±0.09 (1.42-1.75)	20.9±1.9 (17.2-22.9)	20.6±5.2 (13.2-29.2)

Resting metabolic rate (RMR) was measured using a mobile indirect calorimeter (MIC) designed and reported by our group [48, 104] (See Chapter 3.2.1). This device evaluates energy expenditure (EE) by detecting the rate of oxygen consumption and carbon dioxide generation in breath [154]. It is based on a flow meter for breath flow rate and a chemical sensing cartridge for breath oxygen and carbon dioxide measurements. As reported previously [48, 104], the device connects wirelessly to an iOS/Android mobile device via Bluetooth®. A QR code with pre-calibrated sensor information will be scanned with a cell phone camera and the calibration factors for the single-use sensor cartridge will be applied to the measurement.

Participants were required to adhere to the following pre-test conditions: no food or caffeine intake in the past 4 hours, no strenuous exercise performed for the past 12 hours, and no moderate exercise performed 4 hours before the test. Participants were introduced to the testing procedure in the beginning. Physical parameters were then recorded. Three RMR measurements were done in the same morning once the resting state was assured.

All participants adhered to testing instructions.

During the measurement, participants breathed through a disposable mouthpiece attached to the Breezing® device. The data received on the mobile device was processed and displayed on the user interface. The Weir equation was used to determine RMR from the measured oxygen consumption and CO_2 production rates [154]. Validation of this device has been previously described [104].

A portable low cost VOC monitor for free-living conditions has been reported before by our group [121, 131, 155, 156] (See Chapter 4.2.4). It is a selective polymer (molecularly imprinted polymer) modified quartz tuning fork based sensor, which is a mass sensitive piezoelectric resonator. The change in resonant frequency of the sensor correlates with the amount of targeted analyte the sensor is exposed to. Each measurement takes approximately 3 minutes. The device connects wirelessly to an Android smart phone via Bluetooth®. Validation tests of the VOC monitor were reported in our previous publications [121, 131, 155, 156].

VOCs exposure concentration was monitored with our tuning fork VOC monitor. 18 participants out of the 36 participants were randomly selected to have their VOCs exposure measured throughout the day. As mentioned before, one of the participants is an auto mechanic who handles toluene related chemicals for as part of his job. The participants wore the portable monitor in an armband and had their VOCs exposure assessed for two one-hour-long periods during the day and at night respectively.

5.2.3. Epidemiological Equation

As one of the most popularly used predictive equation in estimating RMR, Mifflin-St Jeor equation (MSJE) was used in this study to predict the participants' RMR from their age, gender, weight, and height. The equation is a result of the regression from 498 healthy individuals [139]:

RMR (kcal/day) = 9.99×weight (kg) + 6.25×height (cm) – 4.92×age (y) + 166×sex (males, 1; females, 0) – 161 Equation 5-1

5.3. Results and Discussion

5.3.1. RMR Measurement Results Using Portable IC and Comparison with MSJE

The RMR of every participant was measured three times using the portable IC and the results were averaged. In the meantime, RMR value was calculated using MSJE and the collected physical parameters. A comparison of measured and calculated RMR is shown in Figure 5-1.

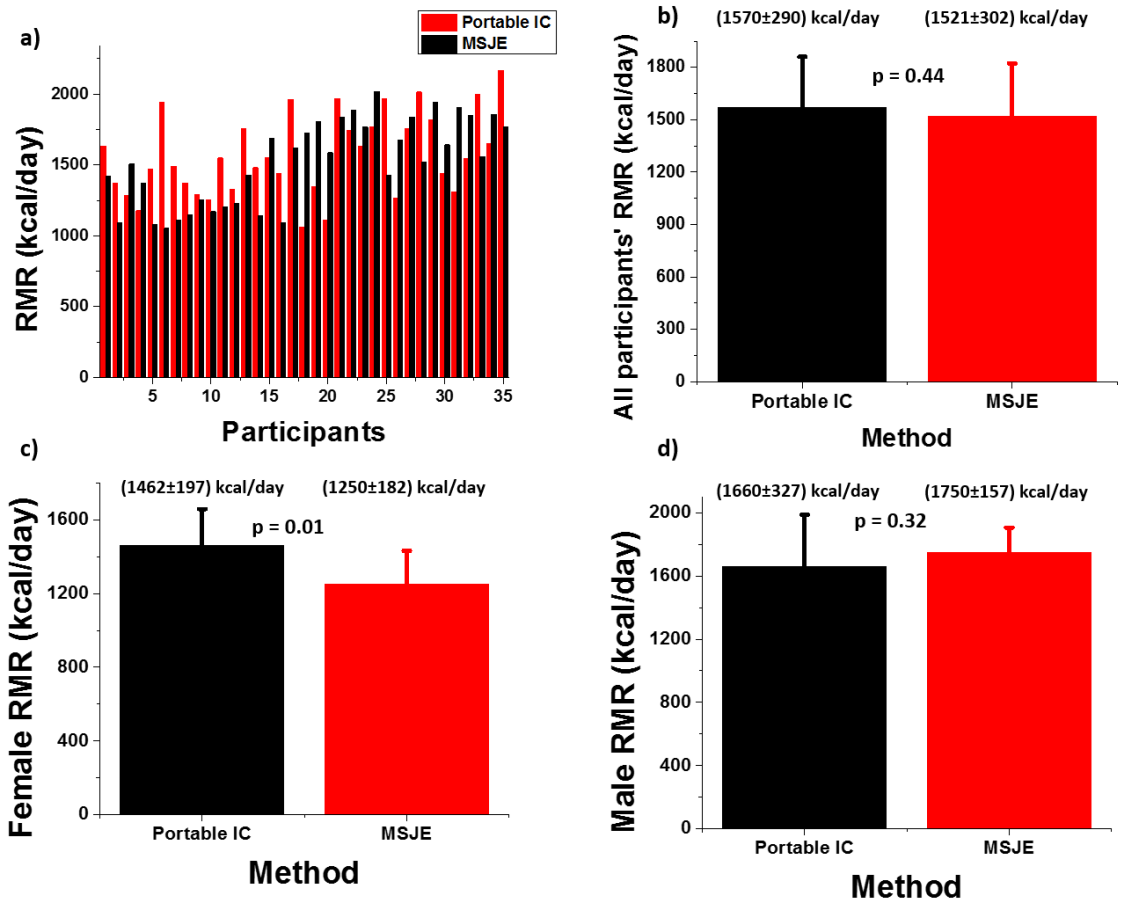

Figure 5-1. RMR results comparison between IC measurement and MSJE prediction [143] a) Raw RMR data from the two methods; b) Averaged RMR comparison between the two methods for all participants; c) Averaged RMR comparison between the two methods for female participants only; d) Averaged RMR comparison between the two methods for male participants only.

The raw RMR values from the two methods are presented in part a, and the averaged RMRs for different participant groups (all participants, female and male) are shown in parts b, c, and d. Paired t-tests were performed and an $\alpha=0.01$ and $p<0.01$ were set for statistical significance. The p values for the three paired t-test are 0.44, 0.01, and 0.32 respectively. Results show that there is no significant difference between predicted and

calculated RMRs for any of the groups. It is noted that the p value for female participants is 0.01, which is just above the cut-off value for our statistical significance.

5.3.2. RMR Difference between the Two Methods

Based on this study and our previously published results [143], that there is no statistical difference in the RMR values between the portable IC measurement and the MSJE calculation. However, as shown in Figure 5-2, the distribution of differences between these two methods (ΔRMR= RMR from MSJE – RMR from portable IC) varies from -887 kcal/day to 665 kcal/day, which is a wide range with physiological significance. Taking into account the precision of the portable IC and the potential experimental errors, a range of ±200 kcal/day for the difference was set to determine the agreement of the measured and calculated RMRs. Although the average difference is -48 kcal/day, which is quite close to the line of equality (x=0), the RMR differences for only 10 out of 35 participants (28.6%) fell within ±200 kcal/day. Since the MSJE is the result of a regression model of a large population study, it represents the average RMR value of the population and is not expected to reflect an individual's unique RMR particularly well. Therefore, we can conclude that for a large portion of the population, their individual RMR likely differs from the MSJE predicted average by more than ±200 kcal/day.

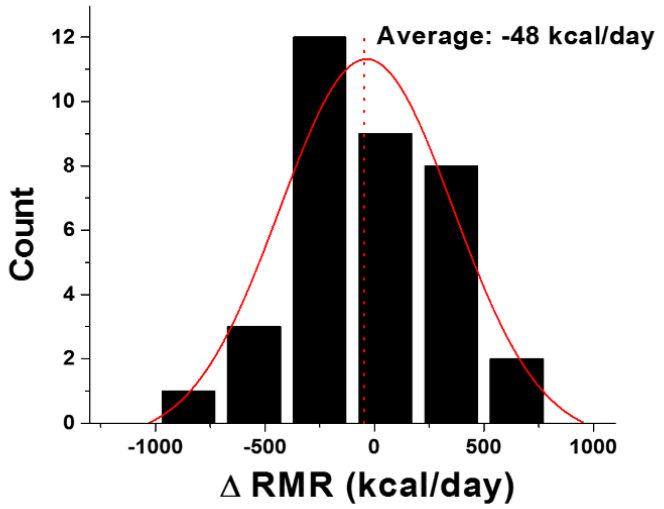

Figure 5-2. Distribution of RMR difference between the two methods, ΔRMR = RMR from MSJE – RMR from portable IC

5.3.3. VOCs Exposure Measurement

Based on the ΔRMR, participants were divided into three groups: Group A includes 10 participants with ΔRMR > 200 kcal/day; Group B includes 10 participants with -200 kcal/day < ΔRMR < 200 kcal/day; Group C includes the remaining 15 participants with ΔRMR < -200 kcal/day. As mentioned above, out of the 36 participants, 17 sedentary office lifestyle participants were recruited with their daily VOC exposure measured as described below.

Among the 17 sedentary lifestyle participants, 6 participants were from Group A, 6 participants were from Group B, and 5 participants were from Group C. They were asked to wear the VOCs monitor for about an hour at work and at home for a total of two hours in a day. The monitor was placed inside an armband and real-time data was recorded on

an Android phone. No discomfort or hindrance during their activity was reported.

Figure 5-3 shows the summary of the study. The average VOCs concentration of each test was plotted against the ΔRMR of each participant. The daytime and nighttime VOCs concentrations are presented in Figure 3 a) and b). On average, participants reported spending 10 hours at work and over 12 hours at home. To simplify the calculation for an individual's 24-hours hydrocarbon exposure, we used their average time spent at work and home as weights for the measured VOC exposure level as shown in the equation below.

$$24\ hour\ exposure\ concentration = \frac{10}{24} * daytime\ area\ VOCs\ concentration + \frac{14}{24} * nighttime\ area\ VOCs\ concentration$$

Equation 5-2

(a)

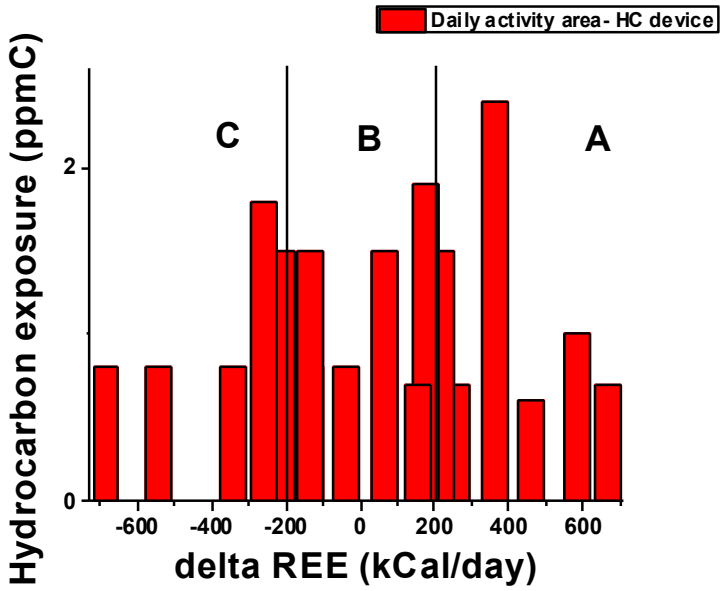
Daily activity area- HC device
Hydrocarbon exposure (ppmC)
C
B
A
2
0
-600
-400
-200
0
200
400
600
delta REE (kCal/day)

(b)

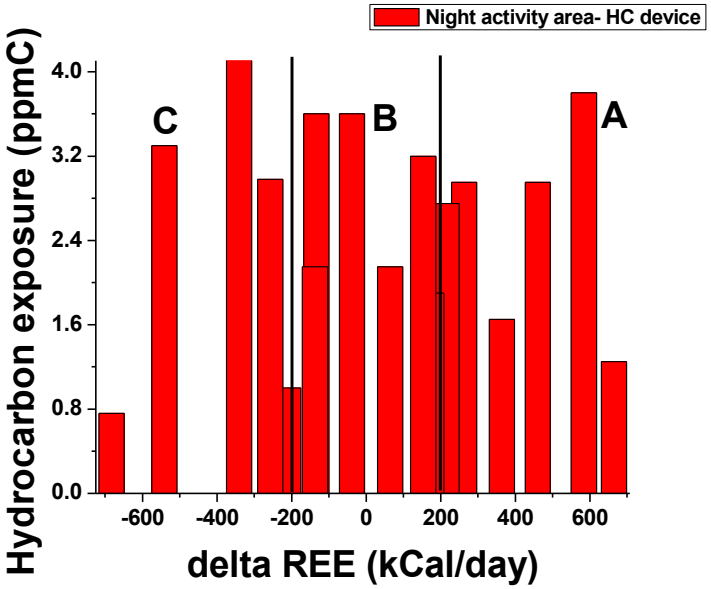
Night activity area- HC device
Hydrocarbon exposure (ppmC)
C
B
A
4.0
3.2
2.4
1.6
0.8
0.0
-600
-400
-200
0
200
400
600
delta REE (kCal/day)

(c)

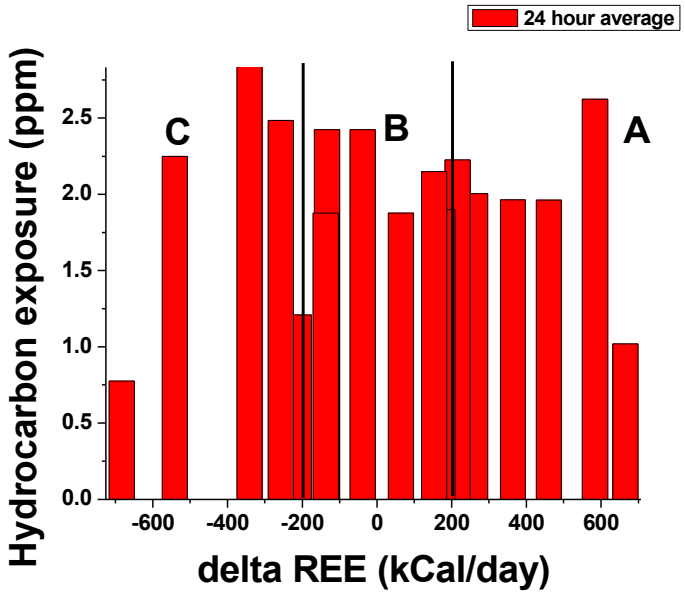

Figure 5-3. Average VOCs concentration for each test: a) participants' work area; b) participants' home; c) prediction of 24-hours exposure level by applying average time spent in each location. See text for details.

As reported in the previous publication, the total VOCs concentration obtained from this VOCs device is in terms of volume in total carbon concentration (ppmC) [157]. From Figure 5-3, it can be observed that for most cases, the participants' homes have higher VOCs concentrations compared to their work area. This may due to better ventilation in most office buildings than in residential constructions.

ANOVA analysis [158] has been applied to quantitatively analyze the VOCs exposure concentration within the three groups. Table 5-2 shows the average VOCs exposure in each test and the statistics from the ANOVA analysis. The average VOCs exposures for all three groups under each condition were similar. The p value for all three conditions are higher than 0.01, indicating no significant difference within the three groups. In

addition, the F values from the ANOVA analysis are smaller than the F critical values. Thus the null hypothesis that there is no significant difference within the three groups is not rejected.

Table 5-2. Average VOCs exposure and ANOVA analysis.

	Day time activity area VOCs exposure (ppmC)	Night activity area VOCs exposure (ppmC)	24 hour average VOCs exposure (ppmC)
Group A	1.15±0.63	2.56±0.48	1.97±0.48
Group B	1.20±0.45	2.77±0.24	2.11±0.24
Group C	1.14±0.43	3.05±1.30	2.25±1.30
p value	0.98	0.88	0.86
F	0.018	0.134	0.147
F critical	3.74	3.74	3.74

For sedentary office lifestyle population, there is no evidence in our study that suggests a correlation between amount of VOCs exposure and the RMR difference between the portable IC and the predictive equation. This is can be attributed to that fact that VOCs exposures of these participants were not high.

However, one may wonder if the same answer could be concluded from people who are expose to high VOC levels. In this study, we also recruited one participant who is an auto mechanic to show to gain insights into that question.

For this specific participant, his RMR value from the MSJE is 2081 kcal/day and his actual measured RMR from the portable IC is 1425 kcal/day with a difference of more than 500 kcal/day. Designing a fitness plan using the epidemiological equation (e.g. MSJE) can lead to a daily energy surplus and result in weight gain. Figure 4 shows his exposure level was at 18.2 ppmC during work, and was much higher than his home

VOCs exposure concentration. This concentration was also much higher than all the sedentary participants' work exposure, while his home VOCs exposure concentration (1.7 ppmC) was comparable to the other 17 participants. Applying the same 24-hours hydrocarbon exposure equation to this set of data, this participant was exposed to 8.6 ppmC VOCs per day, which is three times higher than the sedentary office lifestyle participants.

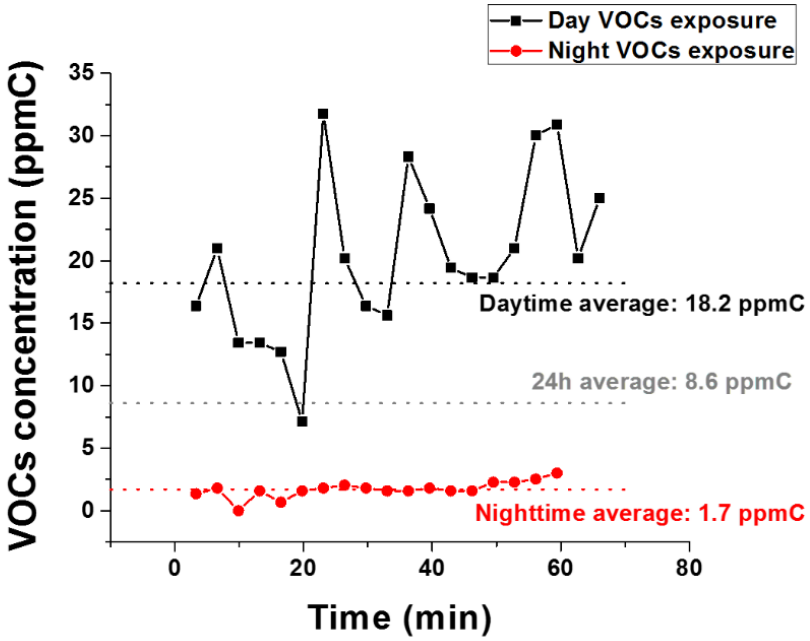

Figure 5-4. VOCs exposure concentration for the auto mechanic.

From the single participant, we cannot conclude whether high level of VOCs exposure will have a long term effect on metabolism. However, this example draws attention to the importance of tracking personal exposure in real-time and demonstrate our protocol in studying health-environment interactions.

There are many factors that contributes to metabolic rate such as body composition,

diet, etc. [137]. It is a complex biometrics that maybe influenced by many cross-talking factors. To the best of our knowledge, although VOCs in blood (partially contributed from external exposure) may potentially influence one's metabolism, there is no report that associates the external exposure to people's metabolic rate. The purpose of this study is to preliminary investigate the correlation between environmental VOCs exposure and RMR in a direct way, specifically, to measure different populations' VOCs exposure concentration and their RMR.

In this study, the use of two portable devices helped in our experimental proceedings as they are easy to operate and provide real-time tracking. It makes collecting real-time data at low cost and in free-living conditions feasible. Comparing to traditional bulky lab-based instruments, portable real-time devices provide immediate information for measurement.

5.4. Conclusion

To conclude, we presented a preliminary study noting the individual RMR difference between the measured results from a portable IC device and calculated results using a widely accepted predictive equation. To investigate whether there is any correlation between VOCs exposure and the noted RMR difference, we investigated 17 sedentary office lifestyle participants' VOCs exposure using a mobile VOC monitor. ANOVA analysis was applied to analyze the data. Results showed that there is no obvious correlation between an individual's RMR difference and VOCs exposure at low level. In addition, we reported an example of a participant with high VOCs exposure. The results

showed the potentials of mobile real-time sensors in studying health-environment interactions.

Acknowledgments

The authors would like to thank NIH/NIEHS (GEI, #5U01ES016064 and SBIR 1R44ES021678 program) for their financial support in the development of the VOCs sensor and Dr. NJ Tao for his support to our work.

Conflict of interest

F. Tsow, NJ. Tao, X. Xian, and E. Forzani declare conflict of interest.

Publications

Yue Deng, Nai-Yuan Liu, Francis Tsow, Xiaojun Xian, Rosa Krajmalnk-Brown, Nongjian Tao, Erica Forzani, *Tracking personal health-environment interaction with novel mobile sensing devices,* Sensors, 2018, 18(8). pii: E2670. doi: 10.3390/s18082670.

CHAPTER 6

CONCLUSIONS AND FUTURE WORK

In this work, I demonstrated how the field sensing devices need to be for connected health and environment. In the first part of work, I showed an example of how to build a diagnostic sensing device through an example. In this example, we designed and created a total-ammonia sensing device for urine. This device is able to monitor the total-ammonia level in biological samples. Pilot study has shown that disorders of the kidney and/or liver may produce rapid changes in total ammonia. This device is able to capture this change continuously in semi-real time without additional labor work compared to standard method such as enzymatic method and ion-selective electrode.

In the second part of work, I demonstrated the improvement of mobile sensing devices to fit the idea of connected health and environment. First of all, we investigated the requirement of the flow meter for breath-related measurements through modifications on the flow meter of an existing mobile indirect calorimeter (MIC). The calorimeter was found to have lots of resistance while subjects were breathing through it, giving an underestimated result. The original design is a differential flow meter with an orifice plate. We resigned the device with a larger diameter of flow channel with a thermistor flow meter since it doesn't require a shrinkage on the flow channel, which releases possible resistance one could feel. The result shows that thermistor flow sensor reduces the resistance and measures the same result as the reference method (Medical Graphics) that was often used in hospital. However, the moisture in breath could affect the reading of the thermistor flow meter.

Other than that, I also demonstrated the improvement on the life time of an environmental sensor. A quartz tuning fork (QTF) coated with molecularly imprinted polymer (MIP) is a very sensitive sensor to monitor the environmental hydrocarbons. However, it suffers from a very short life-time to be applied in the field. With the introduction of the polystyrene to the MIP QTF, we showed the life-time of the sensors increased by 8 times.

In the last part of work, I demonstrated how the mobile sensing devices applied to correlate the environmental conditions to health as a realization of the idea of connected health and environment in the field sensing aspect. The MIC and MIP QTF sensing device described previously were used to see the effect of environmental hydrocarbons to resting metabolic rate (RMR) on sedentary people and people working in environment having potentially high-level of hydrocarbons. We presented a preliminary study noting the individual RMR difference between the measured results from the MIC device and calculated results using a widely accepted predictive equation. For sedentary people, there is no difference between the measurement and calculation. However, we found that there is a great difference on a participant with high hydrocarbons exposure. The results showed the potentials of mobile real-time sensors in studying health-environment interactions.

In sum, I demonstrated different sensing devices that are able to capture the biological information (NH_3, CO_2 and O_2) non-invasively and environmental information (hydrocarbons) continuously. All the devices are portable and wirelessly connected to smart devices (Android or iOS system). The big picture of this technology is to gather all the health data and environmental data altogether in a data storage unit, which could be

transmitted to places such as hospital for further use. For example, if a patient's total-ammonia level drops rapidly, it could be a warning that there is a problem with your kidney. The patient's smart device can warn you in advance. Since the data is transmitted to hospital, ambulance could also be sent.

This work shows the field sensing aspect of the connected health and we extended the idea to the environment as well by showing the applications of a mobile indirect calorimeter and a sensing device for environmental hydrocarbons to investigate the correlation of the health condition and the possible environmental effect. In this aspect, future work will be focused on making all this devices wearable. For example, for the total-ammonia sensing, instead of using the urine as media, sweat could be also used. Using the sweat as media could let us rely on the capillary force if we made the sensor attached to skin. As consequence, these sensing devices could be designed to be to be wearable to monitor the kidney condition to those patients' who potentially have higher risk to have kidney failure without asking the patient to urinate. The same idea could be applied to the environmental sensor. However, this will bring out the question about how to make it small enough to be wearable. The design we have now relies on a pump for sampling, which occupies lots of space. Ideally, we would like a passive measurement, which means the pump is excluded from the design. However, how to make sure the device remains sensitive without the pump could be very challenging. Overall, the idea is to make all these devices to be as portable as possible and as passive as possible to make the technology more attractive and convenient to the public.

REFERENCES

[1] N. Carroll, "Key Success Factors for Smart and Connected Health Software Solutions," *Computer*, vol. 49, pp. 22-28, 2016.

[2] (Sep 30, 2017). *White paper on connected health*. Available: https://www.academia.edu/9447836/WHITE_PAPER_ON_CONNECTED_HEALTH

[3] (Sep 20). *iOS - Health*. Available: https://www.apple.com/ios/health/

[4] R. Atkinson and J. Arey, "Atmospheric degradation of volatile organic compounds," *Chemical Reviews*, vol. 103, pp. 4605-4638, Dec 2003
.

[5] K. Brown, R. Sim, J. Abramson, and N. Gray, "Concentrations of Volatile Organic Compounds in Indoor Air – A Review," *Indoor air*, vol. 4, pp. 123-134, 06/01 1994.

[6] T.-T. Win-Shwe, H. Fujimaki, K. Arashidani, and N. Kunugita, "Indoor Volatile Organic Compounds and Chemical Sensitivity Reactions," *Clinical and Developmental Immunology*, vol. 2013, p. 8, 2013.

[7] H. K. Chagger, J. M. Jones, M. Pourkashanian, A. Williams, A. Owen, and G. Fynes, "Emission of volatile organic compounds from coal combustion," *Fuel*, vol. 78, pp. 1527-1538, 10// 1999.

[8] S. C. Sofuoglu, G. Aslan, F. Inal, and A. Sofuoglu, "An assessment of indoor air concentrations and health risks of volatile organic compounds in three primary schools," *Int J Hyg Environ Health*, vol. 214, pp. 36-46, Jan 2011.

[9] R. K. Hsu, C. E. McCulloch, R. A. Dudley, L. J. Lo, and C. Y. Hsu, "Temporal changes in incidence of dialysis-requiring AKI," *J Am Soc Nephrol*, vol. 24, pp. 37-42, Jan 2013.

[10] C. Y. Hsu, C. E. McCulloch, D. Fan, J. D. Ordonez, G. M. Chertow, and A. S. Go, "Community-based incidence of acute renal failure," *Kidney Int*, vol. 72, pp. 208-12, Jul 2007.

[11] T. D. Boyer and Z. J. Haskal, "The role of transjugular intrahepatic portosystemic shunt in the management of portal hypertension," *Hepatology*, vol. 41, pp. 386-400, Feb 2005.

[12] J. S. Bajaj, J. B. Wade, and A. J. Sanyal, "Spectrum of neurocognitive impairment in cirrhosis: Implications for the assessment of hepatic encephalopathy," *Hepatology,* vol. 50, pp. 2014-21, Dec 2009.

[13] M. Romero-Gomez, F. Boza, M. S. Garcia-Valdecasas, E. Garcia, and J. Aguilar-Reina, "Subclinical hepatic encephalopathy predicts the development of overt hepatic encephalopathy," *Am J Gastroenterol,* vol. 96, pp. 2718-23, Sep 2001.

[14] J. Haberle, N. Boddaert, A. Burlina, A. Chakrapani, M. Dixon, M. Huemer, *et al.*, "Suggested guidelines for the diagnosis and management of urea cycle disorders," *Orphanet J Rare Dis,* vol. 7, p. 32, 2012.

[15] M. B. Robinson, K. Hopkins, M. L. Batshaw, B. A. McLaughlin, M. P. Heyes, and M. L. OsterGranite, "Evidence of excitotoxicity in the brain of the ornithine carbamoyltransferase deficient sparse fur mouse," *Developmental Brain Research,* vol. 90, pp. 35-44, Dec 21 1995.

[16] N. Ah Mew, L. Krivitzky, R. McCarter, M. Batshaw, and M. Tuchman, "Clinical outcomes of neonatal onset proximal versus distal urea cycle disorders do not differ," *J Pediatr,* vol. 162, pp. 324-9 e1, Feb 2013.

[17] A. Tizianello, G. Deferrari, G. Garibotto, C. Robaudo, N. Acquarone, and G. M. Ghiggeri, "Renal ammoniagenesis in an early stage of metabolic acidosis in man," *J Clin Invest,* vol. 69, pp. 240-50, Jan 1982.

[18] A. Gougoux, P. Vinay, M. Cardoso, M. Duplain, and G. Lemieux, "Immediate adaptation of the dog kidney to acute hypercapnia," *Am J Physiol,* vol. 243, pp. F227-34, Sep 1982.

[19] G. Lemieux, E. Junco, R. Perez, E. Allignet, C. Lemieux, M. R. Aranda, *et al.*, "Renal metabolism during four types of lactic acidosis in the dog including anoxia," *Can J Physiol Pharmacol,* vol. 64, pp. 169-75, Feb 1986.

[20] A. Tizianello, G. Garibotto, C. Robaudo, S. Saffioti, R. Pontremoli, M. Bruzzone, *et al.*, "Renal ammoniagenesis in man with chronic potassium depletion," *Contrib Nephrol,* vol. 92, pp. 114-8, 1991.

[21] M. M. Manore, N. L. Meyer, and J. Thompson, "Sport Nutrition for Health and Performance," *Human Kinetics (Ed.),* vol. Second Edition, 2009.

[22] I. Weiner, W. Mitch, and J. Sands, "Urea and Ammonia Metabolism and the Control of Renal Nitrogen Excretion," *CJASN,* vol. July, p. doi: 10.2215/CJN.10311013, 2014.

[23] G. Lemieux, P. Vinay, and P. Cartier, "Renal hemodynamics and ammoniagenesis. Characteristics of the antiluminal site for glutamine extraction," *J Clin Invest*, vol. 53, pp. 884-94, Mar 1974.

[24] J. P. Ong, A. Aggarwal, D. Krieger, K. A. Easley, M. T. Karafa, F. Van Lente, *et al.*, "Correlation between ammonia levels and the severity of hepatic encephalopathy," *Am J Med*, vol. 114, pp. 188-93, Feb 15 2003.

[25] B. Lee, G. A. Diaz, W. Rhead, U. Lichter-Konecki, A. Feigenbaum, S. A. Berry, *et al.*, "Blood ammonia and glutamine as predictors of hyperammonemic crises in patients with urea cycle disorder," *Genet Med*, vol. 17, pp. 561-8, Jul 2015.

[26] J. B. D. Weir, "New Methods For Calculating Metabolic Rate With Special Reference To Protein Metabolism," *Journal Of Physiology-London*, vol. 109, pp. 1-9, 1949.

[27] C. Warneke, J. A. de Gouw, W. C. Kuster, P. D. Goldan, and R. Fall, "Validation of Atmospheric VOC Measurements by Proton-Transfer- Reaction Mass Spectrometry Using a Gas-Chromatographic Preseparation Method," *Environmental Science & Technology*, vol. 37, pp. 2494-2501, 2003/06/01 2003.

[28] D. Zhao, "A Novel Handheld Real-time Carbon Dioxide Analyzer for Health and Environmental Applications," Arizona State University, 2014.

[29] S. Smith, H. Burden, R. Persad, K. Whittington, B. de Lacy Costello, N. M. Ratcliffe, *et al.*, "A comparative study of the analysis of human urine headspace using gas chromatography–mass spectrometry," *Journal of Breath Research*, vol. 2, p. 037022, 2008.

[30] Z. Krkosova, R. Kubinec, L. Sojak, and A. Amann, "Temperature-programmed gas chromatography linear retention indices of all C-4-C-30 monomethylalkanes on methylsilicone OV-1 stationary phase - Contribution towards a better understanding of volatile organic compounds in exhaled breath," *Journal Of Chromatography A*, vol. 1179, pp. 59-68, Jan 25 2008.

[31] C. Grote and J. Pawliszyn, "Solid-phase microextraction for the analysis of human breath," *Analytical Chemistry*, vol. 69, pp. 587-596, Feb 15 1997.

[32] G. F. Fine, L. M. Cavanagh, A. Afonja, and R. Binions, "Metal oxide semi-conductor gas sensors in environmental monitoring," *Sensors*, vol. 10, pp. 5469-5502, 2010.

[33] N. Barsan, M. Schweizer-Berberich, and W. Göpel, "Fundamental and practical aspects in the design of nanoscaled SnO2 gas sensors: a status report," *Fresenius' journal of analytical chemistry*, vol. 365, pp. 287-304, 1999.

[34] N. Barsan and U. Weimar, "Understanding the fundamental principles of metal oxide based gas sensors; the example of CO sensing with SnO2 sensors in the presence of humidity," *Journal of Physics: Condensed Matter*, vol. 15, p. R813, 2003.

[35] V. Vaishanv, P. Patel, and N. Patel, "Indium tin oxide thin-film sensor for detection of volatile organic compounds (VOCs)," *Materials and manufacturing processes*, vol. 21, pp. 257-261, 2006.

[36] P. K. Clifford and D. T. Tuma, "Characteristics Of Semiconductor Gas Sensors .1. Steady-State Gas Response," *Sensors And Actuators*, vol. 3, pp. 233-254, 1983.

[37] C. Imawan, F. Solzbacher, H. Steffes, and E. Obermeier, "Gas-sensing characteristics of modified-MoO3 thin films using Ti-overlayers for NH3 gas sensors," *Sensors And Actuators B-Chemical*, vol. 64, pp. 193-197, Jun 10 2000.

[38] G. Sberveglieri, "Recent Developments In Semiconducting Thin-Film Gas Sensors," *Sensors And Actuators B-Chemical*, vol. 23, pp. 103-109, Feb 1995.

[39] R. K. Srivastava, P. Lal, R. Dwivedi, and S. K. Srivastava, "Sensing Mechanism In Tin Oxide-Based Thick-Film Gas Sensors," *Sensors And Actuators B-Chemical*, vol. 21, pp. 213-218, Sep 1994.

[40] H. P. Hubner and S. Drost, "Tin Oxide Gas Sensors - An Analytical Comparison Of Gas-Sensitive And Non-Gas-Sensitive Thin-Films," *Sensors And Actuators B-Chemical*, vol. 4, pp. 463-466, Jun 1991.

[41] (Sep 20). *Semiconductor Gas Sensors*. Available: http://www.versaperm.com/semiconductor_gas_sensors.php

[42] W. R. Haag and C. Wrenn, *The PID Handbook - Theory and Applications of Direct-Reading Photoionization Detectors (PIDs)*, 2nd ed. San Jose, CA: RAE Systems Inc., 2006.

[43] (Sep 30). *Introduction to photoionization*. Available: http://www.equipcoservices.com/support/tutorials/introduction-to-photoionization/

[44] (Sep 20). *Operating principle*. Available: http://www.figaro.co.jp/en/technicalinfo/principle/electrochemical-type.html

[45] F. Da Fonseca-Wolheim, "Enzymatic assay based on 2-oxoglutarate with glutamate dehydrogenase for detection of ammonia in biological samples (Direkte Plasmaarnmoniakbestimmung ohne Enteiweissung.)," *J Clin Chem Clin Biochem*

- *Mira Plus (Roche Diagnostic Systems, Mijdrecht, The Netherlands).* vol. 11, pp. 421-31., 1973.

[46] B. Timmer, W. Olthuis, and A. van den Berg, "Ammonia sensors and their applications - a review," *Sensors And Actuators B-Chemical,* vol. 107, pp. 666-677, Jun 29 2005.

[47] R. Goggs, S. Serrano, B. Szladovits, I. Keir, R. Ong, and D. Hughes, "Clinical investigation of a point-of-care blood ammonia analyzer," *Vet Clin Pathol,* vol. 37, pp. 198-206, Jun 2008.

[48] D. Zhao, X. Xian, M. Terrera, R. Krishnan, D. Miller, D. Bridgeman, *et al.*, "A pocket-sized metabolic analyzer for assessment of resting energy expenditure," *Clinical Nutrition,* vol. 33, pp. 341-347, 2014.

[49] K. D. v. d. Kant, L. J. v. d. Sande, Q. Jöbsis, O. C. v. Schayck, and E. Dompeling, "Clinical use of exhaled volatile organic compounds in pulmonary diseases: a systematic review," *Respiratory Research,* vol. 13, p. 117, 2012.

[50] R. KL, G. S, and I. JH, "Urine Anion Gap to Predict Urine Ammonium and Related Outcomes in Kidney Disease," *Clin J Am Soc Nephrol.*, 2018.

[51] M. L. Batshaw and S. W. Brusilow, "Treatment Of Hyperammonemic Coma Caused By Inborn-Errors Of Urea Synthesis," *Journal Of Pediatrics,* vol. 97, pp. 893-900, 1980.

[52] S. W. Brusilow and N. E. Maestri, "Urea cycle disorders: diagnosis, pathophysiology, therapy. In: Barness LA, DeVivo DC, Kaback MM, Morrow G, Oski FA, Rudolph AM (eds). Advances in Pediatrics. Chicago: Mosby," vol. 43, p. 127, 1996.

[53] M. A. Agha and R. A. E. Wahsh, "Basal metabolic rate in bronchial asthma and chronic obstructive pulmonary disease patients," *The Egyptian Society of Chest Diseases and Tuberculosis,* vol. 62, pp. 39-44, 2013.

[54] R. Barsotti, "Measurement of ammonia in blood," *The Journal of Pediatrics,* vol. 138, pp. S11-S20, 2001.

[55] J. Georges, "Determination of Ammonia and Urea in Urine and of Urea in Blood by Use of an Ammonia-Selective Electrode," *Clin. Chem.*, vol. 25/11, pp. 1888-1890, 1979.

[56] (09/05). *Orion™ High-Performance Ammonia Electrode*. Available: https://www.thermofisher.com/order/catalog/product/9512HPBNWP

[57] (08/04). *NEPHROLUX™: Breath Ammonia Analyzer*. Available: http://www.pranalytica.com

[58] T. Hibbard and A. Killard, "Breath Ammonia Analysis: Clinical Application and Measurement," *Critical Reviews in Analytical Chemsitry,* vol. 41, pp. 21-35, 2011.

[59] P. Spanel and D. Smith, "Progress in SIFT-MS: breath analysis and other applications," *Mass Spectrom Rev,* vol. 30, pp. 236-67, Mar-Apr 2011.

[60] C. Tuner, P. Spanel, and D. Smith, "A longitudinal study of ammonia, acetone and propanol in the exhaled breath of 30 subjects using selected ion flow tube mass spectrometry, SIFT-MS," *Physiological Measurement,* vol. 27, pp. 321-337, 2006.

[61] T. Wang, A. Pysanenko, K. Dryahina, and P. Spanel, "Analysis of breath, exhaled via the mouth and nose, and the air of oral cavity," *J. Beath Res.,* vol. 2, p. 037013, 2008.

[62] P. Spanel, S. Davies, and D. Smith, "Quantification of Ammonia in Human Breath by the Selected ion flow tube analitical method using H3O+ and O2 precursor ion.," *Radid communications in mass spectrometry,* vol. 12, pp. 763 - 766, 1998.

[63] S. Davies, P. Spanel, and D. Smith, "Quantitative analysis of ammonia on the breath of patients in end-stage renal failure," *Kidney Int,* vol. 52, pp. 223-8, Jul 1997.

[64] S. Smith, H. Burden, R. Persad, K. Whittington, B. de Lacy Costello, N. M. Ratcliffe, *et al.,* "A comparative study of the analysis of human urine headspace using gas chromatography–mass spectrometry - NOTE: reference study for interference analysis in the current study," *Journal of Breath Research,* vol. 2(3), pp. 037022. doi:10.1088/1752-7155/2/3/037022, 2008.

[65] S. Smith, H. Burden, R. Persad, K. Whittington, B. de Lacy Costello, N. M. Ratcliffe, *et al.,* "A comparative study of the analysis of human urine headspace using gas chromatography–mass spectrometry. ," *Journal of Breath Research,* vol. 2(3), pp. 037022. doi:10.1088/1752-7155/2/3/037022, 2008.

[66] A. Airoudj, D. Debarnot, B. Beche, and F. Poncin-Epaillard, "A new evanescent wave ammonia sensor based on polyaniline composite," *Talanta,* vol. 76, pp. 314-319, Jul 15 2008.

[67] A. Airoudj, D. Debarnot, B. Beche, and F. Poncin-Epaillard, "New sensitive layer based on pulsed plasma-polymerized aniline for integrated optical ammonia sensor," *Analytica Chimica Acta,* vol. 626, pp. 44-52, Sep 19 2008.

[68] B. M. Jayawardane, I. D. McKelvie, and S. D. Kolev, "Development of a gas-diffusion microfluidic paper-based analytical device (muPAD) for the determination of ammonia in wastewater samples," *Anal Chem,* vol. 87, pp. 4621-6, 2015.

[69] M. B. Filho, M. G. da Silva, J. C. Polidoro, F. J. Luna, M. B. M. Monte, A. Miklos, *et al.*, "Detection of ammonia released from zeolite by the quantum cascade laser based photoacoustic set-up," *European Physical Journal-Special Topics,* vol. 153, pp. 547-550, Jan 2008.

[70] M. B. Filho, M. G. da Silva, M. S. Sthel, D. U. Schramm, H. Vargas, A. Miklos, *et al.*, "Ammonia detection by using quantum-cascade laser photoacoustic spectroscopy," *Applied Optics,* vol. 45, pp. 4966-4971, Jul 10 2006.

[71] J. Manne, O. Sukhorukov, W. Jager, and J. Tulip, "Pulsed quantum cascade laser-based cavity ring-down spectroscopy for ammonia detection in breath," *Applied Optics,* vol. 45, pp. 9230-9237, Dec 20 2006.

[72] V. M. N. Passaro, F. Dell'Olio, and F. De Leonardis, "Ammonia optical sensing by microring resonators," *Sensors,* vol. 7, pp. 2741-2749, Nov 2007.

[73] A. Diaz Aguilar, E. Forzani, I. Amlani, L. Nagahara, R. Tsui, and N. Tao, "A Breath Ammonia Sensor Based on Conducting Polymer Nanojunctions," *IEEE SENSORS JOURNAL,* vol. 8, pp. 269 - 273, 2008.

[74] H. J. Kharat, K. P. Kakde, P. A. Savale, K. Datta, P. Ghosh, and M. D. Shirsat, "Synthesis of polypyrrole films for the development of ammonia sensor," *Polymers For Advanced Technologies,* vol. 18, pp. 397-402, May 2007.

[75] A. L. Kukla, Y. M. Shirshov, and S. A. Piletsky, "Ammonia sensors based on sensitive polyaniline films," *Sensors And Actuators B-Chemical,* vol. 37, pp. 135-140, Dec 1996.

[76] I. Lahdesmaki, W. W. Kubiak, A. Lewenstam, and A. Ivaska, "Interferences in a polypyrrole-based amperometric ammonia sensor," *Talanta,* vol. 52, pp. 269-275, Jun 21 2000.

[77] G. K. Prasad, T. P. Radhakrishnan, D. S. Kumar, and M. G. Krishna, "Ammonia sensing characteristics of thin film based on polyelectrolyte templated polyaniline," *Sensors And Actuators B-Chemical,* vol. 106, pp. 626-631, May 13 2005.

[78] D. S. Sutar, N. Padma, D. K. Aswal, S. K. Deshpande, S. K. Gupta, and J. V. Yakhmi, "Preparation of nanofibrous polyaniline films and their application as

ammonia gas sensor," *Sensors And Actuators B-Chemical,* vol. 128, pp. 286-292, Dec 12 2007.

[79] I. Lahdesmaki, A. Lewenstam, and A. Ivaska, "A polypyrrole-based amperometric ammonia sensor," *Talanta,* vol. 43, pp. 125-134, Jan 1996.

[80] X. Ji, C. Banks, D. Silvester, L. Aldous, C. Hardacre, and R. Compton, "Electrochemical ammonia gas sensing in nonaqueous systems: A comparison of propylene carbonate with room temperature ffonc liquids," *ELECTROANALYSIS,* vol. 19, pp. 2194-2201, 2007.

[81] K. Toda, J. Li, and P. K. Dasgupta, "Measurement of ammonia in human breath with a liquid-film conductivity sensor," *Analytical Chemistry,* vol. 78, pp. 7284-7291, Oct 15 2006.

[82] (02/07). *Analysis of urine with "dipstick" strips - Manufacturer's specifications*. Available: http://craigmedical.com/urine_diagnostics.htm

[83] A. K. Kaplan and A. J. E. Pesce, "Clinical Chemistry: Theory, Analysis, Correlation," *Mosby, Inc.,* 1989.

[84] PrecisionLabs. (Feb). *Ammonia Test Strips*. Available: https://preclaboratories.com/product/ammonia-test-strips/

[85] H.-X. Jia, S.-L. Wang, Z.-R. Xu, and Z.-L. Fang, "A microfluidic chip-based flow injection system with gas diffusion separation and photometric detection," *Chemical Journal of the Chinese Universities,* vol. 27, pp. 1621-1625, 2006.

[86] J. Ferreira and E. M. Girotto, "pH effects on the ohmic properties of bromophenol blue-doped polypyrrole film," *Journal of the Brazilian Chemical Society,* vol. 21, pp. 312-318, 2010.

[87] D. Zhao, D. Miller, D. D. Shao, X. J. Xian, F. Tsow, R. A. Iglesias, *et al.*, "A personal device for analyzing carbon dioxide in real time and real breath: Experimental investigation and computational simulation," *Sensors and Actuator B-Chemical,* vol. 183, pp. 627-635, Jul 2013.

[88] W. Haynes, "CRC Handbook of Chemistry and Physics," vol. 95th Edition, 2014.

[89] I. Weiner and J. Verlander, "Renal ammonia metabolism and transport," *Compr. Physiol.,* vol. 3, pp. 201-220., 2013.

[90] E. Childs and N. Collis-George, vol. 201, pp. 393-405, 1950.

[91] A. Rushton, A. Ward, and R. G. Holdich, *Solid-Liquid Filtration and Sepration Technology*: Wiley-VCH, 2000.

[92] A. Prabhakar, R. A. Iglesias, X. Shan, X. Xian, L. Zhang, F. Tsow, *et al.*, "Online sample conditioning for portable breath analyzers," *Anal Chem,* vol. 84, pp. 7172-8, Aug 21 2012.

[93] E. Pines, B.-Z. Magnes, M. J. Lang, and G. R. Fleming, "Direct measurement of intrinsic proton transfer rates in diffusion-controlled reacctions," *Chemical Physics Letters,* vol. 281, pp. 413-420 1997.

[94] J. K. K. James A. Goodrich, *Binding and Kinetics for Molecular biologists*: CSHL Press, 2006.

[95] C. J. Geankoplis, A. A. Hersel, and D. H. Lepek, *Transport Processes and Separation Process Principles*, 4th ed.: PHI Learning Private Limited, 2009.

[96] E. S. Lukacz, E. L. Whitcomb, J. M. Lawrence, C. W. Nager, and K. M. Luber, "Urinary frequency in community-dwelling women: what is normal?," *Am J Obstet Gynecol,* vol. 200, pp. 552 e1-7, May 2009.

[97] (02/08). *Gold standard method for analysis of ammonium levles in urine*. Available: http://www.biovision.com/ammonia-colorimetric-assay-kit.html

[98] D. Smith and P. Spanel, "Selected ion flow tube mass spectrometry (SIFT-MS) for on-line trace gas analysis," *Mass Spectrom Rev,* vol. 24, pp. 661-700, Sep-Oct 2005.

[99] A. C. P. Volp, F. C. E. d. Oliveira, R. D. M. Alves, E. A. Estevesy, and J. Bressan, "Energy expenditure: components and evaluation methods," *Nutricion Hospitalaria,* vol. 26, pp. 430-440, 2011.

[100] E. Ferranini, "The Theoretical Bases of Indirect Calorimetry: A Review," *Metabolism,* vol. 37, pp. 287-301, March 1988.

[101] R. D. Gupta, R. Ramachandran, P. Venkatesan, S. Anoop, M. Joseph, and N. Thomas, "Indirect Calorimetry: From Bench to Bedside," *Indian Journal of Endocrinology and Metabolism,* vol. 21, pp. 594-599, Jul-Aug 2017.

[102] J. A. Harris and F. G. Benedict, "A biometric study of human basal metabolism," *Proceedings of the National Academy of Sciences,* vol. 4, pp. 370-373, 1918.

[103] Y. Deng, B. Scott, and S. T. S. Jeor, "Comparison of resting metabolic rates between predictive euqations and portable indirect calorimeter," in *Obesity week*, 2017.

[104] X. Xian, A. Quach, D. Bridgeman, F. Tsow, E. Forzani, and N. Tao, "Personalized indirect calorimeter for energy expenditure (EE) measurement," *Global Journal of Obesity, Diabetes and Metabolic Syndrome,* vol. 2, pp. 004-008, 2014.

[105] D. Jackemeyer, E. Forzani, and C. Whisner, "Study of Resting Energy Expenditure and Weight Changes during Pregnancy," *Glob J Obes Diabetes Metab Syndr,* vol. 4, pp. 016-023.

[106] C. S. Stump, D. Jackemeyer, Y. Abidov, K. Herbst, N. Tao, and E. Forzani, "Study of the Effect of Mobile Indirect Calorimeter on Weight Management," *Glob J Obes Diabetes Metab Syndr* vol. 4, pp. 044-050. DOI: http://doi.org/10.17352/2455-8583.000022, 2017.

[107] K. JW and S. FCx, "The accuracy of pneumotachograph measure- ments during mechanical ventilation," *Am J Respir Crit Care Med,* vol. 154, pp. 913-917, 1996.

[108] B. Raton, "Goldstein R. Fluid Mechanics Measurements," ed. Florida: CRC Press, 1996.

[109] G. JS, J. MB, G. N, and P. DA, "Capnography," ed. Cambridge, England: Cambridge University Press, 2011.

[110] L. PJ and U. EL, "Fluid Flow Measurement: A Practical Guide to Accurate Flow Measurement," ed. Oxford, England: Butterworth-Heine- mann, 2014.

[111] B. Smith, "Gas-Metering Alternatives Emerge for the Connected World," ed: Electronic Design, 2010.

[112] W. D. McArdle, F. I. Katch, and V. L. Katch, *Exercise physiology: nutrition, energy, and human performance*: Lippincott Williams & Wilkins, 2010.

[113] L. Thomas, M. Lind, and D. Kulick, "Assessment survey of high impact biomarkers for real-time monitoring " in *Internal Review at Mayo Clinic, Arizona*, ed, 2015.

[114] A. J. Skinner and M. F. Lambert, "Evaluation of a Warm-Thermistor Flow Sensor for Use in Automatic Seepage Meters. . ," *IEEE Sensors Journal,* vol. 9, pp. 1058-1067, 2009.

[115] A. C. M. C. Admésio, M. Ricardo, and A. Q. Divo, "Thermistor based, low velocity isothermal, air flow sensor," *Measurement Science and Technology,* vol. 27, p. 035307, 2016.

[116] M. M.D., S. J. S.T., H. L.A., S. B.J., D. S.A., and K. Y.O., "A new predictive equation for resting energy expenditure in healthy individuals," *American Journal of Clinical Nutrition* vol. 51, pp. 241-247, 1990.

[117] F. Rastrello, P. Placidi, A. Scorzoni, E. Cozzani, M. Messina, I. Elmi, *et al.*, "Thermal Conductivity Detector for Gas Chromatography: Very Wide Gain Range Acquisition System and Experimental Measurements," *Instrumentation and Measurement, IEEE Transactions on,* vol. 62, pp. 974-981, 2013.

[118] A. Cagan, H. Schmidt, J. E. Rodriguez, and G. A. Eiceman, "Fast gas chromatography-differential mobility spectrometry of explosives from TATP to Tetryl without gas atmosphere modifiers," *International Journal for Ion Mobility Spectrometry,* vol. 13, pp. 157-165, 2010/12/01 2010.

[119] C. Deng, X. Yang, N. Li, Y. Huang, and X. Zhang, "A Novel Miniaturized Flame Ionization Detector for Portable Gas Chromatography," *Journal of Chromatographic Science,* vol. 43, pp. 355-357, August 1, 2005 2005.

[120] D. Diamond, S. Coyle, S. Scarmagnani, and J. Hayes, "Wireless sensor networks and chemo-/biosensing," *Chem Rev,* vol. 108, pp. 652-79, Feb 2008.

[121] Y. Deng, C. Chen, X. Xian, F. Tsow, G. Verma, R. McConnell, *et al.*, "A Novel Wireless Wearable Volatile Organic Compound (VOC) Monitoring Device with Disposable Sensors," *Sensors,* vol. 16, p. 2060, 2016.

[122] H. Gottlich, R. W. Stark, J. D. Pedarnig, and W. M. Heckl, "Noncontact scanning force microscopy based on a modified tuning fork sensor," *Review of Scientific Instruments,* vol. 71, pp. 3104-3107, Aug 2000.

[123] X. Su, C. Dai, J. Zhang, and S. J. O'Shea, "Quartz tuning fork biosensor," *Biosensors and Bioelectronics,* vol. 17, pp. 111-117, 1// 2002.

[124] S. Tokonami, H. Shiigi, and T. Nagaoka, "Review: micro- and nanosized molecularly imprinted polymers for high-throughput analytical applications," *Anal Chim Acta,* vol. 641, pp. 7-13, May 8 2009.

[125] C. Chen, K. D. Campbell, I. Negi, R. A. Iglesias, P. Owens, N. Tao, *et al.*, "A New Sensor for the Assessment of Personal Exposure to Volatile Organic Compounds," *Atmos Environ (1994),* vol. 54, pp. 679-687, Jul 1 2012.

[126] F. A. Pitten, J. Bremer, and A. Kramer, "Air contamination with volatile organic compounds (VOC's) and health complaints," *Deutsche Medizinische Wochenschrift,* vol. 125, pp. 545-550, May 2000.

[127] J. Svenson and I. A. Nicholls, "On the thermal and chemical stability of molecularly imprinted polymers," *Analytica Chimica Acta,* vol. 435, pp. 19-24, 5/17/ 2001.

[128] Y. Corre, M. Seredych, and T. J. Bandosz, "Analysis of the chemical and physical factors affecting reactive adsorption of ammonia on graphene/nanoporous carbon composites," *Carbon,* vol. 55, pp. 176-184, Apr 2013.

[129] P. J. Lunde and F. L. Kester, "Chemical and Physical Gas Adsorption in Finite Multimolecular Layers," *Chemical Engineering Science,* vol. 30, pp. 1497-1505, 1975.

[130] K. Munakata, "Reactive vacancy solution theory for correlation and prediction of adsorption equilibria for physical and chemical adsorptions," *Surface Science,* vol. 616, p. 11, 2013.

[131] Y. Deng, C. Chen, X. Qin, X. Xian, T. L. Alford, H. W. Choi, *et al.*, "Aging effect of a molecularly imprinted polymer on a quartz tuning fork sensor for detection of volatile organic compounds," *Sensors and Actuators B: Chemical,* vol. 211, pp. 25-32, 2015.

[132] A. V. Bloshenko, A. V. Roshchin, I. V. Kumpanenko, and N. A. Ivanova, "An analysis of absorption-desorption of volatile organic compounds by molecularly imprinted polymer films," *Russian Journal of Physical Chemistry B,* vol. 5, pp. 332-344, Apr 2011.

[133] L. D. Gelb and K. E. Gubbins, "Characterization of porous glasses: Simulation models, adsorption isotherms, and the Brunauer-Emmett-Teller analysis method," *Langmuir,* vol. 14, pp. 2097-2111, Apr 14 1998.

[134] C. Herdes and L. Sarkisov, "Computer simulation of volatile organic compound adsorption in atomistic models of molecularly imprinted polymers," *Langmuir,* vol. 25, pp. 5352-9, May 5 2009.

[135] R. Wang, F. Tsow, X. Zhang, J. H. Peng, E. S. Forzani, Y. Chen, *et al.*, "Real-time ozone detection based on a microfabricated quartz crystal tuning fork sensor," *Sensors (Basel),* vol. 9, pp. 5655-63, 2009.

[136] Y. Deng, "A Novel Mobile Device for Environmental Hydrocarbon Sensing and Its Applications," Ph. D. Doctoral Dissertation, Chemical Engineering, Arizona State University, Tempe, 2017.

[137] W. D. McArdle, F. I. Katch, and V. L. Katch, "Exercise Physiology: Energy, Nutrition, & Human Performance," *Lippincott Williams & Wilkins,* 2007.

[138] E. Forzani, C. Stump, N. J. Tao, Y. Abidov, D. Jackemeyer, and K. Herbst, "Study of the effect of mobile indirect calorimeter on weight management," *Surgery for Obesity and Related Diseases,* vol. 13, p. S88, 2017.

[139] M. D. Mifflin, S. T. St Jeor, L. A. Hill, B. J. Scott, S. A. Daugherty, and Y. Koh, "A new predictive equation for resting energy expenditure in healthy individuals," *The American journal of clinical nutrition,* vol. 51, pp. 241-247, 1990.

[140] R. J. Morris, "Lavoisier and the caloric theory," *The British Journal for the History of Science,* vol. 6, pp. 1-38, 1972.

[141] E. Ferrannini, "The theoretical bases of indirect calorimetry: a review," *Metabolism,* vol. 37, pp. 287-301, 1988.

[142] D. Frankenfield, L. Roth-Yousey, and C. Compher, "Comparison of predictive equations for resting metabolic rate in healthy nonobese and obese adults: a systematic review," *Journal of the American Dietetic Association,* vol. 105, pp. 775-789, 2005.

[143] S. B. a. S. J. S. Deng Y., "Comparison of Resting Metabolic Rates Between Predictive Equations and Portable Indirect Calorimeter.," in *The Obesity Society*, Washington D.C., 2017.

[144] D. C. Nieman, G. A. Trone, and M. D. Austin, "A new handheld device for measuring resting metabolic rate and oxygen consumption," *Journal of the American Dietetic Association,* vol. 103, pp. 588-593, 2003.

[145] F. Wania and D. Mackay, "Peer reviewed: tracking the distribution of persistent organic pollutants," *Environmental science & technology,* vol. 30, pp. 390A-396A, 1996.

[146] A. Tremblay, C. Pelletier, E. Doucet, and P. Imbeault, "Thermogenesis and weight loss in obese individuals: a primary association with organochlorine pollution," *International journal of obesity,* vol. 28, pp. 936-939, 2004.

[147] C. Pelletier, E. Doucet, P. Imbeault, and A. Tremblay, "Associations between weight loss-induced changes in plasma organochlorine concentrations, serum T3 concentration, and resting metabolic rate," *Toxicological Sciences,* vol. 67, pp. 46-51, 2002.

[148] R. S. Pardini, "Polychlorinated biphenyls (PCB): effect on mitochondrial enzyme systems," *Bulletin of environmental contamination and toxicology,* vol. 6, pp. 539-545, 1971.

[149] P. Imbeault, A. Tremblay, J.-A. Simoneau, and D. R. Joanisse, "Weight loss-induced rise in plasma pollutant is associated with reduced skeletal muscle oxidative capacity," *American Journal of Physiology-Endocrinology and Metabolism,* vol. 282, pp. E574-E579, 2002.

[150] L. Hagmar, L. Rylander, E. Dyremark, E. Klasson-Wehler, and E. M. Erfurth, "Plasma concentrations of persistent organochlorines in relation to thyrotropin and thyroid hormone levels in women," *International archives of occupational and environmental health,* vol. 74, pp. 184-188, 2001.

[151] M. Sala, J. Sunyer, C. Herrero, J. To-Figueras, and J. Grimalt, "Association between serum concentrations of hexachlorobenzene and polychlorobiphenyls with thyroid hormone and liver enzymes in a sample of the general population," *Occupational and environmental medicine,* vol. 58, pp. 172-177, 2001.

[152] D. A. Sarigiannis, S. P. Karakitsios, A. Gotti, I. L. Liakos, and A. Katsoyiannis, "Exposure to major volatile organic compounds and carbonyls in European indoor environments and associated health risk," *Environment international,* vol. 37, pp. 743-765, 2011.

[153] M. Phillips and J. Greenberg, "Ion-trap detection of volatile organic compounds in alveolar breath," *Clinical Chemistry,* vol. 38, pp. 60-65, 1992.

[154] J. Weir, "New methods for calculating metabolic rate with special reference to protein metabolism. 1949," *Nutrition (Burbank, Los Angeles County, Calif.),* vol. 6, pp. 213-221, 1989.

[155] Y. Deng, N.-Y. Liu, F. Tsow, X. Xian, and E. S. Forzani, "Adsorption Thermodynamic Analysis of a Quartz Tuning Fork Based Sensor for Volatile Organic Compounds Detection," *ACS Sensors,* vol. 2, pp. 1662-1668, 2017/11/22 2017.

[156] C. C. Yue Deng, Francis Tsow, Xiaojun Xian, Erica Forzani, "Unraveling Fabrication and Calibration of Wearable Gas Monitor for use under Free-Living Conditions," *3th Annual International Conference of the IEEE Engineering in Medicine and Biology Society,* 2016.

[157] C. Chen, K. D. Campbell, I. Negi, R. A. Iglesias, P. Owens, N. Tao, *et al.*, "A new sensor for the assessment of personal exposure to volatile organic compounds," *Atmospheric environment,* vol. 54, pp. 679-687, 2012.

[158] D. C. Hoaglin and R. E. Welsch, "The hat matrix in regression and ANOVA," *The American Statistician,* vol. 32, pp. 17-22, 1978.

APPENDX A

SUPPLEMNTARY INFORMATION FOR CHAPTER 2

Table A. 1. Cross-talking measurement table of a PVDF sensor substrate

		Average	Standard Deviation	error (%)
Original	Sensing	0.30	0.002	0.75
	Reference	0.54	0.002	0.45
black sensing	Sensing	0	0	N/A
	Reference	0.46	0.003	0.7
black ref.	Sensing	0.30	2.5*10^-4	0.08
	Reference	0	0	N/A

Table A. 2. Cross-talking measurement table of a hydrophobic PTFE sensor substrate

		Average	Standard Deviation	error (%)
Original	Sensing	1.654	0.004	0.75
	Reference	1.571	0.004	0.45
black sensing	Sensing	0	0	N/A
	Reference	1.761	0.002	0.7
black ref.	Sensing	1.651	0.015	0.08
	Reference	0	0	N/A